Master's thesis

NTNU
Norwegian University of Science and Technology
Faculty of Economics and Management
Dept. of Industrial Economics and Technology Management

Ivar Borge Nore
Kristoffer Winther

Optimizing Hybrid Hydro-Solar Power Systems Using Two-Stage Stochastic Programming

Master's thesis in Industrial Economics and Technology Management
Supervisor: Stein-Erik Fleten
Co-supervisor: Carl Fredrik Tjeransen
June 2023

NTNU
Norwegian University of Science and Technology

Ivar Borge Nore
Kristoffer Winther

Optimizing Hybrid Hydro-Solar Power Systems Using Two-Stage Stochastic Programming

Master's thesis in Industrial Economics and Technology Management
Supervisor: Stein-Erik Fleten
Co-supervisor: Carl Fredrik Tjeransen
June 2023

Norwegian University of Science and Technology
Faculty of Economics and Management
Dept. of Industrial Economics and Technology Management

NTNU
Norwegian University of
Science and Technology

NTNU
Kunnskap for en bedre verden

Department of Industrial Economics and Technology Management

TIØ4905 - Managerial Economics and Operations Research, Master's Thesis

Optimizing Hybrid Hydro-Solar Power Systems Using Two-Stage Stochastic Programming

Authors:
Kristoffer Winther and Ivar Borge Nore

Supervisor:
Stein-Erik Fleten

Co-Supervisor:
Carl Fredrik Tjeransen

June, 2023

Preface

This masters' thesis is the final assessment in a Master of Science degree in Applied Economics and Operations Management at the Department for Industrial Economy and Technology Management at Norwegian University of Science and Technology. The thesis has been written during the spring of 2023 and builds on a project report written in the fall of 2022.

We would like to express our gratitude to everyone involved in this project, who have provided us with valuable insights and guidance. Firstly, we want to thank our supervisor, Professor Stein-Erik Fleten, and our co-supervisor, Carl Fredrik Tjeransen. Their expertise and help have been instrumental in helping us understand important aspects of the literature and construct our masters thesis. We would also like to sincerely thank Ruben van Beesten, who has been an invaluable resource in helping us understand the aspects of Disjunctive Decomposition. Finally, we would like to thank Professor Lewis Ntaimo of Texas A&M University for taking the time to discuss our implementation of his algorithm.

Additionally, we would like to extend our thanks to SINTEF and Scatec for providing us case specific data.

Trondheim, June 11, 2023
Ivar Borge Nore, Kristoffer Winther

Abstract

The integration of renewable energy sources into the energy mix has gained significant attention due to the demand for reliable and sustainable energy. Hybrid power systems that combines renewable energy technologies and dispatchable power sources offer enhanced grid stability and resource utilization. This thesis focuses on the application of two-stage stochastic optimization techniques for the day-ahead load commitment of a hybrid hydro-solar power plant in Guinea. We seek to bridge a gap in literature regarding hybrid power system scheduling by combining state of the art methods from hydropower scheduling, solar scenario generation, and stochastic programming. We develop a scheduling framework through optimization models that maximize resource utilization while minimizing costs. The framework incorporates uncertainties associated with solar power and maintains accuracy in the complexities of hydropower production scheduling. The study highlights the importance of hybrid production planning in off-grid locations with grid congestion issues, comparing it to planning and operating separately. We show a significant advantage in hybrid power production in these settings, as the resource utilization of hybrid configurations is much more efficient. We also explore the effects of representing the hybrid power production as a stochastic problem and accurately representing the hydropower production function. The study is inconclusive regarding advantages to including stochasticity but explicate the significance in accurate representation. The developed framework can be adapted to suit different supply and demand structures and has potential applications in spot markets worldwide. Additionally, the thesis discusses the applicability of a Branch-and-Cut algorithm based on Disjunctive Decomposition for stochastic programming in hydropower production planning.

Sammendrag

Inkluderingen av fornybare energikilder i kraftmiksen har de senere årene fått økt oppmerksomhet på grunn av etterspørselen etter fornybare og bærekraftige energikilder. Hybride kraftsystemer som kombinerer fornybar energi og kontrollerbare energikilder tilbyr økt stabilitet i kraftproduksjonen og økt ressursutnyttelse. Denne masteroppgaven fokuserer på bruken av to-stegs stokastiske optimeringsteknikker i planleggingen av produksjonsforpliktelser ved et hybrid vann- og solkraftverk i Guinea. Masteroppgaven fyller gapet i literatur om kraftplanlegging i hybride kraftsystemer ved å kombinere avanserte teknikker innen vannkraftsproduksjon, solscenariogenerering og stokastisk programmering. Vi utvikler et planleggingsrammeverk gjennom optimeringsmodeller som maksimerer ressursutnyttelse ved å minimere kostnader. Rammeverket innkorporerer usikkerhet i solkraftproduksjon og representerer en nøyaktig tilnærming av vannkraftproduksjonen. Oppgaven understreker viktigheten av hybrid produksjonsplanlegging ved å sammenligne et tilsvarende produksjonssystem der vann- og solkraftprodusentene planlegger og produserer uten kommunikasjon. Vi ser en tydelig fordel av hybrid kraftproduksjon i slike settinger gjennom vesentlig mer effektiv ressursbruk. Vi ser også på effekten av å implementere stokastikk i solproduksjonen, samt forskjellene ved å planlegge eksakt og planlegge tilnærmet. Resultatene er inkonklusive rundt fordelene ved å inkludere stokastikk, men tydeliggjør viktigheten av nøyaktig representasjon av kraftproduksjonen. Det utviklede rammeverket kan modifiseres til forskjellige tilbud- og etterspørselstrukturer, og har potensiale i spot-markeder. I tillegg diskuterer denne masteroppgaven anvendeligheten av en Branch-and-Cut algoritme basert på Disjunktiv Dekomponering for stokastisk programmering i produksjonsplanlegging av vannkraft.

Table of Contents

List of Figures vi

List of Tables vii

List of Abbreviations viii

1 Introduction 1

2 Background 3

2.1 Hybrid Power Production . . . 3

2.2 Hydropower Electricity Production . . . 3

2.3 Solar Power Production . . . 4

2.4 Electricity Markets . . . 4

3 Literature Review 6

3.1 Hybrid Power Production Planning . . . 6

3.2 Hydropower Production Planning . . . 7

3.3 Solar Modeling . . . 11

3.4 Solar Power Estimation . . . 12

3.5 Stochastic Programming . . . 13

4 Problem Description 17

5 Mathematical Models 19

5.1 Modelling choices . . . 19

5.2 Short-Term Model . . . 20

5.3 Mid-Term Model . . . 25

6 Solution Method 27

6.1 Handling of Non-Linearities in the Short-Term Model . . . 27

6.2 Handling of Non-Linearities in the Mid-Term Model . . . 31

6.3 Solar Scenario Generation and Selection . . . 31

6.4 Model Simulation and Testing Procedure . . . 34

6.5 Disjunctive Decomposition . . . 35

7 Computational Study 44

7.1 The Guinean Hybrid Power System . . . 44

7.2 Data Handling . . . 45

7.3 Scenario Generation Hyperparameter Tuning 51
7.4 Simulation 52
7.5 Results 55
7.6 Implementation and Testing of the D2-CBAC Algorithm 60

8 Concluding Remarks **64**
8.1 Future Research 64

Bibliography **66**

Appendix **70**
A Short-Term Model 70
B Mid-Term Model 72

List of Figures

1 Mesh View of HPF 28
2 SOS2-Constrained Weights 29
3 Prediction Interval of PV power 33
4 Simulation Overview 35
5 D2 Cut Convex Approximation 40
6 Disjunct Set of Epigraph 41
7 Guinean Hydropower System Visualization 44
8 Hill Chart 45
9 Turbine Efficiency Curves 47
10 Turbine Efficiency Curved Plane 47
11 Net Head Linear Approximation 49
12 Measured and Interpolated Inflow 50
13 Average Monthly Inflow 50
14 PV Power Generation Scenarios 53
15 Hybrid Configuration Overview 54
16 Seperate Configuration Overview 54
17 Hybrid vs Deterministic Accumulated Profits 58
18 Hybrid vs Seperate Load and Costs 59

List of Tables

1 Nomeclature used in PV power generation 32

2 Data for the Planned Power System 45

3 Turbine Efficiencies Frankonédou 46

4 Turbine Efficiencies Kogbédou 46

5 Breakpoints Frankonédou 48

6 Breakpoints Kogbédou 48

7 Daily Average Inflow 50

8 Hyperparameters in Scenario Generation 51

9 Accumulated Results 56

List of Abbreviations

C3-SLP	-	Common Cut Coefficent Stochastic Linear Program
CBAC	-	Continuous Branch-and-Cut
CDF	-	Cumulative Distribution Functions
D2	-	Disjunctive Decomposition
D2-CBAC	-	A Continuous Branch-and-Cut Algorithm with Disjunctive Decomposition
HPF	-	Hydropower Production Function
LP	-	Linear Program
MILP	-	Mixed-Integer Linear Program
NWP	-	Numerical Weather Prediction
PPA	-	Power Purchasing Agreement
PV	-	Pohotovoltaic
SDE	-	Stochastic Differential Equation
SLP	-	Stochastic Linear Program
SOS2	-	Special Ordered Set Type 2
WC	-	Water Cost

1 Introduction

In recent years, the integration of renewable energy sources into power grids has gained significant attention due to the growing demand for sustainable and reliable energy. Hybrid power systems, which combine multiple renewable energy technologies, have emerged as a promising approach to enhance power grid stability and resource utilization. Among these hybrid systems, the combination of hydro and solar power holds great potential for maximizing energy generation while mitigating the inherent intermittency and uncertainty of renewable sources. In this thesis, we focus on the day-ahead unit commitment of a hybrid hydro-solar power plant in Guinea and the application of two-stage stochastic optimization techniques for this problem.

Solar power is rapidly emerging as one of the most cost-effective options for energy generation worldwide. Development, installations, and investments of solar power technologies are expected to rise further in the coming years (IEA 2022). The low operating costs and high scalability makes solar power an increasingly attractive energy source. However, solar energy poses certain challenges due to its inherent uncertainty and volatility. Photovoltaic solar panels solely produce electricity when exposed to sunlight, rendering power generation vulnerable to rapidly changing weather. Consequently, ensuring a reliable power supply necessitates the integration of solar energy with other technologies.

One promising approach is to combine solar power with storage hydropower (Beluco, Kroeff de Souza and Krenzinger 2012). Storage hydropower plants consist of reservoirs connected to power facilities, enabling the storage of water's potential energy. This reservoir-based setup essentially functions as a large-scale battery, facilitating on-demand power production that is both dispatchable and renewable. A natural compatibility between hydropower and solar power arises from the fact that sun and rain rarely appears at the same time. This synergy highlights the potential of combining hydro and solar power as a promising solution. Moreover, in regions characterized by distinct dry and wet seasons, this combination could prove advantageous as neither technology alone can meet the energy demands throughout all seasons (Bhandari et al. 2014). Additionally, standard battery technology may not alone be able to store enough power to balance the supply in seasons with very little solar irradiance. Hydropower reservoirs may therefore be a better fit with solar energy than other energy sources.

The specific context of our research is a hybrid hydro-solar power plant in Guinea. We classify the Guinean power grid that the hybrid plant is connected to as "off-grid". This means that there is limited energy production and the grid is not connected to a well balanced power market. Consequently, there are no market powers that ensure balance between supply and demand, such as in the Nordics. Guinea has abundant hydro and solar resources, that can be harnessed to meet its growing energy demand. However, the efficient utilization of these resources and the integration of renewable energy into the existing power grid pose significant technical and operational challenges. Additionally to being off-grid, the power grid has insufficient transmission capacity as a result of the hybrid plant being a new, large energy producer, which introduces bottlenecks in production. We address these challenges through a comprehensive and advanced stochastic optimization framework, specifically tailored for the day-ahead unit commitment problem in the context of the hybrid hydro-solar power plant.

The main objective of this research is to solve the scheduling problem for the hybrid power plant in Guinea. We do this by developing and implementing a two-stage stochastic optimization model that takes into account the uncertainties associated with solar power and the complex factors associated with hydropower generation. By incorporating uncertainties, we aim to create a scheduling framework based on this optimization model that maximizes the utilization of available resources by minimizing the expected costs of the power producers. The intricacy of the hydropower modeling makes the optimization problem complex, as it involves non-linear and non-convex functions.

The literature on scheduling hybrid power systems is rather scarce. We have identified a gap in the literature in between the long-term scheduling of large hydro-solar power systems, such as in F. Li and Qiu (2016), and short-term scheduling of hybdrid power systems that use thermal power instead of water, such as in Asensio and Contreras (2016). The short-term scheduling of hybrid hydro-solar power systems is unchartered territory. This thesis seeks to bridge the identified gap

by combining state of the art methods from hydropower scheduling, solar scenario generation, and stochastic programming.

The approach is to create an optimization program that schedule short-term production planning for larger hydro-solar power systems. Using data from the mentioned Guinea setting, we open the door for the development of more sophisticated power production that utilizes renewables in off-grid locations. We also create a new form of integrated short- and mid-term hydropower scheduling optimization framework. Here, the short-term and mid-term models run in tandem so that after each planning period of the short-term model, the mid-term model automatically runs, updated with information from the short-term. This updates the water value and water trajectory estimates for the short-term scheduling, which allows hybrid power producers to take long term considerations into their short-term planning by running just one program.

Our contribution to stochastic optimization is tied to hydropower production planning, were stochastic optimization has been widespread for several years. Common methods are Stochastic Dynamic Programming and Stochastic Dynamic Dual Programming (Wallace and Fleten 2003). However, there are several methods for stochastic programming that have been developed in recent years, making it interesting to see their applicability in hydropower production planning. We have implemented a Branch-and-Cut algorithm developed by Ntaimo and Sen (2007) which is based on the Disjunctive Decomposition algorithm by Sen and Higle (2005). We show the potential in using this method in hybrid hydro-solar scheduling and highlight the importance of tailoring the method to the specific problem.

Even though this thesis focuses on the optimal scheduling of a hybrid power system in Guinea, it can be generalized to other cases of hybrid hydro-solar power production in off-grid locations. This is because storage hydropower production planning is rather similar no matter where the power plant is located. The same accounts for solar power. The aspects that tie the case to Guinea are mostly related to the input data and other configurations in the initialization of the scheduling problem. All these aspects are easily changed in order to translate the scheduling problem to another case with a similar supply and demand structure. Additionally, very few changes are necessary in order to translate the problem to suit hybrid hydro-solar production planning in a spot market, which is relevant many places in the world.

In the following sections we will first present the fundamentals of hybrid power production, hydropower production, solar power production, and electricity markets in Section 1. Then, we will provide an overview of the relevant literature to present the current state of hybrid hydro-solar production in stochastic optimization. After the literature review we present the reader with the problem description, describing the hybrid power plant in Guinea and the necessary considerations related to it. Based on the problem description, we design and present our optimization models in Section 5, before we introduce the methods we have used to solve these models in Section 6. Finally, we will briefly introduce the data used in this thesis and the processes used to structure this data. We present and discuss the computational results obtained from our simulations and analyses, highlighting the benefits and implications of our approach. Lastly we present our concluding remarks and future research.

2 Background

In this section we present the fundamentals of hybrid power production, hydropower production, solar power production, and electricity markets. The purpose of this part is to introduce well known concepts in key topics for our thesis, which will make it possible to understand the problem description and literature review for readers with little prior knowledge in these fields. Since this thesis is an extension of Nore and Winther (2022), some similarities will occur.

2.1 Hybrid Power Production

Hybrid power plants, which generate electricity using multiple power sources, have been defined by Paska, Biczel and Kłos (2009) as a "small set of co-operating units, generating electricity or electricity and heat, with diversified primary energy carriers (renewable and non-renewable)". In this thesis, the terms "hybrid power systems" and "hybrid power plants" will be used interchangeably.

As the world's energy needs shift towards renewables, hybrid power plants have become increasingly attractive. Although renewables such as wind and solar power have low marginal costs, their unpredictable nature necessitates the use of a power sources that are more controllable in order to create more reliable power plants and ensure stable electricity supply. These controllable power sources, known as dispatchable power sources, can be fossil fuels, hydrogen cells, batteries, or other technologies.

Hybrid power plants are particularly common in isolated power grids such as islands or developing regions, where there may be limited power sources. Typically, hybrid power plants combine renewable sources with dispatchable power sources in form of thermal power production based on fossil fuels, such as coal or crude oil (Asensio and Contreras 2016; Beluco, Kroeff de Souza and Krenzinger 2012). Unfortunately, this often leads to the use of non-renewable energy when renewable resources are unavailable, which has negative environmental consequences.

Replacing fossil fuel based thermal power production with stored hydropower can maintain reliability and supply certainty while using only renewable energy sources. This implies that, if these hybrid power plants are designed and operated efficiently and on a sufficiently large scale, more of the world's reliable energy production can be renewable, even in isolated power grids.

2.2 Hydropower Electricity Production

The term hydropower production usually includes all terms where power is produced from the potential energy of water, including run-of-the-river power plants and storage hydropower plants where water is stored in reservoirs and discharged at will. For the continuation of this thesis, the term hydropower will be used to describe storage hydropower.

The principles behind hydropower production are rather simple. Water from higher altitudes stream into rivers which flow downwards. By building dams, the energy of the flowing water is stored and power can be produced at will, making hydropower a dispatchable power source. The water turns turbines connected to generators, which generates electricity. The process of discharging water from higher altitudes through turbines transforms the potential energy of the water into electrical power. The energy production capacity of a hydropower plant is dependent on the *head* of the power plant, as well as the mass of the water discharged. The term *head* describes two values in hydropower production: gross head and net head. The gross head is the height difference between the water level of the reservoir and the level of the water beneath the turbine. Net head is the gross head adjusted for friction and other loss factors as a consequence of the water being discharged through a tunnel. The water is discharged through one or several turbines, connected to a generator. A hydropower plant may consist of several turbines and generators, and a hydropower system may consist of several reservoirs and power plants, usually connected in a cascade.

Consequentially, the power produced from a hydropower plant is dependent on both the head and

the discharge. Since the head varies with the water level, a power plant will be able to produce less energy when the water level in the reservoir is low compared to when it is high. The future water level is determined by two factors: the discharge and the amount of inflow to the reservoir. Depending on the geographical location of the hydropower system, the inflow may have large seasonal variations.

The energy-storing ability of hydropower makes it a key energy source in the global energy transition. Reservoirs function as large batteries, enabling the plants to produce how much energy they want when most beneficial to them, not on nature's decree like with wind- or solar power. The ability to choose when to produce presents the need for power production planning. This has been done with the use of optimization programs in this field since the mid-1900s (Wallace and Fleten 2003).

Since hydropower systems are able to store energy in the form of water and then sell this energy at a later time, there is an opportunity cost for using water to generate power. This opportunity cost is often called the water value and refers to the marginal value of having one extra unit of water in the reservoir. The water value is dependent on the future price of electricity and the expected inflow to the reservoirs, as well as the amount of water currently in the reservoir. If the reservoir is full, any additional water will only lead to overflow and not produce power. This implies a water value of zero. Lower water levels lead to less potential energy per unit of water in the reservoir, but the risk of overflow is lower. Combined with seasonality, these properties mean that the water value varies over time and with the amount of water in the reservoir. Since flooding is always a possibility with stochastic inflow, the water value decreases with higher head even if this leads to increased marginal production for each unit of water (Fosso et al. 1999).

Hydropower scheduling is usually split into different categories based on time horizon: long- and short-term. The long-term planning is typically concerned with time horizons of several years or longer, and is ususally dependent on some medium-term model in order to be transferable to the short-term model. The difference between medium-term and long-term models are rather vague, and they are therefore often both categorized as long-term. Short-term models usually span one to fourteen days and concern the detailed production planning of the hydropower plant. The purpose of long-term models are to determine the water trajectory and the current water value of the reservoir. The water value is a necessary input value to the short-term planning.

2.3 Solar Power Production

Solar power is produced by turning the energy from the sun into power, either by turning solar radiation or solar thermal energy into electricity (Qazi 2017). Most commonly, solar power is generated by photovoltaic (PV) panels that convert the radiation from the sun into power (Singh 2013). PV panels consists of several PV cells that are made from semiconducting materials, usually silicon. The power is generated as the energy from solar rays knocks loose electrons of the PV cells. Electric fields in the PV-panel create an electrical current of these electrons. The panels are not able to store the power produced. The unpredictable nature of weather means PV power generation is highly volatile. Under certain cloud conditions, for example, the changes can be drastic and fast, greatly reducing the PV panels power output (Singh 2013). In order to fully cover power demand in an area and balance the power production, solar power has to be coupled with more reliable and controllable energy sources.

2.4 Electricity Markets

Electricity markets differ somewhat in different parts of the world, leading to differences in power production planning. In the Nordics, the electricity market has been decentralized since 1991. In these markets, the power producers trade power day-ahead with delivery next day. The main volume of power is traded in this spot market. In addition, actors are allowed to trade some power intra-day, meaning that they can trade until 30 minutes before delivery. This trading is on a continuous market, while the day-ahead trading is on auction form. The market clearing price

is created in the intersection between demand and supply (Fleten and Kristoffersen 2007). This leads to highly efficient markets, with few imperfections. In developing countries, however, the electricity markets are often regularized. In Brazil, for example, an independent system operator performs the system scheduling. This means that an independent body decides the amount of power each plant is to produce, based on long-, medium- and short-term analysis. This is called the hydro unit loading and commitment problem, and means that all power scheduling is centrally planned and controlled (Finardi and Scuzziato 2013). In other less developed countries, such as Guinea, the electricity market is not completely defined. In other cases again there is no market at all, only a grid operator that sells energy to consumers in a monopoly.

3 Literature Review

To gain insight in the most relevant and up-to-date approach to hybrid hydro-solar planning, we have conducted a literature search. The search focuses on articles and papers related to hybrid power systems, hydropower production planning, solar power forecasting, and stochastic programming, in that sequence. The aim of this section is to provide a comprehensive understanding of the extensive research conducted in these quite different areas.

3.1 Hybrid Power Production Planning

The existing literature on hybrid power systems primarily focuses on three main aspects: the complementary features of different power sources, the advantages of implementing them together in a hybrid system, and the optimal design considerations for such systems. However, this master thesis specifically concentrates on the production planning aspect of a hydro-solar hybrid power system, an aspect only addressed in a limited number of research papers. In the following section, we will discuss the scheduling and optimization approaches employed in these studies. Subsequently, we will present literature findings regarding the advantages of utilizing hybrid power systems, comparing their efficiency with that of independently-operated power plants. Through this comparison we want to elucidate the potential benefits of integrating different energy sources in hybrid operations.

Advantages of Using Hybrid Power Systems

One of the notable advantages of employing hybrid power systems is the enhanced reliability in renewable energy sources, which can contribute to increased load commitment. The intermittent nature of many renewable energy sources is the main challenge of extensive integration into existing grids, markets, and power systems (Bhandari et al. 2014). By combining different energy carriers, hybrid power systems facilitate a stable energy supply to the market (Zhang et al. 2021). This can be achieved by leveraging energy sources with complementary properties. To a certain degree, renewables, e.g., solar, are predictable and periodic. The sun rises in the morning and sets in the afternoon. However, the volatility is ever present, as a single cloud can significantly reduce the irradiance. In instances where the power system includes a renewable source that is both periodic and highly volatile, such as solar energy, incorporating at least one dispatchable power source in a hybrid system enhances stability. Various battery technologies, for example, can enhance the value of the renewable power source, distributing generated power more evenly throughout a time period. In certain markets, this enables power producers to increase their load commitment, resulting in higher revenues (Beluco, Kroeff de Souza and Krenzinger 2012).

Optimization of Hybrid Power Systems

Most research papers addressing the operation of hybrid power systems face stochastic optimization problems. This is because hybrid systems often involve at least one non-dispatchable power source. The literature presents various approaches to solving these stochastic optimization problems, but a common strategy involves handling the different power systems separately and subsequently combining them in a final optimization model. Typically, the stochastic power source is represented through scenarios, while the controllable power source is optimized (Bhandari et al. 2014; F. Li and Qiu 2016). M. Deshmukh and S. Deshmukh (2008) argue that the optimization of hybrid power systems is primarily dependent on the performance of the individual components. Therefore, it is essential to first model and evaluate the individual parts before combining them.

Once the individual power systems have been modeled, there are several approaches to solve the combined optimization problem. F. Li and Qiu (2016) utilize a multi-objective optimization model for an integrated PV and hydropower system. Their objectives include minimizing power variance and maximizing power output over multi-year time horizons. They employ a Genetic Algorithm to generate the Pareto front of solutions. However, since the time horizon extends over several

years, the model does not provide insights into the daily operation of the hybrid system. In a short-term multi-objective model with the same objectives, Zhang et al. (2021) investigate the optimal production of a cascaded hybrid hydro-PV system. Neither of these models incorporates any kind of market structure nor supply obligation.

Raygani (2019) focuses on unit commitment modeling with solar power and proposes an improved model based on classical robust approaches that plan for worst-case realizations of stochastic sun conditions. Using only three scenarios (overcast, clear, and uncertain), they achieve cost reductions of approximately 0.5%. However, robust approaches tend to be overly pessimistic and provide little flexibility in the optimization model. In a similar vein, Ming et al. (2018) focus on modeling large hydro-PV hybrid power plants and also adopt a robust approach to PV production. They address the hydropower unit commitment using three different nested heuristics, specifically tailored for the optimization of these extensive power production systems.

In smaller power grids or configurations, the approaches are different. Looking at isolated island communities, Asensio and Contreras (2016) propose a two-stage stochastic unit commitment model that incorporates solar power generation with recourse in thermal production. Their objective is to minimize conditional values at risk and they solve their problem using the deterministic equivalent. By considering 125 scenarios and a 20% share of renewable power, their model successfully reduces the conditional values at risk by 1% (Asensio and Contreras 2016). This two-stage stochastic programming model proves to be a viable option for hybrid production planning, particularly when considering day-ahead commitment requirements. While islands and isolated communities face a challenge of producing enough, generating too much power can also present problems. Renewables often share infrastructure with existing power producers, introducing the possibility for congestion problems. Matevosyan and Soder (2007) presents a day-ahead planning algorithm for hybrid wind-hydro power production in this setting. They implement uncertainty in wind production and compares hybrid planning to the two producers planning separately. With a replanning algorithm, they find that coordinated operation increases revenue for the hydro producer while reducing wind power curtailment. The setting is set to a spot marked context, showing the potential gains of hybrid power systems even in developed power markets.

3.2 Hydropower Production Planning

The planning of hydropower production is a highly intricate task, necessitating careful consideration of multiple modeling choices. The selection of an appropriate objective function is one of these choices, and plays an important role in determining the operational framework of the program. The objective of all hydropower planning programs is either to maximize profits or minimize cost in some form. How this is represented in the objective function is however depending on various factors, such as market dynamics and the time horizon of the problem at hand. Consequently, it is crucial to address the choice of factors in the objective in order to ensure effective planning outcomes.

In addition to the objective function, another significant challenge in hydropower production planning arises from the complexity involved in modeling the hydropower production function itself. The intricate nature of this function gives rise to a vast array of approaches found within the existing literature. With a multitude of perspectives and methodologies available, careful consideration must be given to understanding and evaluating the different approaches.

To provide a comprehensive overview of hydropower production planning, this section will begin by exploring the existing literature pertaining to the objectives of production planning. Subsequently, the section will examine various approaches and techniques employed for handling the complexity of the power production function, hereby including turbine efficiency curves and varying head. This sheds light on the methods used to model and optimize hydropower production.

Objectives of the Hydropower Production Planning Problem

The objective function of the hydropower production planning model exhibits variations depending on both the time horizon of the model and the specific market characteristics of the power system. In the context of the Brazilian market, the primary objective of the scheduling problem is to ensure the efficient generation of power while meeting the predetermined demand. A study by Finardi and Scuzziato (2013) addresses this objective by minimizing two key factors: the discharge of water from each reservoir during each timestep and the frequency of starting and stopping each generator throughout the planning period. These factors directly contribute to the objective function proposed in Finardi and Scuzziato (2013) model.

In contrast, alternative methods employed in similar markets may prioritize different aspects. For instance, some approaches concentrate on maximizing the volume of water stored in reservoirs (L. Guedes et al. 2016). Others emphasize minimizing the water consumption per unit of power generated to meet production demands (Cordova et al. 2014). However, both aforementioned approaches lack the inclusion of monetary values within their objective functions. Consequently, comparing the value of water discharge to the power produced becomes challenging.

In liberalized markets like the Nordics, power system operators operate with the goal of maximizing their profits, adopting a strategic approach to power production and trading. To achieve this, operators carefully assess market dynamics and adjust their production and sales strategy accordingly. The key principle is to generate and sell electricity during periods when prices are high, while conserving water resources for later use during periods when prices are low. This profit-maximizing behavior is evident in the day-ahead market, where the market clearing price is determined based on the intersection of supply and demand curves (Fleten and Kristoffersen 2007).

Power producers in these markets actively participate in electricity trading, leveraging market opportunities to maximize their profits. Their decision-making process involves evaluating price forecasts and adjusting their production and trading strategies accordingly. By effectively timing their power generation and sales activities, they can capitalize on periods of high market prices and optimize their revenue streams. This strategic behavior is a fundamental component of the objective function in short-term hydropower scheduling models. In these models, a term for the power sold each hour multiplied by the hourly prize is incorporated into the objective function. By including this term, operators align their scheduling decisions with the goal of maximizing their financial gains in the market.

However, it is important to note that in most liberalized markets, the day-ahead hourly prices are subject to uncertainty. They are often influenced by various factors such as demand fluctuations, weather conditions, bottlenecks in supply and availability of other power sources. As a result, power producers face a level of uncertainty in their potential profits. This, combined with uncertainty in other factors such as inflow, leads to the fact that stochastic optimization problems could be implemented to find optimal production schedule in hydropower planning (Fleten and Kristoffersen 2008).

In liberalized markets, where power producers aim to maximize their revenue, it is important to consider costs as well. The alternative cost of using water is the most prominent cost in hydropower production according to Kong, Skjelbred and Fosso (2020). Water is the means of storing energy that potentially could be sold at a later time, and it therefore it becomes imperative to consider the value of water. In the realm of short-term planning, two common approaches are employed to incorporate this consideration. Firstly, some models focus on maximizing the remaining water volume in the reservoir by the end of the planning period (Skjelbred, Kong and Fosso 2020). Alternatively, others seek to minimize the cost associated with water usage throughout the planning period (Kong, Skjelbred and Fosso 2020). Both approaches enable the comparison of the opportunity cost of utilizing water against other cost factors, i.e., the water value.

However, to implement these methods effectively, the determination of the water value becomes necessary. Obtaining this value typically involves employing a long-term production planning model. The water value at the end of the planning horizon is the most interesting value, as it represents the alternative cost of having a greater water supply available for future power production. Notably,

in short-term planning scenarios with extensive reservoir capacities, the total discharge of water has minimal impact on the overall water volume and, consequently, does not significantly affect the water value either (Catalão et al. 2009). As a result, updating the water value during the production planning process is unnecessary in such cases.

According to Kong, Skjelbred and Fosso (2020), apart from the alternative cost of using water, the most significant expenses in hydropower production are the start-up and shut-down costs associated with the generating units, which is the combination of a turbine and the generator it is connected to. Producers often prefer to sell power only when it is profitable, which may tempt them to frequently initiate and halt the generating units. However, this approach entails various additional expenses, including increased turbine wear and tear, the risk of false starts, and additional monitoring costs. Moreover, there is a cost related to the loss of water as the turbines accelerate to generate electricity (Bakken and Bjorkvoll 2002). These costs are collectively referred to as start-up costs, which are incurred each time a turbine begins generating power. Consequently, these costs are commonly incorporated into the objective functions of short-term hydro scheduling optimization models (Finardi and Scuzziato 2013; Fleten and Kristoffersen 2008; Kong, Skjelbred and Fosso 2020). However, many medium- and long-term models tend to ignore these costs, as seen in for example Carpentier, Gendreau and Bastin (2013) and Cassano et al. (2021).

Hydropower Production Function

The complexity of hydropower production planning is primarily attributed to the inherent non-linearity and non-concavity of the hydropower production function (HPF). The power production is determined by the net head h, discharge q, a constant denoted as G, and the efficiency factors of both the turbine and generator in the power plant, denoted η_t and η_g respectively. Consequently, the HPF can be expressed as:

$$P = G\eta_g\eta_t hq \tag{3.1}$$

Here, the constant G encompasses the gravity constant and water density, typically set to a standard value of 9.81×10^{-3} kg·m^2/s^2 (Kong, 2020). The head changes with the reservoir's water volume, and the discharge directly impacts it. Additionally, the relationship between head and water volume is often nonlinear. Both generator and turbine efficiencies are nonlinear as well and influenced by the discharge and net head. While power producers can directly control the discharge, it affects all other variables in the HPF. The combination of these non-linear efficiency factors results in a non-convex solution space. Additionally, the HPF contains various interdependencies, further contributing to the intricate non-linear and non-convex nature of hydropower production planning. Numerous approaches have been developed to address these challenges, enabling the problem to be solved through optimization programs.

The efficiency curves of both generators and turbines are non-linear and the turbine efficiencies are additionally not monotonically increasing. This leads to a non-convex relation when multiplied in the power production function (Breton, Hachem and Hammadia 2004). To simplify this complexity, a common approach is to treat turbine efficiency as a fixed value and disregard the generator efficiency or combine it with the turbine efficiency term. This simplification ignores the effects of head and discharge on both efficiencies, sacrificing some accuracy for increased computational speed. Alternatively, a more accurate representation involves considering the turbine and generator efficiencies as a unified factor dependent solely on discharge. This is practical in short-term modeling of power plants connected to large reservoirs. That is because in these cases, the head rarely changes enough during the planning period to affect the power production, making the actual head effects minimal (Mariano et al. 2008). This is a simple and accurate way of handling the turbine efficiency in these cases, as seen in Catalão et al. (2009) and Séguin et al. (2017). It is also possible to represent the turbine efficiency by using high-order polynomials. This results in a convex problem. However, the power production function remains non-linear, necessitating the use of heuristics or non-linear solvers (Finardi and da Silva 2005). Another way to represent turbine efficiency is through a piecewise linear function (Kong, Skjelbred and Fosso 2020; Skjelbred, Kong and Fosso 2020). This method is practical, as turbine producers typically provide the

turbine efficiencies as a Hill chart or Hill diagram, making it possible to calculate turbine efficiency as sets of triplets that relate efficiency values to discharge and head. This enables the creation of breakpoints on the efficiency curves and linearization of turbine efficiency.

The influence of head and discharge in each timestep adds complexity to the HPF. The approach to addressing this issue depends on factors such as the size, shape, and time horizon of the reservoir. As mentioned earlier, reservoirs with significant storage capacity and short planning periods may reasonably assume constant head, according to Mariano et al. (2008). However, variable head should be considered for small and medium reservoirs, as well as for long-term planning of larger reservoirs (Kong, Skjelbred and Fosso 2020).

Excluding the effect of variable head from the optimization problem would fail to incentivize maintaining high water levels, which directly affects actual power production. To incorporate the incentive for a high head, the optimization model can include rewards for high water levels and penalties for low water levels in the objective function (Gjelsvik, Mo and Haugstad 2010). This method directly avoids the issues relating to variable head, allowing for a simpler production function. However, it is less accurate and increases complexity in other aspects of the model, for example in how to calculate these penalties.

Another method for handling variable head in the HPF is to approximate it using a Taylor expansion around the mean effective discharge and head. The effective discharge is a combination of turbine efficiency and discharge, allowing for dynamic variations in head and discharge while preserving linearity in the HPF (De Ladurantaye, Gendreau and Potvin 2009; Ek Fälth et al. 2022). This approximation proves especially accurate when head and discharge deviate little from their means, and it enables fast computational processing.

Varying head is not trivial to update, as mentioned earlier. This is because nature seldom exhibits reservoirs with vertical walls, which leads to non-linear gross head functions. A common way of handling this is simply by using a linear approximation of the water level trajectory, leading to a head function that is linearly updateable from the volume (Catalão et al. 2009). A more accurate method is approximating the head/volume relation as a piecewise linear function (Skjelbred, Kong and Fosso 2020).

A final way of handling the HPF is by a piecewise linearization of the entire expression. This method relies on creating breakpoints on the multi-dimensional HPF and is a common approach in the literature (Garcia-Gonzalez and Castro 2001; L.S.M. Guedes et al. 2017; Kong, Skjelbred and Fosso 2020; Tong, Zhai and Guan 2013). If the turbine efficiency has been linearized using the breakpoints computed from the Hill chart, the complete linearizarion may simply be done by just expanding these triplets. Using these triplets, it is possible to create a set of discrete points that describe the power output for net head and discharge combinations. These points can then be used as breakpoints for the linear approximation of the hydropower production function, for example by combining them with a weighting variable (Garcia-Gonzalez and Castro 2001; Kang, Guo and Wang 2017). With a piecewise approximation the accuracy of the HPF increases, but the problem becomes increasingly complex (Diniz and Maceira 2008). This is largely because of the amount of binary variables that need to be introduced in order to model the breakpoints and linear pieces between them. As a result, sophisticated solution methods are often needed when optimizing a detailed hydropower scheduling problem.

In Kang, Guo and Wang (2017), the piecewise linearization is constrained using Special Ordered Sets type 2 (SOS2) to decrease the amount of binary variables that are necessary to introduce. SOS2 were implemented by Beale and Forrest (1976) in order to make it easier to find global optimum in problems with non-linear constraints. The concept of a SOS2 set is a set in which at most two variables are allowed to be non-zero, and these must be adjacent. In Kang, Guo and Wang (2017), the SOS2 sets are used to constrain the weights that create the linear approximation of the HPF. This method was proven to be both computationally efficient and accurate (Kang, Guo and Wang 2017).

Mid- and Long-Term Models

Determining the value of the remaining water in a reservoir at the conclusion of a short-term planning period involves considering various long-term factors. This implies that to ascertain the water value for short-term hydropower scheduling, it is typically necessary to address a long-term scheduling problem. Long- and medium-term models typically optimize aggregated hydropower systems, meaning that some aspects are simplified or concatenated to make the model manageable over longer time periods. (Fosso et al. 1999) (Saad et al. 1994). Since both long- and short-term models aim to optimize power production in hydropower systems, most constraints for long-term optimization resemble those for short-term optimization. One notable distinction is however that start-up costs are often disregarded in longer-term scheduling problems, as seen in Carpentier, Gendreau and Bastin (2013), Cassano et al. (2021) and Finardi and Silva (2006).

When running a mid-term optimization to calculate the water value, the planning horizon must be set so far into the future so that the solution is not affected by the value of the remaining water at the end of the period (Flatabø et al. 1998). One common way to ensure this, is to plan to the next flood season, where the inflow is larger than the turbine max capacity over a sufficient period of time. This requires the need to open bypass gates to prevent flooding, thus any extra water at that time will not give any extra profit.

3.3 Solar Modeling

The successful integration of solar and wind energy into short-term power production planning relies heavily on the use of different forms of forecasts. These forecasts are typically considered as stochastic processes that involve a power variable, taking into account numerous physical processes and parameters. Due to the complexity and uncertainties associated with these processes, the power variable is subject to significant uncertainties (Morales et al. 2014). Both solar- and wind power share common characteristics of being intermittent and uncertain. However, in this thesis, our focus will primarily be on solar power forecasting, unless otherwise specified. Furthermore, different models exist for different time horizons, and we will specifically discuss day-ahead and intraday forecasting.

Forecasts, in general, can be seen as a form of extrapolation, where a model is fitted to historical data, assuming that the future will follow a similar pattern based on its inputs. Morales et al. (2014) categorizes forecasts into four main groups: point forecasting, probabilistic forecasting, scenarios, and event-based prediction. For the purpose of this thesis, event-based predictions will not be discussed, as their value in addressing operational problems is limited (Morales et al. 2014).

Point forecasting is the simplest category, providing a forecast at time t for a future realization at time t + k, where k represents the lead time or forecasting horizon. Point forecasting yields a single value, which can be interpreted as the most likely or average outcome. While the stochastic and deterministic versions of point forecasts are similar, the stochastic version acknowledges the uncertainty that the estimate for time t + k may not materialize. Pedro and Coimbra (2012) compare various models that do not incorporate exogenous data and find that artificial neural networks (ANNs) optimized by genetic algorithms outperform other models. Recent research in the field of PV power production planning often incorporates or revolves around the use of ANNs. These networks are powerful tools for capturing non-linear relationships between inputs and outputs but require substantial amounts of high-quality data for training purposes. In the context of forecasting, most of the ANNs reviewed for this report produce point forecasts as their output (P. Li, Zhou and Yang 2018; Munir et al. 2019; Pedro and Coimbra 2012).

The point forecasting models that do not incorporate exogenous data face challenges in capturing seasonality, which is an important aspect of PV forecasting (Pedro and Coimbra 2012). To address this limitation, Lorenz et al. (2009) discuss a clear sky model for PV production, which represents the production under the assumption of no irradiance absorption or reflection in the atmosphere. They find that the standard error of the model is primarily influenced by the standard error in the exogenous irradiance forecast. Clear sky point forecasting serves as a crucial input for more advanced models that assess the available solar resources (Antonanzas-Torres et al. 2019). Among

the most known clear sky models is Bird and Hulstroms model from 1981. They combine five tested models to create a clear sky model with a minimal number of input parameters. Although outperformed by more advanced models in a comparison of seventy clear sky models (Antonanzas-Torres et al. 2019), it remains widely used due to its accuracy compared to other simple models (Annear and Wells 2007).

In contrast to point forecasts, probabilistic forecasts provide a quantification of potential outcomes, expressing uncertainty through statistical quantiles, prediction intervals, or time-dependent probability densities. Various methods exist for generating these forecasts. Iversen, Morales et al. (2014) highlight that stochastic differential equations (SDEs) are commonly employed to create probabilistic forecasts in wind production but have limitations in the solar domain. Their approach involves using numerical weather predictions (NWPs), or point forecasts, to construct stochastic differential equations that, through Monte Carlo simulations, quantify the uncertainty associated with the point forecasts. Their methodology follows a second-order moment representation of solar irradiance dynamics. They compare their results to more conventional approaches such as general linearized models (GLMs) (Thyregod and Madsen 2011). The SDE models outperform the best GLM, although GLMs require less data input for model construction.

Probabilistic forecasts provide insights into the marginal densities of predictions at each lead time. However, operational problems may lose important information when utilizing these forecasts as inputs. Morales et al. (2014) emphasizes that probabilistic forecasts disregard all spatio-temporal dependencies, which are crucial aspects that can be captured through scenario forecasts.

Scenario forecasts appear as point forecasts. They do, however, capture the uncertainty expressed by probabilistic forecasts while respecting the interdependence structure of prediction errors through the different scenarios, something single point forecasts do not (Pinson et al. 2009).

Various approaches exist for generating scenarios. Generally, a procedure is employed to discretize the continuously evolving stochastic parameter. This procedure can involve sampling, construction, or reduction techniques (King and Wallace 2012). Similar to probabilistic forecasts, ANNs play a prominent role in scenario generation research. Vagropoulos et al. (2016) present an approach that has been widely adopted in subsequent publications. They utilize historical NWPs and weather data to train an ANN for generating a point forecast. Scenarios are constructed around the point forecast, and reduction techniques are then applied to generate the final set of scenarios.

Alternative approaches to scenario generation extend beyond the realm of ANNs. Iversen and Pinson (2016) consider stochastic variables for each timestep as points from a multivariate normal distribution. They construct multivariate normals through quantile regression in the spatio-temporal domain. Scenarios are constructed using a technique called copula estimation. Pinson et al. (2009) also employ similar techniques in scenario generation but do not incorporate the spatial domain. Staid et al. (2017) calculate cumulative distribution functions (CDF) and utilize path-dependent cut points at each timestep to generate realizations from the inverse CDF. When comparing their method to scenarios generated by treating the stochastic forecast as a multivariate normal distribution, they find that their approach performs better. A similar technique is employed by Rios, Wets and Woodruff (2015) in their scenario generation. Here, uniformly distributed variables at each timestep are used instead of cut points. This simpler technique is based on sampling, and the interdependency is captured by weighting the hourly uniform variables with the temporal error correlation coefficient. After generating N number of scenarios, they use a reduction methodology described in Eichhorn, Heitsch and Roemisch (2010) to reduce the number of scenarios. All the reviewed papers incorporate NWPs and observed realizations as inputs to their models.

3.4 Solar Power Estimation

Irradiance forecasts or scenarios are not directly translatable to solar power generation, as the irradiance conversion factor is not constant. It depends on, among other factors, temperature, wind and the angle of the PV cell (Huld, Šúri and Dunlop 2008). All PV cells are tested under standardized testing conditions to give a rating of the technologies nominal efficiency. The power produced is a product of the voltage and the current the PV cell is able to deliver, given the

exogenous variables. Huld, Šúri and Dunlop (2008) proposes a simplified model to calculate the power produced under various conditions. They introduce PV technology specific constants based on tests conducted in standardized conditions. In their model, the PV cell's relative temperature is an important input. There are several ways of calculating this temperature, but the European Commission suggests a model proposed by Faiman (2008), taking wind, air temperature, irradiance and technology specific constants into account (European Commission 2022). The model by Huld, Šúri and Dunlop (2008) does not take into account degrading of cells or weather phenomena like snow or dust covering the PV equipment.

3.5 Stochastic Programming

Stochastic programming is a term denoting optimization methods that involve some form of uncertainty. For the case where one has to make a present day, permanent decision based on future uncertainties, a two-stage or multi-stage stochastic optimization program is reasonable (Kall and Wallace 1994). A two-stage stochastic program is a program where a decision is made in the first stage based on a future with one or several uncertain factors. In the second stage, the value of these factors are realized and recourse decisions are made. Modeling a stochastic hydropower scheduling problem with a two-stage stochastic model is well-reputed, especially in cases with liberalized day-ahead markets (Beltrán, Finardi and de Oliveira 2021; Fleten and Kristoffersen 2007; Wallace and Fleten 2003).

In most two-stage stochastic models, several possible futures are evaluated in order to allow the model to plan with flexibility (Wallace and Fleten 2003). These possible futures represented as discretized realizations of the stochastic variables, called scenarios. Since the second-stage decisions are made after the scenarios occur, they enable flexibility to be modeled in the stochastic program. If the model is evaluated over several scenarios, the room for flexibility is increased as the model gains information about several possible futures. This makes flexibility more valuable than if the model is only presented with one possible future, for example the expected value of the stochastic variables. This included flexibility implies that the two-stage stochastic model with several scenarios will have a worse objective function than a deterministic model before the future is realized. Additionally, in instances where the single-point prediction and actual outcome are in agreement, the scenario based model will seem worse than the deterministic. This is because the flexibility included in the scenario-based model comes at a cost. This cost will never be included in a deterministic model, making it seem better than it is when only looking at the objective function value (Wallace and Fleten 2003).

Deterministic Equivalent

The canonical formulation of a two-stage stochastic optimization problem is

$$\begin{aligned} min \quad & c^\top x + d^\top y \\ s.t \quad & Ax \geq b \\ & Wy \geq h - Tx \\ & x, y \geq 0 \end{aligned} \tag{3.2}$$

where x is the first-stage decision and y is the stochastic second-stage stochastic variable. To be able to make a first-stage decision which takes the stochastic nature of the second-stage variable into account, we introduce a set $\mathcal{S}$ of S different scenarios. This allows us to extend the model to sum over S different realizations of the stochastic second stage variable y, with π_s being the probability that scenario $s \in \mathcal{S}$ realizes. We thus get the new formulation

$$
\begin{aligned}
min \quad & c^\top x + \sum_{s \in \mathcal{S}} \pi_s d^\top y_s \\
s.t \quad & Ax \geq b \\
& W y_s \geq h - Tx \quad \forall s \in \mathcal{S} \\
& x, y \geq 0
\end{aligned}
\tag{3.3}
$$

If we write this formulation in extended form, it compares to any other deterministic optimization problem, treating all y_s as a deterministic variable. This is why this formulation of a two-stage stochastic problem is commonly referred to as the *deterministic equivalent* (Wets 1974).

Even though a deterministic equivalent formulation of a problem can be solved by most commercial solvers, the problem size grows rapidly with the number of scenarios introduced. When the problem additionally is MILP, the computational complexity is further increased, making it nearly impossible to solve with conventional methods. To counter this rapid expansion, several decomposition approaches and methods have been proposed.

Stage decomposition

Stage decomposition methods are methods where the stochastic problem is split into first-stage and second-stage problems. In this approach, the first-stage solution $\hat{x}$ is produced by a master problem and the second-stage problem, called the scenario subproblem, is then solved with the first-stage solution fixed (Sherali and Zhu 2009). Several methods have been proposed in order to solve these problems. One common approach is a version of Benders' Decomposition method, more often referred to as the L-shaped method in stochastic optimization (Rahmaniani et al. 2017). Benders' decomposition was first described in Benders (1962), while the L-shaped method was described a few years later in Van Slyke and Wets (1969)

L-Shaped

The L-shaped method is a stage decomposition method used to solve complex two-stage problems. The L-shaped decomposition is essentially the same as Benders' decomposition applied to stochastic problems (Van Slyke and Wets 1969). Both methods are based on fixing complicating variables and solving the rest of the problem with these values fixed. Dual information about this solution is then used to update both the feasibility and the optimality of the fixed variables in an iterative process (Benders 1962; Van Slyke and Wets 1969). The standard L-shaped decomposition is designed for *recourse problems*, meaning problems with second-stage decisions, where both first-stage variables and second-stage variables are continuous (Laporte and Louveaux 1993). A recourse problem is on the following form:

$$
\begin{aligned}
& min \quad c^T x + Q(x) \\
& s.t. \quad Ax = b, \quad x \geq 0
\end{aligned}
$$

where

$$
Q(x) = \sum_{s \in \mathcal{S}} \pi_s (Q(x, \xi_s))
\tag{3.4}
$$

and

$$
Q(x, \xi) = min\{q(\xi) y : W(\xi)\, y = h(\xi) - T(\xi)\, x, y \geq 0\}
$$

$Q(x, \xi)$ called the *recourse function*. Here, x is a deterministic first-stage decision value, while ξ is a stochastic factor with S discrete realizations. As mentioned, the method is based on iteratively updating feasibility- and optimality cuts based on the dual variables of the optimized recourse function over all possible scenarios. Mathematically, we solve the a master problem on the following form:

$$
\begin{aligned}
&min \quad c^T x + \theta \\
&s.t. \quad Ax = b, \quad x \geq 0 \\
&\theta \geq Q(x) \\
&x \geq 0
\end{aligned}
\tag{3.5}
$$

where as before

$$Q(x) = \sum_{s \in \mathcal{S}} \pi_s (Q(x, \xi_s))$$

and

$$Q(x, \xi) = min\{q(\xi)y : W(\xi)\, y = h(\xi) - T(\xi)\, x, y \geq 0\} \geq 0\}$$

If for every feasible first-stage solution there exists at least one feasible second-stage solution for all scenarios, then we have the problem characterstic known as *relatively complete recourse*, and there is no need for feasibility cuts. We will focus these types of problems. After solving the master problem, we get a solution x^k that is optimal with the current constraints. We now need to check if $\theta \geq Q(x^k, \xi_s)$. We do this by solving $Q(x^k, \xi_s)$. If it is, we have an optimal solution and the algorithm terminates. If not, we observe that because of strong duality we can introduce optimality cuts based on the dual of the optimal solution of the subproblem:

$$\theta \geq \sum \pi_s (\sigma_s^k)^\top (h(\xi_s) - T(\xi_s)x \tag{3.6}$$

Here, σ_s^k is a vector of the duals of the optimal solution of the subproblems for all scenarios s, given the current first stage solution x^k. These are essentially Benders' type optimality cuts and are commonly added to the problem on the following form

$$\beta_k x + \theta \geq \alpha_k \tag{3.7}$$

where $\beta_k = \sum_{s \in \mathcal{S}} \pi_s (\sigma_s^k)^\top T(\xi_s)$ and $\alpha_k = \sum_{s \in \mathcal{S}} \pi_s (\sigma_s^k)^\top h(\xi_s)$. This means that the method finds the optimal decision of the second-stage problem $\hat{y}$, given a first-stage solution $\hat{x}$. Since the optimality cuts are based on dual information, this implies that the subproblem must be LP and convex for all scenarios in order to use the L-shaped. If this is not the case, the dual values may not be well-defined which yields the cuts useless. In these cases, the method does not guarantee solutions in finite time (Laporte and Louveaux 1993). There exists L-shaped methods that are modified to work for problems with different structures, for example integer recourse (Carøe and Tind 1998). We will not elaborate further on these.

Scenario decomposition

Another way of decomposing the problem is scenario-wise. The only relation between the second-stage problems is through the first stage solution. Suppose we have a set $\mathcal{S}$ of scenarios. By creating first stage variables $x_1, x_2, ..., x_s$ for each scenario $s \in \mathcal{S}$ and forcing these to be equal in what is called a non-anticipativity condition, $x_1 = x_2 = x_3 = ... = x_s$, we can create a block-angular structure for the two-stage problem. Carøe and Schultz (1999) propose using a Lagrangian relaxation on this non-anticipativity constraint, effectively creating independent second-stage solutions that can be solved in parallel. Their method is based on using the Lagrangian dual as a lower bound in a branch and bound process. The first-stage solutions that do not fulfill the integer requirement are rounded to an integer value, and then branched on based on this rounding. This algorithm is finitely convergent if the feasible area of x is bounded and the x-variables are purely integer restricted.

Disjunctive decomposition

In programs where there are integrality or binary constraints in both stages of the problem, stage decomposition or scenario decomposition alone may not suffice. With discrete values in the second-stage problem, the expected recourse function becomes non-convex and in general not even continuous (Küçükyavuz and Sen 2017). This makes approximating the expected recourse value challenging, as one can no longer utilize approximations deriving from the LP dual of the subproblem. When solving problems with challenging characteristics, utilizing specialized algorithms that exploit the concrete problem structure is generally a good idea.

Ntaimo and Sen (2007) has developed a Branch-and-Cut algorithm for two-stage stochastic mixed integer programs with continuous first stage variables and mixed-binary second stage variables. This method branches on the continuous first stage variables while the branching is guided by valid inequalities computed for the second-stage problem. These cuts are generated by a Disjunctive Decomposition (D2) algorithm, which is a core part of this branch-and-cut method.

Disjunctive Decomposition is a class of methods developed by Sen and Higle (2005) and is based on the theory of disjunctive programming. Disjunctive programming is in short a line of work that studies the convex hull of a solution space that is composed of several disjunctive sets. These disjunctive sets can for example represent different scenarios or different variable configurations. This convexification is also what the main part of the D2 algorithm is about. The purpose of D2 is to sequentially convexify and build an approximation of the convex hull of the second-stage problem so that the LP relaxation of the second-stage problem can be solved. This convex hull contains all the disjunctive sets. Information about the approximation of the subproblem is then passed to the master problem in the form of Benders' type optimality cuts and updated lower bounds, which leads to an updated optimal value. This happens iteratively until an optimal solution is found. This convexification makes it possible to solve large scale two-stage MILP-problems, especially problems where the subproblem is challenging and computationally expensive to solve (Sen and Higle 2005).

The convexification process of the subproblem is done by creating *disjunctive cuts*. After solving the LP-relaxation of the subproblem, variables that violate their binary constraints are identified and one of them are selected as the *disjunction variable*. Two new disjunctive set are then created, one where the disjunction variable is zero and one where it is one. A new problem is then introduced with the purpose of creating a cut for the union of these sets. This cut is called a disjunctive cut, and is essentially a Lift-and-Project cut, as described in Balas, Ceria and Cornuéjols (1993). The purpose of this disjunctive cut is to cut away the fractional solution of the binary variable, only allowing it to take on binary values while still solving the LP relaxation (Balas, Ceria and Cornuéjols 1993). By iteratively creating disjunctive cuts that cut away one and one fractional solution, a convex approximation of the binary solution space is concieved. This allows us to solve the LP-relaxation of the complex subproblem while keeping the solutions feasible for the non-relaxed problem.

Since the scenario subproblem will be different for different scenarios and different first-stage values, convexification and relaxation of all these different problems may be cumbersome. The convexification process in the D2 algorithm is therefore done by creating disjunctive cuts that holds for all scenarios and all first-stage values. This is possible because of the C3 theorem (Sen and Higle 2005). The general idea of the C3 theorem is that it is possible to translate a cut that is valid for a pair of a first-stage solution and a scenario, $\bar{x}$ and $\bar{\omega}$, into a cut that is valid for all pairs of x and ω. This allows for convexification of the second-stage problem for all scenarios and first-stage solutions, leading to general cuts that can be added to the subproblem. Since these cuts depend on both the first stage solution and the scenarios, the D2 can be said to be both a stage wise and scenario wise decomposition.

4 Problem Description

This problem concerns the short-term power production scheduling of a hybrid hydro-solar power plant located in Guinea. This specific power plant is in development by Scatec, a Norwegian listed company, and was presented to us as a case study through Scatec's cooperations with SINTEF and NTNU. The problem revolves around scheduling the hydropower production combined with the stochastic solar power production so that a load requirement is met. Both these problems are stochastic in nature, where the capacity of the hydropower production is dependent on the natural inflow to the reservoirs and the solar power production is dependent on the irradiance from sunlight on its solar panels.

There is no power market in Guinea. The power is supplied under a Power Purchasing Agreement (PPA), determining load and price requirements. The PPA in this case study is based assumptions made by Scatec, based on their conversations with the local authorities in Guinea. It is assumed that the power plants will get a fixed price for power sold in the time periods during the day where the need for power is greatest. These periods are denoted peak periods. The power plant has to deliver the same amount of power during all these hours, which are typically from 07:00 to 22:00. This is the peak load commitment. All power produced in excess of the load commitment is sold at a significantly lower price, called the intermittent price. Finally, the power produced outside of the peak hours, called the off-peak hours, is sold at an off-peak price, which is lower than the peak price but higher than the intermittent price.

Further, we assume that the PPA works in a way that lets the power plants control their own supply during the peak periods. The power plants report their production capacity day-ahead, and they have to deliver according to this load commitment. If the power plants under-deliver according to their load commitment, it is assumed that they must pay a penalty cost for each unit of under-delivered power.

In this thesis we will focus on the short-term scheduling of the hybrid power plant. As the PPA is assumed to involve day-ahead nominations, a natural time horizon is one day. This means that the problem will concern how much power the producer is able to nominate day-ahead, based on the solar forecasts and the water level in the reservoir. In other words, the problem has a two-stage structure. Firstly, the decision on the day-ahead commitment is made. This decision is made before the power plant has certain knowledge of the solar power generation the following day. The following day the power plant has to produce power in order to fulfill its load obligation. This is the second stage of the problem. Here, the solar power generation is realized, and the power plant has to decide when it wants to generate hydropower and when it wants to only supply solar power based on this realization.

The hydropower plant in this thesis consists of two reservoirs in cascade. Both reservoirs are connected to one power plant each, and each of these power plants have two turbines. The turbines in each power plant are identical and situated at the same height. This means that the power plant head value is equal for both turbines in the same power plant. The turbines are connected to the reservoirs through the same penstock, but it is still possible to control how much water is discharged to each turbine through valves. This means that it is possible to have one idle and one active turbine in the same power plant.

As the power plants are connected in cascade, the water discharged from the top reservoir will become inflow to the bottom reservoir. Both reservoirs also have natural inflow. If overflow of the top reservoir occurs, this water will not be usable in the bottom reservoir. It is consequently only controlled discharge from the top reservoir that is reusable water.

The PV-panels connected to the power plant are not connected to any batteries. It is not possible to pump water from the lower reservoir to the higher reservoir, a characteristic that is called pumped-storage hydro. Consequently, there are no possibilities of storing solar power. Solar power is, however, easy to curtail. This way, if the PV power generation is higher than the grid capacity, this electricity can be curtailed.

In order to perform short-term scheduling optimization of a power plant, it is necessary to know the alternative cost of discharging water. Since the actual power plant is not yet built, there is

no current data on historical fill level during different times of the year. The same is the case for the water value. In order to find these values it is necessary to build a medium-term hybrid optimization model. This model finds the water value in each reservoir based on a two-year cycle of the production plant. It also finds the initial reservoirs water volume in each planning period, which is necessary in our case study since the reservoir is not yet built. If the reservoir had been built, the water level could simply be measured before the planning starts. In order to simplify the mid-term problem, it is assumed that the hydro-reservoirs are completely filled during the rainy season in Guinea, leading to a natural reset of the water value. This natural reset occurs because there is a large chance of flooding during the rainy season, which would lead to a water value of zero.

5 Mathematical Models

In this section, the mathematical model for the day-ahead power planning as well as the mid-term model will be introduced. Firstly, we will present and explain different modelling choices and assumptions made in both the short-term and the mid-term model. Then, both models will be presented in full, with the necessary explanations of both constraints and objective functions.

Both the short-term and the mid-term model are extensions of models created in Nore and Winther (2022). Therefore, some similarities, especially in the nomenclature, will occur.

5.1 Modelling choices

Several modelling choices have been made in order to represent hybrid power production plant as accurately as possible. These choices are made based on the most fitting approaches from the literature. The choices are mostly tied to the hydropower production, as solar power modelling is mostly tied to scenario generation which will be explained in Section 6.

As per the work of M. Deshmukh and S. Deshmukh (2008), the individual components of the hybrid power system has been modeled separately before being combined in the optimization model.

Hydropower Modeling

The hydropower scheduling problem has been modeled with a short-term and a mid-term model. Both the mid-term and the short-term have been modeled with full detail, meaning that they are modeled with reservoirs in cascade with respective power plants and generating units. Recall from Section 3.2 that a generating unit is the term for the combination of a turbine and the generator this is connected to. In our model we include the generator efficiency in the turbine efficiency term, meaning that we often address these two entities as one, i.e., a generating unit. Water inflow is viewed as a deterministic parameter both models. For the short-term model it is easy to predict inflow accurately from day to day, making it sufficiently accurate to represent this as deterministic. Regarding the mid-term, we have observed from data that the inflow changes little from year to year in the same seasons. For simplicity, we have kept inflow deterministic in this model as well. This choice is addressed in Section 7.4.

There are different demands in accuracy for the short and mid-term, leading to some simplifications in the mid-term model. These will be explained later in this section. Both models contain the non-linear and non-convex hydropower production function, as well as the relationship between volume and head values. How we handle these non-linearities will be explained in Section 6, and they are merely introduced as functions in this section.

Solar Power Modeling

The solar power generation in this problem is simply represented by two factors; ξ_t, representing the amount of power produced by the PV panels during the current timestep, and ξ_t^{CURT}, representing any excess power generated that is not sent into the grid. This representation is due to the fact that solar power has no inherent storage capacity, and that power producers cannot increase the amount of solar power generated. Additionally, since the marginal cost of solar power is close to zero, there is no need to optimize solar production further, and it is instead included as a stochastic term in the total power produced.

5.2 Short-Term Model

Time Horizon

The problem we are modelling is a short-term production planning problem. Therefore, the chosen time horizon is one day, with the peak and off-peak periods included in this day. The time sets do however contain two days, and the model is run over 48 hours. Even though we are only really interested in the next 24 hours, we run it for twice as long to incentivise scheduling that takes the following day into account. Since the HPF is dependent on head, keeping the water volume high will allow for more power output per unit of water. A model that does not plan any timesteps into the future might be incentivised to discharge more water than what is optimal in the final timesteps, lowering the head and compromising the production the next day. However, as we are not interested in the actual schedule from day two, the peak and off-peak commitment constraint for this period is relaxed. Therefore, we have four time set in the nomenclature; one set for all timesteps, one set for each day, one set for peak, and one set for off-peak periods. The peak and off-peak periods only contain timesteps in the first day.

An additional note regarding the nomenclature is the overlapping generating unit sets, $\mathcal{K}$ and $\mathcal{K}_r$. In total, these contain the same generating units, but in $\mathcal{K}_r$ they are tied to respective reservoirs. This is done in order to make the model more understandable and easier to read.

Nomenclature

Sets and Indices

$\mathcal{R}$	-	set of reservoirs, index $r \in \mathcal{R}$
$\mathcal{K}$	-	set of power generating units, index $k \in \mathcal{K}$
$\mathcal{K}_r$	-	set of power generating units connected to reservoir r, index $k \in \mathcal{K}_r$
$\mathcal{T}$	-	set of timesteps in the planning period, index $t \in \mathcal{T}$
$\mathcal{T}_d$	-	set of timesteps in the days of the planning horizon, index $t \in \mathcal{T}_d$. $d \in \{1, 2\}$
$\hat{\mathcal{T}}$	-	set of peak period timesteps in the planning horizon, index $t \in \hat{\mathcal{T}}$, $\hat{\mathcal{T}} \subset \mathcal{T}_1$
$\tilde{\mathcal{T}}$	-	set of off-peak period timesteps in the planning horizon, index $t \in \tilde{\mathcal{T}}$, $\tilde{\mathcal{T}} \subset \mathcal{T}_1$

Parameters

P_t	-	power selling price at timestep t (\$/MWh)
P^I	-	intermittent power selling price (\$/MWh)
C^U	-	penalty cost of not meeting load commitment (\$/MWh)
C_k^S	-	start-up cost of generating unit k (\$)
V_r^{MIN}, V_r^{MAX}	-	minimum and maximum water volume in reservoir r (m^3)
Q_r^{MIN}	-	environmental restriction on minimum water discharge from reservoir r (m^3/h)
Q_k^{MIN}, Q_k^{MAX}	-	minimum and maximum amount of water dischargeable to unit k (m^3/h)
D^{MAX}	-	grid capacity (MW)
ξ_t	-	solar power production in timestep t (MWh)
$\delta_{k,0}$	-	input status for generating unit k (bin)
ϕ_r	-	water value in reservoir r at end of planning horizon (\$/m^3)
V_r^{INIT}	-	water volume in reservoir r at start of planning horizon (m^3)
$Q_{r,t}^{NI}$	-	natural inflow to reservoir r in timestep t (m^3/h)

Variables

$v_{r,t}$	-	water volume in reservoir r in timestep t (m^3)
$q_{k,t}$	-	water discharge to unit k in timestep t (m^3)
$h_{r,t}$	-	net head level in reservoir r in timestep t (m)
$h^G_{r,t}$	-	gross head level in reservoir r in timestep t (m)
$q^{BP}_{r,t}$	-	controlled water spillage through bypass gate in reservoir r in timestep t (m^3)
$q^{OF}_{r,t}$	-	water overflow in reservoir r in time t (m^3)
$q^{TOT}_{r,t}$	-	total regulated water discharge from reservoir r at time t (m^3)
$\delta_{k,t}$	-	status of unit k in timestep t (bin)
$\lambda_{k,t}$	-	status change of production at plant k in timestep t (bin)
ξ^{CURT}_t	-	excess solar power in time t (MWh)
$p_{k,t}$	-	hydropower production at unit k in timestep t (MWh)
p^U_t	-	total unfulfilled commitment based on the load commitment in timestep t (MWh)
p^I_t	-	total amount of power delivered in excess of the load commitment in timestep t (MWh)
x_t	-	firm power commitment in timestep t (MWh)
x^P	-	firm power commitment in the peak period (MWh)
x^O	-	firm power commitment in the off-peak period (MWh)

Functions

$h^G_r(v_{r,t})$	-	gross head of reservoir r at timestep t (m)
$h_r(h^G_{r,t}, q_{k,t})$	-	net head for the power plant in reservoir r in timestep t (MWh)
$p_k(h_{r,t}, q_{k,t})$	-	hydropower production function for unit k in timestep t (MWh)

Objective Function

The objective of this hybrid power system production problem is to deliver according to the load commitment in the PPA while minimizing costs. The most prevalent costs in hydropower production are the alternative cost of using water during the time horizon, the start-up costs and the costs of not delivering according to the load commitment. The alternative cost of discharged water is found by multiplying the marginal water value at the end of the planning period ϕ_r with the value of amount of water used during the planning period for each reservoir, $V^{INIT}_r - v_{r,T}$, where T is the final timestep of the planning period. Water value in $\$/m^3$ multiplied by the change in water volume in m^3 leads to a term in \$.

$$\sum_{r \in \mathcal{R}} \phi_r (V^{INIT}_r - v_{r,T}) \tag{5.1}$$

All the costs of starting and stopping a generating unit are combined in a single term C^S_k which is in \$. This is assumed to be identical for all generating units. The term is multiplied with the amount of times each generator starts during the planning period, yielding

$$\sum_{t \in \mathcal{T}} \sum_{k \in \mathcal{K}} C^S_k \lambda_{k,t} \tag{5.2}$$

The penalty of not delivering according to the load commitment is given by the total unfulfilled commitment based on the load commitment in each timestep multiplied with the unit penalty cost. The penalty cost is in \$/MWh and the unfulfilled commtiment is in MWh

$$\sum_{t \in \mathcal{T}} C^U p^U_t \tag{5.3}$$

The power system sell the power in accordance with the PPA. Power can be sold on both intermittent price and the regular selling price for each hour, which is either the peak price or the off-peak

price depending on the timestep. The intermittent price is the same for all timesteps. Both prices are in \$/MWh and both the unit commitment and the intermittent production is in MWh.

$$\sum_{t \in \mathcal{T}} (P_t x_t + P^I p_t^I) \tag{5.4}$$

The sum of all these terms make up the objective function. As all terms are in \$, so is the objective function. The problem is formulated to minimize costs, which means that the earnings have a negative sign and the costs a positive sign.

$$min \quad \sum_{r \in \mathcal{R}} \phi_r (V_r^{INIT} - v_{r,T}) + \sum_{t \in \mathcal{T}} \sum_{k \in \mathcal{K}} C_k^S \lambda_{k,t} + \sum_{t \in \mathcal{T}} C^U p_t^U - \sum_{t \in \mathcal{T}} (P_t x_t + P_t^I p_t^I) \tag{5.5}$$

Constraints

The first four constraints concern the water flow in the reservoirs. Constraint (5.6) initializes the water level in each of the reservoirs with the value given by the starting state.

$$v_{r,1} = V_r^{INIT}, \quad r \in \mathcal{R} \tag{5.6}$$

Constraint (5.7) models the amount of water in each reservoir at the start of each timestep. This is done by adding flow of water to the water volume in the previous timestep, $v_{r,t-1}$. The flow into a reservoir is given by the natural inflow, $Q_{r,t-1}^{NI}$, and the total discharge from the reservoir directly upstream, $q_{r+1,t-1}^{TOT}$. The flow out of a reservoir is given by the total discharge from the reservoir, $q_{r,t-1}^{TOT}$ as well as the possible overflow, $q_{r,t-1}^{OF}$.

$$v_{r,t} = v_{r,t-1} + Q_{r,t-1}^{NI} + q_{r+1,t-1}^{TOT} - q_{r,t-1}^{TOT} - q_{r,t-1}^{OF}, \quad r \in \mathcal{R}, t \in \mathcal{T} \backslash \{1\} \tag{5.7}$$

For the reservoirs at the top of the cascade, R, the total discharge of upstream reservoirs will naturally be zero, modeled by Constraint (5.8).

$$q_{R+1,t}^{TOT} = 0, \quad t \in \mathcal{T} \tag{5.8}$$

The overflow variable $q_{r,t}^{OF}$ is introduced in order to allow the mathematical model to operate in the unlikely event that there is so much inflow that the max volume restriction is broken and the plant is unable to handle this by increasing total discharge. The overflow leads to unused water that cannot be used downstream, which means that the model will always try to minimize this variable. The overflow restriction says that overflow must be more than the total amount of water in the timestep, subtracted by the highest regulated volume V_r^{MAX}. The total amount of water in the reservoir in this timestep is given by the current water volume $v_{r,t}$ plus the total inflow $Q_{r,t}^{NI} + q_{r+1,t}^{TOT}$ minus the total regulated outflow $q_{r,t}^{TOT}$,

$$q_{r,t}^{OF} \geq v_{r,t} + Q_{r,t}^{NI} + q_{r+1,t}^{TOT} - q_{r,t}^{TOT} - V_r^{MAX}, \quad r \in \mathcal{R}, t \in \mathcal{T} \tag{5.9}$$

Constraint (5.10) keeps the water volume in each reservoir between the highest and lowest regulated levels.

$$V_r^{MIN} \leq v_{r,t} \leq V_r^{MAX}, \quad r \in \mathcal{R}, t \in \mathcal{T} \tag{5.10}$$

The total discharge is given by the discharge to each turbine connected to the power plant in each reservoir $q_{k,t}$, as well as the discharge through the bypass gate connected to each reservoir, $q_{r,t}^{BP}$. There is only one power plant connected to each reservoir.

$$q_{r,t}^{TOTAL} = \sum_{k \in \mathcal{K}_r} q_{k,t} + q_{r,t}^{BP}, \quad r \in \mathcal{R}, t \in \mathcal{T} \tag{5.11}$$

Environmental restrictions may force the hydropower system to discharge a certain amount of water at all times, which is modeled in Constraint (5.12)

$$Q_r^{MIN} \leq q_{r,t}^{TOT}, \quad r \in \mathcal{R}, t \in \mathcal{T} \tag{5.12}$$

Each turbine has a maximum capacity Q_k^{MAX} before it is unable to handle more water. In addition, a turbine needs a certain amount of water Q_k^{MIN} to start up and can only produce power above this level.

$$Q_k^{MIN} \delta_{k,t} \leq q_{k,t} \leq Q_k^{MAX} \delta_{k,t}, \quad k \in \mathcal{K}, t \in \mathcal{T} \tag{5.13}$$

In many hydropower models, there is a constraint is similar to the minimum and maximum discharge that limits the power production in an interval between minimum power and maximum power. This often comes in addition to the discharge constraint. However, in our case the minimum and maximum power production capacity is less constraining than the minimum and maximum discharge, meaning that this constraint is redundant in this model.

The bypass discharge does not produce power, and is therefore only limited by the size of the bypass tunnel, Q_r^{BP}.

$$q_{r,t}^{BP} \leq Q_r^{BP}, \quad r \in \mathcal{R}, t \in \mathcal{T} \tag{5.14}$$

The gross head level $h_{r,t}^G$ is a function of the water level in the reservoir at the current timestep $v_{r,t}$, as well as the maximum of the water level in the reservoir directly below or the outlet line height. In our case, the outlet line is higher than the maximum regulated water level below for both reservoirs, meaning that this part is a constant. Therefore, the gross head level is only dependent on the volume of the current reservoir.

$$h_{r,t}^G = h_r^G(v_{r,t}), \quad r \in \mathcal{R}, t \in \mathcal{T} \tag{5.15}$$

To keep the net head of a power plant, $h_{r,t}$, as accurate as possible, we model this as a function of both the gross head and the discharge to each turbine in the power plant, $q_{k,t}$. Therefore, it cannot be directly computed from the water volume alone, and we therefore need this in its own expression.

$$h_{r,t} = h_r(h_{r,t}^G, q_{k,t}) \quad r \in \mathcal{R}, k \in \mathcal{K}_r, t \in \mathcal{T} \tag{5.16}$$

The hydropower production function is a complex multivariate relation that depends on both net head and discharge. The turbine efficiency curves combined with the varying net head values and discharge values creates a non-linear, non-convex expression. Here, the power production $p_{k,t}$ is represented as a function.

$$p_{k,t} = p(h_{r,t}, q_{k,t}), \quad r \in \mathcal{R}, k \in \mathcal{K}_r, t \in \mathcal{T} \tag{5.17}$$

How we handle the production function, the non-linear relationship between gross head and volume as well as the linearization of the net head function will be explained in detail in Section 6.

In order to model the start-up costs, Constraint (5.18) gives λ_{kt} the value of 1 whenever a generating unit switches state from idle to active production.

$$\lambda_{k,t} \geq \delta_{k,t} - \delta_{k,t-1}, \quad k \in \mathcal{K}, t \in \mathcal{T} \tag{5.18}$$

The power balance constraint, Constraint (5.19), captures the quantity of power supplied in each timestep. On the left-hand side, it represents the solar power generation ξ_t, hydropower generation $p_{k,t}$, and the amount of power under-delivered according to the load commitment, p_t^U. The inclusion of p_t^U allows the model to plan to under-deliver if it is advantageous to pay the penalty cost instead of generating additional power. Moreover, it ensures the feasibility of power balance when running the model.

The right side of the equation comprises the load obligation x_t, the power produced in excess of the load commitment p_t^I, and the solar curtailment ξ_t^{CURT}. ξ_t^{CURT} is introduced to guarantee feasible solutions when solar production exceeds the capacity of the power grid, necessitating the curtailment of solar power. The existence of p_t^I arises due to the assumed conditions of the Power Purchase Agreement (PPA), where the hybrid power system is obliged to supply a consistent amount of power during all peak hours. However, solar production can vary significantly during these hours, possibly creating a profitable scenario to commit to a lower power output and only sell the excess solar power at the intermittent price.

$$\xi_t + \sum_{k \in \mathcal{K}} p_{k,t} + p_t^U = x_t + p_t^I + \xi_t^{CURT}, \quad t \in \mathcal{T} \tag{5.19}$$

The unit commitment must be equal in all timesteps in the peak period and similarly in the off-peak. We model this by introducing the variables x^P and x^O, which are the load obligations for the peak and off-peak periods respectively. As mentioned earlier, these are not included in the second day

$$x_t = x^P, \quad t \in \hat{\mathcal{T}} \tag{5.20}$$

$$x_t = x^O, \quad t \in \tilde{\mathcal{T}} \tag{5.21}$$

The total amount of power supplied cannot be greater than the capacity of the outline power grid.

$$x_t + p_t^I \leq D^{MAX}, \quad t \in \mathcal{T} \tag{5.22}$$

Finally, the binary nature of $\lambda_{k,t}$ and $\delta_{k,t}$ as well as the non-negativity of the other decision variables is declared

$$\lambda_{k,t}, \delta_{k,t} \in \{0, 1\}, \quad k \in \mathcal{K}, t \in \mathcal{T} \tag{5.23}$$

$$p_{k,t}, q_{k,t} \geq 0, \quad k \in \mathcal{K}, t \in \mathcal{T} \tag{5.24}$$

$$q_{r,t}^{BP}, q_{r,t}^{TOT}, q_{r,t}^{OF}, v_{r,t}, h_{r,t}^G, h_{r,t} \geq 0, \quad r \in \mathcal{R}, t \in \mathcal{T} \tag{5.25}$$

$$\xi_t^{CURT}, p_t^I, p_t^U, x_t \geq 0, \quad t \in \mathcal{T} \tag{5.26}$$

$$x^O, x^P \geq 0 \tag{5.27}$$

5.3 Mid-Term Model

In this section we will explain the mid-term model. This model has the purpose of finding the water value for each short-term planning period. Different purpose combined with a longer time horizon means that there is less need for high accuracy in the mid-term model, which makes it possible to make some simplifications compared to the short-term. Consequently it is appropriate with changes to some of the modelling aspects. However, the mid-term does share several similarities with the short-term, as it is built with this as a basis. Therefore, only new aspects will be explained while we will refer to Section 5.2 for aspects that are identical in the short-term.

The most important differences between the mid-term and short-term model lie in the functions for head values and power production. Similar to the short-term, these will be explained in Section 6. Additionally, while the short-term model plans with stochastic PV power generation, this is deterministic in the mid-term model. As the mid-term models' purpose is finding the water value, stochastic PV power generation is unnecessary. The rest of the mid-term model will be presented with a brief explanation of the aspects that differ from the short-term model.

Nomenclature

Sets and Indices

$\mathcal{R}$	-	set of reservoirs, index $r \in \mathcal{R}$
$\mathcal{K}$	-	set of power generating units, index $k \in \mathcal{K}$
$\mathcal{K}_r$	-	set of power generating units connected to reservoir r, index $k \in \mathcal{K}_r$
$\mathcal{T}$	-	set of timesteps in planning horizon, index $t \in \mathcal{T}$

Parameters

P_t	-	power selling price at timestep t (\$/MWh)
P^I	-	intermittent power selling price (\$/MWh)
C^U	-	penalty cost of not meeting load commitment (\$/MWh)
V_r^{MIN}, V_r^{MAX}	-	minimum and maximum water volume in reservoir r (Mm^3)
Q_r^{MIN}	-	environmental restriction on minimum water discharge from reservoir r (Mm^3/day)
Q_k^{MAX}	-	maximum amount of water dischargeable to unit k (Mm^3/day)
D^{MAX}	-	grid capacity (MW)
ξ_t	-	solar power production in timestep t (MWh)
V_r^{INIT}	-	water volume in reservoir r at start of planning horizon (Mm^3)
$Q_{r,t}^{NI}$	-	natural inflow to reservoir r in timestep t (Mm^3)

Variables

$v_{r,t}$	-	water volume in reservoir r in timestep t (Mm^3)
$h_{r,t}$	-	net head level in reservoir r in timestep t (m)
$q_{k,t}$	-	water discharge to unit k in timestep t (Mm^3)
$q_{r,t}^{BP}$	-	controlled water spillage through bypass gate in reservoir r in timestep t (Mm^3)
$q_{r,t}^{OF}$	-	water overflow of reservoir r in time t (Mm^3)
$q_{r,t}^{TOTAL}$	-	total regulated water discharged from reservoir r at time t (Mm^3)
ξ_t^{CURT}	-	excess solar power in time t
$p_{k,t}$	-	hydropower production at unit k in timestep t (MWh)
p_t^U	-	total unfulfilled commitment based on the load commitment in timestep t (MWh)
p_t^I	-	total amount of power delivered in excess of the load commitment in timestep t (MWh)
x_t	-	firm power commitment in timestep t (MWh)

Functions

$h_r(v_{r,t})$	-	net head for the power plant in reservoir r in timestep t. (MWh)
$p_k(h_{r,t}, q_{k,t})$	-	hydropower production function for unit k in timestep t. (MWh)

$$min \sum_{t \in \mathcal{T}} (C^U p_t^U) - \sum_{t \in \mathcal{T}} (P_t x_t + P_t^I p_t^I) \tag{5.28}$$

such that

5.6 - 5.12 , 5.14 and 5.22

$$q_{k,t} \leq Q_k^{MAX}, \quad k \in \mathcal{K}, t \in \mathcal{T} \tag{5.29}$$

$$h_{r,t} = h_r(v_{r,t}), \quad r \in \mathcal{R}, t \in \mathcal{T} \tag{5.30}$$

$$p_{k,t} = p(h_{r,t}, q_{k,t}), \quad r \in \mathcal{R}, k \in \mathcal{K}_r, t \in \mathcal{T} \tag{5.31}$$

$$p_{k,t}, q_{k,t} \geq 0, \quad k \in \mathcal{K}, t \in \mathcal{T} \tag{5.32}$$

$$q_{r,t}^{BP}, q_{r,t}^{TOTAL}, q_{r,t}^{OF}, v_{r,t}, h_{r,t} \geq 0, \quad r \in \mathcal{R}, t \in \mathcal{T} \tag{5.33}$$

$$\xi_t^{CURT}, p_t^I, p_t^U, x_t \geq 0, \quad t \in \mathcal{T} \tag{5.34}$$

Notice in the nomenclature 5.3 that there are no peak and off-peak periods in the mid-term model. This is because the model has a time horizon of two years and each timestep is one day, which removes the need for peak- and off-peak periods. Another time-related difference is the lack of water value from the model and objective function. This is because the time horizon for the mid-term is structured so that there is a natural reset of the water value at the end of the time horizon, which makes this term unnecessary.

A prominent difference is the lack of on-off and status variables for the generating units. This leads to the removal of start-up costs from the objective function, which is normal in mid- and long-term models as mentioned in Section 3.2. This in turn leads to the fact that the lower bound of discharge has been removed, in order to allow the model to not produce a timestep. This means that constraint (5.29) replaces constraint (5.13). Notice as well that there is no function relating gross head to volume. Instead, the net head values are directly dependent on the volume, meaning that there is a simplification in how the net head is calculated. This will be further explained in Section 6, along with the handling of constraint (5.31).

The removal of status variables in the mid-term model is necessary in order to allow for an LP model. This is necessary as we need to extract meaningful dual variables from the mid-term in order to find the water value. The water value is the value of having one extra unit of water in the reservoir at the end of the timestep, i.e the dual of constraint (5.7). Recall that this constraint gives the current water volume in the reservoirs, accounting for incoming and outgoing flows in the previous timestep. Finding this value is the main purposes of creating the mid-term model, making it important to create an LP mid-term. Dual values are derived from convex analysis and MILP problems are by definition not convex. In MILPs, the dual value of a constraint only makes computational sense if the constraint is binding, and it is no guarantee that constraint (5.7) will be binding. Therefore it is important to keep the mid-term LP. This also allows for shorter computational time, which enables us to solve the mid-term for a long time horizon. This is necessary in order to get an accurate water value, as mentioned in Section 3.2

6 Solution Method

The purpose of this thesis is to investigate several questions regarding hybrid hydro-solar power systems. Firstly, we want to quantify the gains of planning in hybrid as opposed to having two separate producers planning for themselves. Secondly, we want to measure the gains or costs of introducing stochasticity in the models. Finally, we want to know the importance of running the planning model precisely as opposed to some approximation or heuristic. This section will outline the details of how we have implemented the models from Section 5 and our approach for testing their performance.

To solve the two-stage stochastic MILP problems, we have implemented the D2-CBAC algorithm by Ntaimo and Sen (2007), as described in Section 3.5. This implementation has faced several issues and is therefore not included in our general solution simulations. However, it is, to the best of our knowledge, an untested approach in hydro scheduling. Thus, we include a detailed explanation of how it works and how we have implemented it. This can be found at the end of this section. In Section 7 we further explore different challenges and possible solutions, enabling future implementations to build on our experiences.

6.1 Handling of Non-Linearities in the Short-Term Model

The short-term hybrid power production planning model has three functions that complicate the solution: the hydropower production function, the volume to gross head function and the gross head to net head function. In order to solve the problem with commercial optimization solvers, these functions must be approximated. Our representation of these functions will be presented in the following subsection.

Hydropower Production Function

In order to accurately represent the hydropower production function, we have chosen to model it as a piecewise linear function as in Kang, Guo and Wang (2017). This method has been proven to be both accurate and computationally efficient, and uses SOS2 sets as described in Section 3.2. We follow the same approach as Kang, Guo and Wang (2017) in our implementation of the HPF, i.e., function (5.17).

Firstly, net head values are represented in a list with $j = 1, ..., m$ discrete values, ranging from the minimum net head value to the maximum net head value. The same is the case for discharge, which is represented in a list with $i = 1, ..., n$ values, from minimum to maximum discharge. These indeces are in sets $\mathcal{M}$ and $\mathcal{N}$ respectively. We introduce weighting variables α_j and β_i that creates linear combinations of net head and discharge. α_j and β_i are contained in SOS2 sets, one set for head weights and one set for discharge weights, with size $|\mathcal{M}|$ and $|\mathcal{N}|$ respectively. Because of the SOS2 sets, at most two of the weighting variables from each set may be non-zero, and they must be adjacent.

The discretized head and discharge values coincide with the discretized triplet values from the Hill chart of the turbines. Consequently, for each combination of head and discharge, there exists a turbine efficiency value. By using these triplets of head, discharge, and efficiency, we create several breakpoints in the production function. This allows for a piecewise linearization of the 3-dimensional curve. Using the turbine efficiencies for the combinations of head and discharge, we have calculated the power produced in each breakpoint. This creates a mesh representation of the HPF. We use a weighting variable $\theta_{i,j}$ that is constrained by α_j and β_i in order to create a linear combination of these breakpoints. Since the weighting variable of the power matrix is constrained by the head and discharge, we get adjacent power weights as well. This leads to a linear approximation of the power production function.

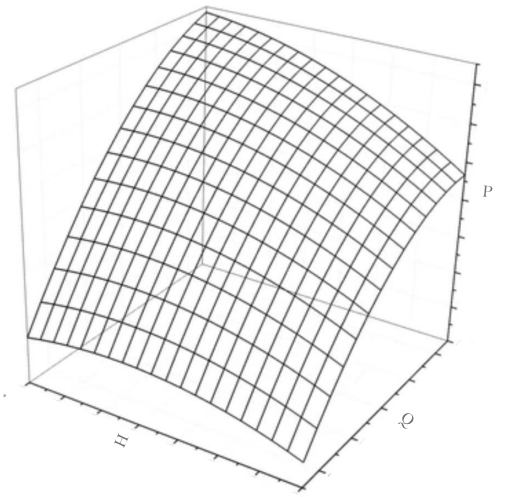

Figure 1: Rough sketch of a mesh representation of an HPF. Inspired by Kang, Guo and Wang (2017).

We generate one matrix for each generating unit. Recall from the nomenclature in Section 5 that $\mathcal{K}$ is the set of generating units and $\mathcal{R}$ is the set of reservoirs. Therefore, j and i indeces mentioned earlier now becomes a part of set $\mathcal{M}_k$ and $\mathcal{N}_k$ respectively. The matrix contains the amount of power produced for each discrete combination of head and discharge. These production values are called $\bar{p}_{i,j}$. Linear combinations of the power values are created by the non-negative value $\theta_{i,j}$. The discretized head and discharge values are denoted $\bar{h}_j$ and $\bar{q}_i$. A linear combination of the values are created by weighting variables α_j and β_i respectively. Using this mesh representation and the principle with a weighting variable and binary constraining variables we get

$$p(h_{r,t}, q_{k,t}) = \sum_{i \in \mathcal{N}_k} \sum_{j \in \mathcal{M}_k} \bar{p}_{k,i,j} \theta_{k,t,i,j}, \quad k \in \mathcal{K}, t \in \mathcal{T} \tag{6.1a}$$

$$\sum_{i \in \mathcal{N}_k} \sum_{j \in \mathcal{M}_k} \theta_{k,t,i,j} = 1, \quad k \in \mathcal{K}, t \in \mathcal{T} \tag{6.1b}$$

$$h_{r,t} = \sum_{j \in \mathcal{M}_k} \bar{h}_{k,j} \alpha_{k,t,j}, \quad r \in \mathcal{R}, k \in \mathcal{K}_r, t \in \mathcal{T} \tag{6.1c}$$

$$q_{k,t} = \sum_{i \in \mathcal{N}_k} \bar{q}_{k,i} \beta_{k,t,i}, \quad k \in \mathcal{K}, t \in \mathcal{T} \tag{6.1d}$$

$$\sum_{i \in \mathcal{N}_k} \theta_{k,t,i,j} = \alpha_{k,t,j}, \quad k \in \mathcal{K}, t \in \mathcal{T}, j \in \mathcal{M}_k \tag{6.1e}$$

$$\sum_{j \in \mathcal{M}_k} \theta_{k,t,i,j} = \beta_{k,t,i}, \quad k \in \mathcal{K}, t \in \mathcal{T}, i \in \mathcal{N}_k \tag{6.1f}$$

$$\theta_{k,t,i,j} \geq 0 \quad k \in \mathcal{K}, t \in \mathcal{T}, i \in \mathcal{N}_k, j \in \mathcal{M}_k \tag{6.1g}$$

$$\alpha_{k,t,j} \geq 0 \quad k \in \mathcal{K}, t \in \mathcal{T}, j \in \mathcal{M}_k \tag{6.1h}$$

$$\beta_{k,t,i} \geq 0 \quad k \in \mathcal{K}, t \in \mathcal{T}, i \in \mathcal{N}_k \tag{6.1i}$$

Here, $(\alpha_1, \alpha_2, ..., \alpha_m)$ and $(\beta_1, \beta_2, ..., \beta_n)$ are SOS2 set. Since at most two values in each of these sets are allowed to be non-zero, (6.1e) constrain $\theta_{i,j}$ to be non-zero in at most two neighboring rows, while constraint (6.1f) allow $\theta_{i,j}$ to be non-zero in at most two neighbouring columns. Thus, $\theta_{i.j}$ may only be non-zero in four neighbouring values in a square (Kang, Guo and Wang 2017). Consequently we may only select one square of the discretized hydropower function.

	α_1	α	α_3	$\cdots$	α_m
β_1	$\theta_{1,1}$	$\theta_{1,2}$	$\theta_{1,3}$	$\cdots$	$\theta_{1,m}$
β_2	$\theta_{2,1}$	$\theta_{2,2}$	$\theta_{2,3}$	$\cdots$	$\theta_{2,m}$
β_3	$\theta_{3,1}$	$\theta_{3,2}$	$\theta_{3,3}$	$\cdots$	$\theta_{3,m}$
$\vdots$	$\vdots$	$\vdots$	$\vdots$	$\ddots$	$\vdots$
β_n	$\theta_{n,1}$	$\theta_{n,2}$	$\theta_{n,3}$	$\cdots$	$\theta_{n,m}$

Figure 2: Visualization of possible θ values constrained by α and β in SOS2 sets.

The SOS2 sets of weighting variables α and β have been modeled by introducing two new binary variables, ω and ζ, one for each SOS2 set and the following constraints:

$$\alpha_{k,t,j} \leq \zeta_{k,t,j} + \zeta_{k,t,j+1}, \quad k \in \mathcal{K}, j \in \mathcal{M}_k, t \in \mathcal{T} \tag{6.2a}$$

$$\sum_{j \in \mathcal{M}_k} \zeta_{k,t,j} = 1 \quad k \in \mathcal{K}, t \in \mathcal{T} \tag{6.2b}$$

$$\beta_{k,t,i} \leq \omega_{k,t,i} + \omega_{k,t,i+1}, \quad k \in \mathcal{K}, i \in \mathcal{N}_k, t \in \mathcal{T} \tag{6.2c}$$

$$\sum_{i \in \mathcal{N}_k} \omega_{k,t,i} = 1 \quad k \in \mathcal{K}, t \in \mathcal{T} \tag{6.2d}$$

Constraints (6.2a) and (6.2c) make sure that α and β can only have values if the binary value with the same, or following, index in the list is 1. Constrains (6.2b) and (6.2d) makes sure that only one of these binary values are 1. Combined, these constraints allow at most two values of α and β to be non-zero, and these two values must be adjacent.

In order to correctly capture edge values in the SOS2 sets, these are hard coded in the actual code implementation.

Gross Head Linearization

The gross head is a function of the water volume in the reservoir at the current timestep. Recall from Section 5 that the volume is denoted $v_{r,t}$. As the relationship is non-linear, the gross head function is represented by a piecewise approximation. We model the non-linear relationship similarly as with the HPF. We create two arrays, H and V, consisting of discretized pairwise values $\bar{h}_u$ and $\bar{v}_u$ for gross head and volume, where $u = 1, ..., U$ for both arrays. The sets of these indeces are denoted $\mathcal{U}_r$, one for each reservoir $r \in \mathcal{R}$. Then the gross head value is given by a weighted linear combination of two neighbouring points in H.

$$h^G_{r,t} = \sum_{u \in \mathcal{U}_r} \bar{h}_{r,u} \gamma_{r,t,u} \quad r \in \mathcal{R}, t \in \mathcal{T} \tag{6.3a}$$

$$v_{r,t} = \sum_{u \in \mathcal{U}_r} \bar{v}_{r,u} \gamma_{r,t,u} \quad r \in \mathcal{R}, t \in \mathcal{T} \tag{6.3b}$$

$$\sum_{u \in \mathcal{U}_r} \gamma_{r,t,u} = 1, \quad r \in \mathcal{R}, t \in \mathcal{T} \tag{6.3c}$$

$$\sum_{u \in \mathcal{U}_r} \kappa_{r,t,u} = 1, \quad r \in \mathcal{R}, t \in \mathcal{T} \tag{6.3d}$$

$$\gamma_{r,t,u} \leq \kappa_{r,t,u} + \kappa_{r,t,u+1}, \quad r \in \mathcal{R}, u \in \mathcal{U}_r, t \in \mathcal{T} \tag{6.3e}$$

$$\gamma_{r,t,u} \geq 0, \quad r \in \mathcal{R}, u \in \mathcal{U}_r, t \in \mathcal{T} \tag{6.3f}$$

$$\kappa_{r,t,u} \in \{0,1\} \quad r \in \mathcal{R}, u \in \mathcal{U}_r, t \in \mathcal{T} \tag{6.3g}$$

Here, $\gamma_{r,t,u}$ is a weighting variable that creates a linear combination of the breakpoints in the gross head approximation and is contained in a SOS2 set defined by $\kappa_{r,t,u}$. Since $v_{r,t}$ is exogenously given and $\bar{h}$ and $\bar{v}$ coincide index-wise, this method creates linearly separable values from a piecewise linear function. This method is essentially the same as the HPF linearization but for a function of only one variable. Similarly to the HPF linearization, the edge values have been hardcoded in the code implementation.

Net Head Linearization

Net head is the gross head adjusted for different loss factors, such as friction and drag loss. These loss factors are represented as a friction coefficient μ multiplied by discharge squared, meaning that this function has to be linearized. Mathematically, this reads

$$h_{r,t} = h^G_{r,t} - \mu_r (\sum_{k \in \mathcal{K}_r} q_{k,t})^2, \quad r \in \mathcal{R}, t \in \mathcal{T} \tag{6.4}$$

This polynomial is represented with a linear approximation in our model. Even though the gross head levels varies, the loss factor stays constant, meaning that the intercept difference and the slope of the approximation line remains constant. To ensure that the intercept is not added to the net head calculation unless water is discharged through the penstock, creating higher than possible net head values, constraint (6.5a) is added. The binary variable ρ is multiplied with the intercept to force it to zero if there is no water discharged. Consequently, the net head calculation is as follows

$$\sum_{k \in \mathcal{K}_r} \delta_{k,t} \leq |K_r| \rho_{r,t}, \quad r \in \mathcal{R}, t \in \mathcal{T} \tag{6.5a}$$

$$h_{r,t} = h^G_{r,t} + a_r \rho_{r,t} - b_r \sum_{k \in \mathcal{K}_r} q_{k,t}, \quad r \in \mathcal{R}, t \in \mathcal{T} \tag{6.5b}$$

$$\rho_{r,t} \in \{0,1\} \quad r \in \mathcal{R}, t \in \mathcal{T} \tag{6.5c}$$

Recall that $\delta_{k,t}$ is a binary variable that is one only if generating unit k is in active production. $|K_r|$ is the amount of generating units in the power plant connected to reservoir r. Constraint (6.5a) forces $\rho_{r,t}$ to be one if at least one of the generating units connected to reservoir r are active in the current timestep. The intercept of the linear approximation is given by $h^G_{r,t}$ which is the gross head of reservoirs r at timestep t plus a constant a_r. The constant factor b_r is the slope of the linear approximation. This linear approximation does not increase the model complexity considerably, and is considered sufficiently accurate to be used in our models.

6.2 Handling of Non-Linearities in the Mid-Term Model

In order to keep the mid-term linear, the HPF has been linearized in differently than in the short term. We implement the HPF linearization from Ek Fälth et al. (2022), with a Taylor expansion around mean discharge and mean head, in order to keep the expression continuous and non-binary. In order to do this, we make the simplification that the turbine efficiency is constant. This simplification is reasonable as the demand for accuracy in the power production in the mid-term is not as high as in the short term. The Taylor expansion of a function of two variables $f(x, y)$ around a point (a, b) if (x, y) is close to (a, b) and the first derivatives of $f(x, y)$ are continuous is

$$f(x,y) \approx f(a,b) + \frac{\partial f}{\partial x}(a,b)(x-a) + \frac{\partial f}{\partial y}(a,b)(y-b) \tag{6.6}$$

In our case, the Taylor expansion of the HPF looks like this

$$\begin{aligned} p(q,h) &\approx p(\bar{Q},\bar{H}) + \frac{\partial p}{\partial q}(\bar{Q},\bar{H})(q-\bar{Q}) + \frac{\partial p}{\partial y}(\bar{Q},\bar{H})(h-\bar{H}) \\ &= G\eta(\bar{Q}\bar{H} + \bar{H}(q-\bar{Q}) + \bar{Q}(h-\bar{H})) \\ &= G\eta(\bar{H}q + \bar{Q}h - \bar{H}\bar{Q}) \end{aligned} \tag{6.7}$$

Here, $\bar{H}$ and $\bar{Q}$ are the average values for head and discharge respectively. Recall from Section 3.2 that G is a constant encompassing the gravity constant and water density and that η is the combined turbine and generator efficiency, a simplification mentioned in Section 5. This makes the power production function in the mid-term take the following form:

$$p(q_{k,t}, h_{r,t}) = G\eta_k(h_{t,r}\bar{Q_k} + \bar{H}_r q_{k,t} - \bar{Q_k}\bar{H}_r), \quad r \in \mathcal{R}, k \in \mathcal{K}_r, t \in \mathcal{T} \tag{6.8}$$

The linearization of the net head in the mid-term is also simplified. Notice that there is no volume-to-gross-head function, but instead the net head is directly dependent on the volume. This relationship is represented as a linear function:

$$h_{r,t} = d_r v_{r,t} + g_r, \quad r \in \mathcal{R}, t \in \mathcal{T} \tag{6.9}$$

Here, d_r is the slope of the linearization and g_r is the intercept. Even though this is not a very accurate representation of the net head, it is seen as sufficiently accurate considering the purpose of the mid-term model.

6.3 Solar Scenario Generation and Selection

In this section, we outline an approach to create PV power generation scenarios. The scenario generation process utilizes different forecasts with minutely resolution. The desired output is a set of distinct PV power generation scenarios Ξ_s. Each scenario comprises several $\xi_{t,s}$, representing the amount of solar energy, in MWh, generated for each hour t in a day.

When selecting a generation method, we primarily considered two factors: simplicity and data quality requirements. Although artificial neural networks (ANNs) may offer better quality scenarios, the stringent demands on data quality and quantity, as discussed in Section 3.3, led us to explore alternative generation procedures. We chose a composite procedure featuring stochastic differential equations (SDE) proposed by Iversen, Morales et al. (2014) as the core component.

The procedure introduces quite a lot of nomenclature used only in this section. To get an understanding of the procedure beyond what is presented in this section, the reader is referred to the original paper (Iversen, Morales et al. 2014). We reuse the nomenclature from the original paper

X_t	-	proportion of clear sky irradiance reaching the ground at time t
Y_t	-	observed irradiance at time t
A_t	-	stochastic process governing the predicted level reversion speed of X_t at time t
$dW_{p,t}$	-	system noise process value at time t for process $p \in \{X, A\}$
n_t	-	numeric weather prediction (NWP) at time t
m_t	-	clear sky irradiance at time t
β_X	-	small auxiliary parameter
δ	-	small auxiliary parameter
γ	-	scaling constant for the clear sky irradiance m_t
ω_1	-	amplitude scaling of time dependant term
ω_2	-	phase scaling of the time dependant term
μ_X	-	local scaling parameter
μ_A	-	mean of A_t
σ_p	-	system noise scaling of process $p \in \{X, A\}$
θ_A	-	speed of reversion to μ_A for A_t
ϵ	-	small error term

Table 1: Nomeclature used in PV power generation

to make parallel reading easier and it is presented in Table 1. This is not to be confused with the nomenclature from the other subsections. The procedure simulates the state of irradiance, i.e., the observed proportion of clear sky irradiance reaching the ground. We denote this state as X_t.

The code implementation simulates the evolution of X_t at every time delta dt (minutes). The change in $X(t)$ at each timestep is denoted $dX(t) = X(t) - X(t-1)$. This gives us (6.10). The clear sky forecast at time t, m_t, multiplied with the proportion state, X_t, yields one possible realization of observed irradiance on the ground at that time (6.11). We denote this observed irradiance Y_t. Note that a small random error term is added to Y_t, representing the measurement error of observed irradiance.

$$X_t = X_{t-1} + dX_t \tag{6.10}$$

$$Y_t = \gamma m_t X_t + \epsilon_t \tag{6.11}$$

A_t is a separate stochastic process, Equation (6.13), governing the speed at which X_t reverts to its predicted level. This represents the fact that NWPs predict some interval into the future. The part of the prediction interval closest to the time it is given has a higher probability of being correct than the part of the NWP interval that is further into the future. The evolution of A_t at each timestep t is shown in (6.12).

$$A_t = A_{t-1} + dA_t \tag{6.12}$$

dA_t is calculated as shown in (6.13). The stochastic nature of the process is governed by system noise in the form of a standard Wiener process, also known as Brownian Motion (Wiener 1923), denoted $dW_{A,t}$. The process will return to its mean, μ_A at a speed governed by θ_A. σ_A scales the system noise at each timestep.

$$dA_t = \theta_A(\mu_A - A_t)dt + \sigma_A dW_{A,t} \tag{6.13}$$

The final part of the simulation is the calculation of $dX(t)$. The calculation is shown in (6.14) and consists of two terms representing a deterministic part and a stochastic part. We start of by explaining the stochastic part, $\sigma_x X_t(1 - X_t)dW_{X,t}$. It is almost identical to the stochastic term in (6.13), with its own independent Wiener process adding stochasticty. As $X(t)$ represents a proportion, it is bounded between 0 and 1. The term $X_t(1 - X_t)$ makes sure the stochastic term does not push $X(t)$ outside its bounds, and σ_X represent a constant scaling of the stochastic term.

The deterministic part, the first term in (6.14), takes the predicted irradiance on the ground, n_t, and the predicted clear sky irradiance, m_t, as input. We see A_t in front of the term, serving the same purpose as θ_A does in (6.13). It governs how rapidly X_t tends to its predicted level. The fraction with n_t and m_t represents what the forecasted proportion of clear sky irradiance reaching the ground is. The auxiliary parameter β_X is added to ensure the process does not tend to 0 at night, and the auxiliary parameter δ is added so that there is no division by 0, should $m_t = 0$. This proportion term is scaled by μ_X. We see the time dependent sine term added to the scaling, representing a varying bias of the process throughout a day. dt is the timestep size, in our simulations one second.

$$dX_t = e^{A_t}\left(\frac{n_t + \beta_x}{\gamma m_t + \delta}\left(\mu_x - \omega_1 \sin\left(\frac{2\pi}{24}t + \omega_2\right)\right) - X_t\right)dt + \sigma_x X_t(1 - X_t)dW_{X,t} \tag{6.14}$$

As X_t solely represents the proportion of potential irradiance, the stochastic process can operate during nighttime as well. Together, (6.10)-(6.14) lets us simulate a possible realisation of the observed irradiance throughout one day, based on the provided NWP. The outcome is a model that, at any given time t, provides an X_t drawn from a distribution unique to that precise time.

The next step involves converting irradiance to electricity in the PV modules. For this conversion process, we follow the model proposed by Huld, Šúri and Dunlop (2008), described in Section 3.4. This method use PV panel specific constants. We adopt appropriate modeling constants from a paper by Koehl et al. (2011). To calculate the PV module temperature required for the conversion, we employ a procedure developed by Faiman (2008). By combining the conversion process (Huld, Šúri and Dunlop 2008) and module temperature calculation (Faiman 2008), we now have a conversion procedure that takes irradiance, temperature, and wind as inputs, returning the numerical power output of the PV module. Scaling this to the entire PV power plant yields a trajectory of its total power output on a per-minute basis.

Next, we derive an inverse cumulative distribution function (CDF). We do this by performing a Monte Carlo simulation, running the SDE process by Iversen, Morales et al. (2014) thousands of times. We determine every percentile for each minute across all realizations, thus obtaining prediction intervals. An example of the prediction intervals can be seen in Figure 3. By averaging the power output over the minutes of every hour within each quantile, we convert the power output to energy output. This process creates an approximation of the inverse CDF of the energy produced each hour t, measured in MWh.

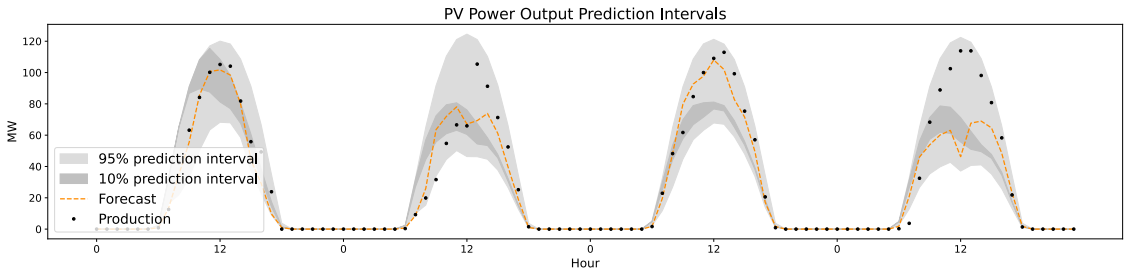

Figure 3: Prediction intervals after Monte Carlo simulation. The 10% prediction interval is between the 55% and the 65% interval.

From the inverse CDF, we want to construct possible PV generation scenarios. If we were to construct all possible scenarios from the 99 quantiles over approximately 12 hours of sunlight, we would be looking at 12^{99} distinct scenarios. To construct a comprehensible number of representative scenarios, we implement a sampling and reduction procedure described in (Rios, Wets and Woodruff 2015). We begin by creating a fairly large number of scenarios by correlated sampling. The correlation dictates how much the power production varies between different quantiles of the inverse CDF between successive hours in each scenario. The correlation coefficient used in this process, ρ, is calculated between the production forecasting errors of successive hours over the previous 14 days. It is calculated by emplying a Durbin-Watson test on the error between the forecasted and actual PV production, a standard approach for calculation auto-correlation (Durbin and Watson

1950). After this procedure, we are left with S scenarios of energy production $\xi_{t,s}$ for each hour t.

Next, we perform scenario reduction to get a selection of a few representative scenarios among the sampled scenarios. The reduction is a form of forward construction, where the construction is performed on cluster centroids calculated by employing k-means clustering on the sampled scenarios. We end up with a reduced scenario set and corresponding probabilities of realisation. In addition, we convert the NWP from the algorithm inputs into a single PV power generation scenario, following the (Huld, Šúri and Dunlop 2008) approach. This single sceario is used as a baseline to assess the value of introducing uncertainty. It is referred to as the deterministic dataset.

6.4 Model Simulation and Testing Procedure

To test and compare the different configurations of hybrid and separate planning, we implement the models from Section 5 in Python and use commercial solver Gurobi to solve all LP and MILP models. Their performance in the setting of this thesis is simulated and tested through a procedure described in this subsection.

The general outline of our simulation is as follows: we choose a date on which to start a simulation. In reality, the water volume on this date would be observed. Because the reservoirs have not been built, there is no historical data on water volumes and we need to approximate these levels. Based on inflow data, the mid-term model runs over two flooding seasons and calculates the water volume of both reservoirs on the given date. We can do this because we assume the water reservoirs are full at the end of every flooding season. Next, the mid-term calculates the water values. This is done by solving the hydro scheduling problem from the current date until the end of next rainy season. If that date is less than 32 weeks away, the mid-term model is run until the end of next years rainy season in order to enable the model to plan far enough ahead into the future as mentioned in Section 3.2. The duals of the constraints on the reservoir volumes two days ahead are returned from the model. This output gives an indication of how much we would be willing to pay to have an extra unit of water two days in the future, i.e., the water value.

The volumes and the water values are then fed into the short-term scheduling model along with inflow and weather data. The short-term model is run for 48 hours, as mentioned in Section 5. After being run to optimallity, the short-term model outputs its day-ahead peak and off-peak commitment. It is then re-run with the commitments fixed. In this step, the weather data is replaced with the dataset containing the actual PV power production data. This step simulates the actual realisation of the stochastic data used in the planning phase, forcing the producers to react based on their commitments from the "the day before". At this point, the model outputs the water volumes of both reservoirs at the end of timestep 24. These volumes are then fed into the mid-term model for the next day. Additionally, the simulation phase of the short-term model outputs its generating unit status variables, δ_k, at the end of timestep 24. This allows the next day model to plan based on the model state the current day.

We run four variations of the simulation procedure:

- Hybrid planning and operation with PV power generation scenarios, referred to as the hybrid configuration.

- Hybrid planning and operation without PV power generation scenarios, using the deterministic dataset, referred to as the deterministic configuration.

- Hybrid planning and operation with heuristic planning and PV power generation scenarios, referred to as the heuristic configuration.

- Separate planning and operation with PV power generation scenarios, referred to as the separate configuration.

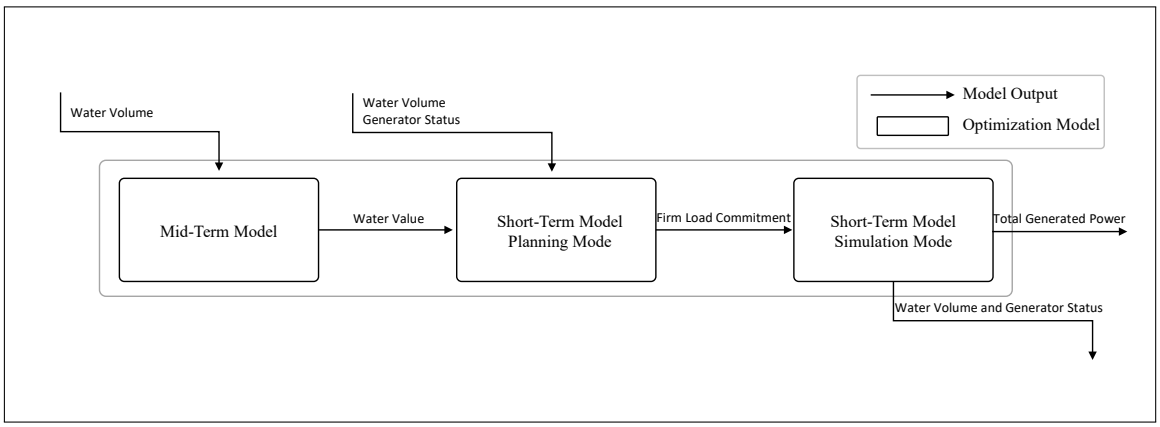

Figure 4: A general overview of one day of simulation for one power system configuration.

All PV power production scenario sets used in these simulations are generated on a day-by-day basis by the generation procedure described in Section 6.3. The same generated scenario set is used for the hybrid, the separate, and the heuristic configuration. Each of them is solved using the deterministic equivalent of the two-stage stochastic problem. With the complexity of our short-term scheduling model, the use of a deterministic equivalent severely limits the number of scenarios we are able to plan over. A proposed alternative is described in detail in Section 6.5. As a heuristic alternative for the planning phase, the heuristic configuration makes day-ahead commitments based on solving the linear version of the deterministic equivalent. We relax all binary restrictions and make a tradeoff between time and precision in the day-ahead commitment planning.

In the separate configuration, we have to make some assumptions. As the power purchasing agreement we assume to be operating under is drawn up for a hybrid setting, we look to the literature to find a realistic alternative for the separate configuration. In the paper from Matevosyan and Soder (2007), there are hydro and intermittent renewables, as well as a combined peak production capacity well above the capacity of the power grid. This setting is comparable to the setting of this thesis, thus we set up the separate planning and operation problem based on Matevosyan and Soder (2007). In scenarios where the two separate producers nominates a combined total above the transmission capacity, the hydro producers takes precedence, forcing the curtailment of PV power generated in excess of the grid capacity. The rationale behind this hierarchy of grid priority is that the hydro producer plans based on a long term allocation of resources. Forcing it to hold back water could potentially lead to negative consequences through flooding.

In the planning phase, the hydro producer nominates a peak and off-peak commitment with no PV power generation. The solar power producer nominates only a peak period load commitment, as there are barely any seasons where there is PV power generation in the off-peak periods. Moving on to the simulation step, the hydro producer proceeds as in the general outline. The load commitment of the PV power producer is however adjusted to $\min(x_{peak}^{PV}, D^{MAX} - x_{peak}^{HYDRO})$, where x_{peak} denotes the load commitment of either producer. Additionally, x_{peak}^{HYDRO} is given as input to the solar producer, reducing its grid capacity in the simulation phase accordingly.

We run the simulation procedure over 14 days periods. More detailed descriptions of the simulation procedure for the different configurations with actual data are described in Section 7.

6.5 Disjunctive Decomposition

Our day-ahead stochastic hybrid power planning program is characterized as a two-stage stochastic program with continuous first-stage variables and mixed-binary recourse. Recall that the first stage decisions are deciding the load commitment for each timestep the next day, while the second stage decision is how to produce this load commitment the following day. This leads to the characteristic that the first-stage problem is rather easy to solve, while the second-stage problem

is computationally expensive. This is a result of the sophisticated and accurate representation of both the HPF and the head variation, which leads to a large amount of binary variables. As a result of these characteristics, a Disjunctive Decomposition algorithm developed by Ntaimo and Sen (2007) was originally selected as the solution method. This algorithm fits the structure of our problem as it is specialized in solving two-stage stochastic MILP problems with continuous first-stage and binary second-stage variables. The method is a Branch-and-Cut algorithm revolving around the D2 method that was introduced in Section 3.5. The method is referred to as the D2-CBAC algorithm. This section will go through the solution method step-by-step, explaining each part of the algorithm.

As the solution method is both a temporal and scenario-wise decomposition, it is necessary to split the problem into a master and subproblem. The master problem is on the following form:

$$\begin{aligned} min \sum_{t \in \mathcal{T}_1} (-P_t x_t) + E[f(x,\omega)] \\ \text{s.t.} \\ x_t = x^P, \quad t \in \hat{\mathcal{T}} \\ x_t = x^O, \quad t \in \tilde{\mathcal{T}} \\ x_t \leq D^{MAX}, \quad t \in \mathcal{T}_1 \\ x_t \geq 0, \quad t \in \mathcal{T}_1 \quad x^P, x^O \geq 0 \end{aligned} \tag{6.15}$$

where $E[f(x,\omega)]$ is the expected value of the second-stage problem and x is a vector containing all first-stage variables. In the second-stage, the x_t values for the first day are locked, while the x_t values for the second day are decision variables. Recall from the nomenclature in Section 5 that $\tilde{T}$ is the set of off-peak timesteps, $\hat{T}$ the set of peak timesteps, and T_1 the set of timesteps in the first day. In the subproblem, the x_t values for the second day are denoted x_t^s in order to distinguish them as second-stage variables. As explained in Section 6.4, these do not need to have the same values for peak and off-peak periods. The subproblem becomes:

$$f(x,\omega) = min \quad \sum_{r \in \mathcal{R}} \phi_r (V_r^{INIT} - v_{r,T}) + \sum_{t \in \mathcal{T}} \sum_{k \in \mathcal{K}} C_k^S \lambda_{k,t} + \sum_{t \in \mathcal{T}} C^U p_t^U - \sum_{t \in \mathcal{T}} P_t^I p_t^I - \sum_{t \in \mathcal{T}_2} P_t x_t^s \tag{6.16}$$

s.t.

$$5.6 - 5.18 \tag{6.17a}$$

$$\sum_{k \in \mathcal{K}} p_{k,t} + p_t^U - p_t^I - \xi_t^{CURT} = x_t - \xi_t(\omega), \quad t \in \mathcal{T}_1 \tag{6.17b}$$

$$\sum_{k \in \mathcal{K}} p_{k,t} + p_t^U - p_t^I - \xi_t^{CURT} - x_t^s = -\xi_t(\omega), \quad t \in \mathcal{T}_2 \tag{6.17c}$$

$$p_t^I \leq D^{MAX} - x_t, \quad t \in \mathcal{T}_1 \tag{6.17d}$$

$$p_t^I + x_t^s \leq D^{MAX}, \quad t \in \mathcal{T}_2 \tag{6.17e}$$

$$\lambda_{k,t}, \delta_{k,t} \in \{0,1\}, \quad k \in \mathcal{K}, t \in \mathcal{T} \tag{6.17f}$$

$$p_{k,t}, q_{k,t} \geq 0, \quad k \in \mathcal{K}, t \in \mathcal{T} \tag{6.17g}$$

$$\xi_t^{CURT}, q_{r,t}^{BP}, q_{r,t}^{TOT}, q_{r,t}^{OF}, v_{r,t}, h_{r,t}^G, h_{r,t} \geq 0, \quad r \in \mathcal{R}, t \in \mathcal{T} \tag{6.17h}$$

$$p_t^I, p_t^U, x_t^s \geq 0, \quad t \in \mathcal{T} \tag{6.17i}$$

Most constraints are identical to the short-term model in Section 5, but the constraints defining the power balance (5.19) and grid congestion (5.22) have been slightly changed to comply with the second-stage nature of this problem, as seen in (6.17c) - (6.17e). Notice that these have been split in two versions, one for the first day and one for the second day in the planning period. This is in order to model the load commitment in the second day as a second-stage variable. Recall from Section 5 that the second day is included to get the model to behave correctly, and the load commitment for this day should therefore be a second-stage variable and not a first-stage variable.

Moving forward in this subsection, the master- and subproblems are represented on canonical form. This is done in order to implement the algorithm efficiently, as well as to increase readability. Indeces and variables in this section do not coincide with nomenclature from the previous sections. This has been done in order to keep the formulation of the method true to the original paper. In this subsection, $c, x, A,$ and b represents the objective function coefficients, the variables, the constraint coefficients, and the right hand sides of the master problem. Similarly, $g, y, W, r(\omega)$ and T represents the objective function coefficients, the variables, and the constraint coefficients and constants of the subproblems.

When solving the master problem, we replace $E[f(x, \omega)]$ in the master problem with an approximation of this expected value. This is represented by a new variable, η. The master problem then takes the following form:

$$\begin{aligned} min \quad & c^\top x + \eta \\ & \text{s.t.} \\ & Ax \geq b \\ & x, \eta \geq 0 \end{aligned} \tag{6.18}$$

$Ax \geq b$ is all constraints in the master problem, and $c^\top x$ is the objective function value. In the process of creating and convexifying disjunctive cuts we need to use Theorem 1 and Theorem 2 from Sen and Higle (2005). Roughly speaking, Theorem 1 states how to find valid inequalitites for the convex hull of a set of disjunct polyhedrons. Theorem 2 states that a valid inequality for a set S is always an extreme point of the reverse polar of this set. Both these theorems can be read in more detail with proofs in Sen and Higle (2005). The creation and convexification process will be explained later in this section. To be able to use these theorems without modification, we impose the constraint $\eta \geq 0$. The constraint $\eta \geq 0$ is guaranteed to hold without loss of generality by simply translating the η value with a constant equal to a lower bound of the sub problem. In the D2-CBAC algorithm, we want to branch on the x-variables. We will therefore iteratively add branching cuts to this formulation, that will be appended on A and b.

The LP-relaxed subproblem is formulated in (6.19). As with the master problem, the subproblem has been written on canonical form.

$$\begin{aligned} f(x, \omega) = min \quad & g^\top y \\ & \text{s.t.} \\ & Wy \geq r(\omega) - Tx \\ & y \geq 0 \end{aligned} \tag{6.19}$$

T is the vector containing the coefficients for all the locked first-stage solutions in the second-stage problem and links the second stage to the first stage. $Wy \geq r(\omega) - Tx$ thereby contains all second

stage constraints. These constraints also include the upper bounds on the binary variables, i.e., $-y \geq -1$. T contains the coefficients for all the first-stage variables in the subproblem, while W contains the coefficients for all the second-stage variables. In our problem, r is the only vector that varies from subproblem to subproblem based on the scenarios, since this contains the PV power production. This can be seen mathematically as it is the only term that is dependent on ω in this formulation. In our algorithm, we want to develop disjunctive cuts on the form $\pi y \geq \pi_0(\omega, x)$ that are valid for all pairs of ω and x. These cuts will be iteratively added to the subproblem in order to aproximate the convex hull of the subproblem. This makes it possible to solve the LP-relaxation of the subproblem and obtain an accurate solution.

In short, the algorithm consists of six steps:

1. Initialization of the branch and bound tree. Here, the algorithm is initialized and the root node of the tree is created.
2. Cut creation. A disjunctive cut is created in order to cut away fractional binary values from the LP-relaxation of the subproblem.
3. Cut convexification. The disjunctive cut is convexified in order to append it to the subproblem.
4. Re-optimizing the subproblem. After the disjunctive cut is added, we re-optimize the subproblem.
5. Re-optimizing the master problem. The master problem is updated with optimality cuts based on the current subproblem solution, and is re-optimized.
6. Branching. Depending on the current solution to the master problem we possibly branch on the feasible first-stage solutions.

Step 2 to 5 is here part of the D2 algorithm, which is a key part of the D2-CBAC. We will now go through all these six steps in detail.

Initialization

The algorithm is initialized by creating a branch-and-bound tree, where the root node is a problem consisting of the master and subproblem, i.e., (6.18) and (6.19). k denotes the number of iterations of the D2 algorithm performed across all nodes. In the root node, we begin by running one iteration of the D2 algorithm before checking for and potentially performing branching in accordance with the CBAC extension from Ntaimo and Sen (2007).

D2 starts of by solving the master problem to find the optimal values of x, denoted x^k. These first-stage variables are then passed to the subproblem as constants, and the subproblem is solved for each scenario ω. After solving each sub-problem, we check if any of the binary restrictions are violated. If not, we have found a feasible solution and can update the upper bound. We find this by subtracting the approximated value of the expected value of the subproblems, η, from the master problem objective function value. Instead we add the actual expected value of all current subproblem objective function values. We then use the dual multipliers from the subproblem solutions over each scenario to create a standard Benders' optimality cut in the master problem and re-solve to get a new lower bound on the problem.

If however, over all scenarios, there is at least one variable in y that violates its binary restriction, we need to add cuts to cut away this solution. The binary variable with the lowest continuous value is selected. We call this variable the *disjunction variable*, $y_{j(k)}$. $\bar{y}_{j(k)}$ is the value of $y_{j(k)}$ in this iteration. J is the set of all second-stage variable indeces, and $j(k) \in J$. We use the disjunction variable to find a cut on the form $\pi y \geq \pi_0(\omega, x)$ that is most violated by the current solution y^k, which contains the fractional variable $y_{j(k)}$. By adding this cut to the subproblem, we will cut away the current fractional solution of $y_{j(k)}$. We want to create a cut that is valid for all pairs of scenarios and first stage solutions, as explained in Section 3.5. This is done by solving a stochastic linear program that is referred to as the C3-SLP (Ntaimo and Sen 2007).

Cut Creation

The C3-SLP is an LP that creates valid inequalities for disjunctive set. Since $y_{j(k)}$ is in fact a binary variable, we know that its feasible values are 0 or 1. We can therefore create two disjunct sets containing the feasible area of the subproblem, given the current x^k but with $y_{j(k)} \in \{0, 1\}$. These sets will not contain the fractional value $\bar{y}_{j(k)}$.

$$S_0 = \{y \in \mathbb{R}_+ | \quad Wy \geq r(\omega) - Tx^k, \, - y_{j(k)} \geq 0\} \tag{6.20}$$

$$S_1 = \{y \in \mathbb{R}_+ | \quad Wy \geq r(\omega) - Tx^k, y_{j(k)} \geq 1\} \tag{6.21}$$

The goal of the C3-SLP is to create valid inequalities for the union of these two sets. If all valid inequalities are generated, this will create the convex approximation of the union of these sets. We are interested in the valid inequality that cuts away the current fractional solution. This can be achieved by using the standard approach for generating valid inequalities for disjunct set, as described by Sherali and Shetty (1980). By using this approach we can create the C3-SLP subproblem:

$$max \quad E[\pi_0(\tilde{\omega})] - E[y^k(\tilde{\omega})]^\top \pi \tag{6.22a}$$

$$\text{s.t.} \quad \pi \geq \lambda_{0,1}^\top W^k - I^k \lambda_{0,2} \tag{6.22b}$$

$$\pi \geq \lambda_{1,1}^\top W^k + I^k \lambda_{1,2} \tag{6.22c}$$

$$\pi_0(\omega) \leq \lambda_{0,1}^\top (r(\omega) - Tx^k) - \lambda_{0,2} \lfloor \bar{y}_{j(k)} \rfloor \quad \forall \omega \in \Omega \tag{6.22d}$$

$$\pi_0(\omega) \leq \lambda_{1,1}^\top (r(\omega) - Tx^k) - \lambda_{1,2} \lceil \bar{y}_{j(k)} \rceil \quad \forall \omega \in \Omega \tag{6.22e}$$

$$-1 \leq \pi \leq 1, -1 \leq \pi_0(\omega) \leq 1 \quad \forall \omega \in \Omega \tag{6.22f}$$

$$\lambda_{0,1}, \lambda_{0,2}, \lambda_{1,1}, \lambda_{1,2} \geq 0 \tag{6.22g}$$

The objective function in Problem (6.22) maximizes a distance measure between the current solution y^k and the cut. This is in order to create the deepest possible valid inequality. In the model, the vector π represents the coefficients of the y variables in our disjunctive cut. π is called the common cut coefficient, as it is independent of both ω and x. $\pi_0(\omega)$ is the right hand side of our disjunctive cut for this current x-solution. Since the inequalities that constrain $\pi_0(\omega)$ contain x^k, the values of $\pi_0(\omega)$ can be said to be dependent on the current x^k. The λ's in (6.22) are weighting variables that are used to create valid cuts, and $r(\omega), T$ and W are vectors from the subproblem. $\lfloor \bar{y}_{j(k)} \rfloor$ and $\lceil \bar{y}_{j(k)} \rceil$ are the rounded values of $\bar{y}_{j(k)}$, i.e., 0 and 1 respectively. I^k is a vector that is 0 in all indices but j(k), where it is 1. To ensure that the generated cut removes the current fractional solution of $y_{j(k)}$, we change the objective function formulation of (6.22) by using *Remark 6* in Sen and Higle (2005). This replaces the expected values in the objective function from the expectation over all scenarios to the expectation only over the scenarios where $\bar{y}_{j(k)}$ is indeed fractional.

Since we want a representation of $\pi_0^k(\omega, x^k)$ as a function of x and not just as a scalar value, we cannot use the $\pi_0(\omega)$ value from the optimal solution of the C3-SLP directly. We create an expression for $\pi_0^k(\omega, x^k)$ based on the weighting variables $\lambda_{0,1}, \lambda_{0,2}, \lambda_{1,1}, \lambda_{1,2}$ in the optimal solution. From the proof from Corollary 4 in Sen and Higle (2005), we know that we can introduce new, real vectors $\bar{\nu}$ and $\bar{\gamma}$ such that

$$\pi_0^k(\omega, x) = \min\{\bar{\nu}_0 - \bar{\gamma}_0^\top x, \bar{\nu}_1 - \bar{\gamma}_1^\top x\} \tag{6.23}$$

when $\pi^k y \geq \pi_0(\omega, x)$ is a valid inequality of a union of two disjunctive sets. The proof also shows how to derive the ν's and γ's. Since creating a valid inequality for the union of two disjunctive sets is exactly what we have done in the C3-SLP, we can use the formulation from the proof to create an expression of π_0 that is dependent on x:

$$\bar{\nu}_0^k = \lambda_{0,1}^\top r^k(\omega), \quad \bar{\nu}_1^k = \lambda_{1,1}^\top r^k(\omega) + \lambda_{1,2} \tag{6.24}$$

$$(\bar{\gamma}_0^k(\omega))^\top = \lambda_{0,1}^\top T^k, \quad (\bar{\gamma}_1^k(\omega))^\top = \lambda_{1,1}^\top T^k \tag{6.25}$$

Since $\pi_0^k(\omega, x^k)$ is the minimum of two lines that are continuous in x, $\pi_0^k(\omega, x^k)$ becomes a piecewise linear concave function on x. This makes it necessary to convexify it in order to implement it as a cut in the subproblem. We denote this convex approximation π_c. Figure 5 is a graphical illustration of $\pi_0(\omega, x)$ and the $\pi_c(\omega, x)$ we need to approximate. In Figure 5, $\varphi(\omega)$ is an auxiliary variable used to represent the value of $\pi_0(x, \omega)$ as a function of x. X is the feasible region of the x-values visualized in two dimensions, with u and l being upper and lower bounds.

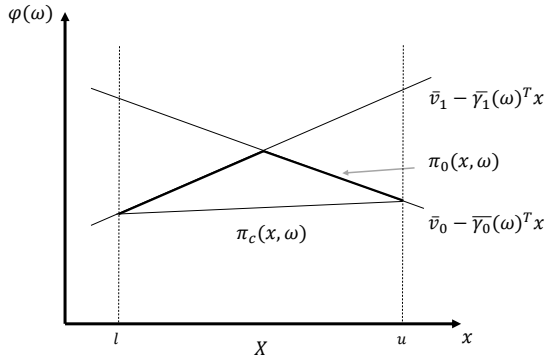

Figure 5: $\pi_0(x, \omega)$ and the convex approximation $\pi_c(x, \omega)$. Illustration inspired by Ntaimo and Sen (2007)

.

Cut Convexification

If $\pi_0 \geq 0$ we can, as previously mentioned, use Theorem 1 and Theorem 2 from Sen and Higle (2005) in the convexification process of π_c. This allows us to use reverse polar sets the way they are described in Sen and Higle (2005). If $\pi_0 < 0$ for some x, we translate $\bar{\nu}$ values with a constant in order to keep π_0 positive.

The first step of the convexification process is to create the epigraph of π_0, as we need π_0 to be represented as the union of two set in order to create our convex approximation. We restrict this epigraph to the feasible values of x, i.e $x \in X$. This is denoted Π_X.

$$\Pi_X(\omega) = \{(\varphi, x) | x \in X, \varphi \geq \pi_0(\omega, x)\} \tag{6.26}$$

ϕ is an auxiliary variable as in Figure 5. Since $\pi_0(\omega, x)$ is piecewise linear, we represent the epigraph as two set, E_0 and E_1. These set are illustrated in Figure 6.

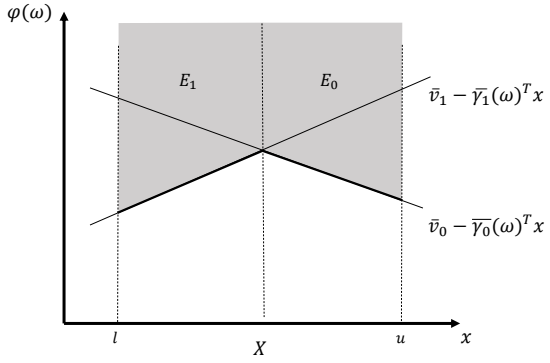

Figure 6: A graphical representation of one of the disjunct sets that constitute Π_X. Illustration inspired by Ntaimo and Sen (2007)

.

We can now create the reverse polar set of the epigraph Π_X represented as the union of the two disjunctive set E_0 and E_1. As in Sen and Higle (2005) we will reference this set as the epi-reverse polar, denoted $\Pi_X^\dagger$. The epi-reverse polar is defined as follows

$$\begin{aligned}
\Pi_X^\dagger = &\{\sigma_0(\omega) \in \mathbb{R}, \sigma(\omega) \in \mathbb{R}^n, \delta(\omega) \in \mathbb{R} \quad \text{such that} && (6.27a)\\
&\forall h \in \{0,1\}, \exists \tau_h \in \mathbb{R}^m, \tau_{0h} \in \mathbb{R} && (6.27b)\\
&\sigma_0(\omega) \geq \tau_{0h}, \quad h \in \{0,1\} && (6.27c)\\
&\sum_h \tau_{0h} = 1 && (6.27d)\\
&\sigma_j(\omega) \geq \tau_h^\top A_j + \tau_{0h}\bar{\gamma}_h(\omega), \quad h \in \{0,1\}, j = 1, ..., n && (6.27e)\\
&\delta(\omega) \leq \tau_h^\top b + \tau_{0h}\bar{\nu}_h(\omega), \quad h \in \{0,1\} && (6.27f)\\
&\tau_h \geq 0, \tau_{0h} \geq 0\} && (6.27g)
\end{aligned}$$

As with the C3-SLP (6.22), this formulation is constructed on the basis of Theorem 1 and Theorem 2 in Sen and Higle (2005). In this formulation, σ, τ and δ are auxiliary variables that are only used to represent the reverse polar of the epigraph of $\pi_0(\omega, x)$. A and b are from the master problem (6.18). $\sigma(\omega)$ is a vector of dimension n, which is the same as the first-stage variables x. τ_h is a vector of dimension m, which is the same as b from the master problem (6.18). The reverse polar $S^\#$ of a set S has the useful property that the its extreme points provide the facets of the convex hull of S (Sen and Sherali 1987). Therefore, the extreme points of $\Pi_X^\dagger$ provide the facets of Π_X. By finding the extreme points of (6.27) for each scenario, we can concatenate the optimal solution to create π_c, a linear, convex approximation of π_0. Since we have extreme points for each scenario ω, π_c is a function of both x and ω. Similarly to the λ's in C3-SLP, τ's are weighting variables, and in accordance with Corollary 5 in Sen and Higle (2005) we can create π_c from σ and δ. The corollary says that

$$\pi_c(\omega, x) = \underset{i \in I}{Max}\{\frac{\delta^i(\omega)}{\sigma_0^i(\omega)} - \frac{(\sigma^i(\omega))^\top}{\sigma_0^i(\omega)}x\} \tag{6.28}$$

where $i \in \mathcal{I}$ are the set of extreme points of $\Pi_X^\dagger$. Therefore we can find $\pi_c^k(\omega, x^k)$ by solving the following problem for each scenario:

$$\begin{aligned} max \quad & \delta(\omega) - \sigma_0(\omega) - \sigma(\omega)x^k \\ & (\delta(\omega), \sigma_0(\omega), \sigma(\omega)) \in (\Pi_X^\dagger)^k \end{aligned} \tag{6.29}$$

We derive $\pi_c^k(\omega, x^k)$ based on the optimal solution of (6.29):

$$\pi_c^k(\omega, x^k) = \nu^k(\omega) - \gamma^k(\omega)^\top x, \quad \nu^k = \frac{\delta^i(\omega)}{\sigma_0^i(\omega)}, \quad \gamma^k = \frac{(\sigma^i(\omega))}{\sigma_0^i(\omega)} \tag{6.30}$$

Re-Optimizing

We have now created a cut in the LP-relaxation of the subproblem that is valid for all combinations of ω and feasible x values in the current iteration. This cut is added to the subproblem so that W^{k+1} is the matrix $[W^k, \pi]$. Similarly, r^{k+1} and T^{k+1} is r^k and T^k appended with ν^k and γ^k, respectively. We re-optimize the subproblems for all scenarios $\omega \in \Omega$. If no binary values in any scenario subprolems are fractional, we update the problem upper bound with the objective function value of the master problem and add the expected value of the subproblem over all scenarios.

After the subproblem reoptimization, we use the dual multipliers σ_s^k from each scenario subproblem to update the approximation of η in the masterproblem (6.18). In our implementation, we use Benders' optimality cuts. As described in Section 3.5, the Benders' optimality cuts take the following form

$$\beta_k^\top x + \eta \geq \alpha_k \tag{6.31}$$

where

$$\beta_k = \sum_{s \in \mathcal{S}} \pi_s (\sigma_s^k)^\top T \quad \text{and} \quad \alpha_k = \sum_{s \in \mathcal{S}} \pi_s (\sigma_s^k)^\top r(\omega_s) \tag{6.32}$$

With this optimality cut added, we re-optimize the master problem and update the current lower bound. At this point, one ordinary iteration of the D2 algorithm is completed and one of three conditions must hold in the current node:

(i) The master problem (6.18) has become infeasible;

(ii) The difference between the upper and lower bound is below some small threshold ϵ;

(iii) The difference between the upper an lower bound is greater than some small threshold ϵ;

If (i) holds, the node is closed and marked as infeasible. We pick a new node from the tree and run the D2 algorithm on that. Note that because our problem has complete recourse, this would never happen in the root node of our problem. If (ii) holds, this node has been run to optimality. If the objective function value is lower than the current upper bound on the entire tree, this node's upper bound is the new upper bound on the tree. All expanded nodes with a lower bound higher than the new tree upper bound are closed by bound. Finally, if (iii) holds, then we need to continue running the D2 algorithm on this node. However, because we have continious variables in our master problem, we might have to branch on the x-variable and create two new nodes.

Branching

In the original D2 algorithm by Sen and Higle (2005), the first stage variables are all integer. It follows that the optimal x^k at each iteration of the master problem is in a vertex of the set of feasible values, X. The disjunctive cuts are created and convexified on a given value x, ensuring

that in the verteces of X, $\pi_0(x^k, \omega) = \pi_c(x^k, \omega)$ for all $\omega \in \Omega$. When the first stage variables are continuous, however, this equality might not hold. If the equality holds, we perform another iteration of the D2 algorithm. If it does not hold, i.e., $\pi_0(x^k, \omega) \neq \pi_c(x^k, \omega)$ for some $\omega \in \Omega$, we branch on the scenario $\bar{\omega}$ where the equality is most violated.

Proposition 1 in Ntaimo and Sen (2007) describes how the feasible region of X is split into two subsets guided by $\pi_0(x^k, \bar{\omega})$. The split is made where the two linear functions that make up the piecewise linear $\pi_0(x, \bar{\omega})$ are equal. These two subsets make up the feasible regions for the first stage variables x^k in two new nodes in the tree. In each new problem, the D2 cut $\pi y \geq \pi_c(\omega, x)$ is replaced by $\pi_0(x, \omega)$ restricted to the new feasible region of X. $\pi_0(x, \omega)$ is thus a linear function in each new node, as illustrated in Figure 6.

We can summarize the D2 iterations and branching scheme by looking at the master and subproblem after $|K|$ iterations, where K is the set of all algorithmic iterations k performed. We introduce the index $q \in Q$, where Q is the set of all expanded nodes. Let B_q be the set of all ancestors of q, including the initial root node, so that $\tau \in B_q$ is an ancestor of q in the branch-and-bound tree. Let $k(\tau)$ denote all algorithmic iterations k performed in node τ so that $k(\tau) \subseteq K$, and let $\kappa(\tau)$ denote the iteration when branching was performed in node τ. The master problem in node q will take the form:

$$
\begin{aligned}
min \quad & c^\top x + \eta && && \text{(6.33a)}\\
\text{s.t.} \quad & Ax \geq b, && && \text{(6.33b)}\\
& \beta_k^\top x + \eta \geq \alpha_k, && k \in k(\tau), \tau \in B_q && \text{(6.33c)}\\
& (\bar{\gamma}_{q_h}^k)^\top x \geq \bar{\nu}_{q_h}^k, && h \in \{0,1\}, k \in \kappa(\tau), \tau \in B_q && \text{(6.33d)}\\
& x \geq 0 && && \text{(6.33e)}
\end{aligned}
$$

(6.33b) is the master problem at the root node. (6.33c) are the Benders' optimality cuts made at every iteration k, and (6.33d) are the branching cuts. For every iteration $k \in k(\tau)$, node q contains either the cut for $h = 0$ or $h = 1$, making the other node born from the parent τ its sibling node.

For the subproblem, we denote the current iteration of the algorithm at node q as k_q to emphsize that the subproblems are functions of the current master problem solution. The subproblem takes the form:

$$
\begin{aligned}
f_c^{k_q}(x^{k_q}, \omega) = min \quad & g^\top y && && \text{(6.34a)}\\
\text{s.t.} \quad & Wy \geq r(\omega) - Tx^{k_q}, && && \text{(6.34b)}\\
& \pi_k^\top y \geq \pi_c^k(x^{k_q}, \omega), && k \in k(\tau) \setminus \kappa(\tau), \tau \in B_q && \text{(6.34c)}\\
& \pi_k^\top y \geq \pi_0^k(x^{k_q}, \omega), && k \in \kappa(\tau), \tau \in B_q && \text{(6.34d)}\\
& y \geq 0 && && \text{(6.34e)}
\end{aligned}
$$

(6.34b) is the subproblem formulation from the root node. (6.34c) are all the disjunctive cuts at every iteration that does not precede a branch. If a disjunctive cut leads to a branch, the cut from (6.34c) for that iteration κ is replaced by (6.34d). The algorithm runs iteratively until there are no more expanded nodes that have not been closed. A node can be closed by branching, by infeasibility, by bound, or by optimality. When the algorithm terminates, it returns the first stage solution of the node that yielded the lowest upper bound, i.e., the best feasible solution.

7 Computational Study

This section outlines how we tested the two-stage stochastic model. It describes how and from where data is gathered, the procedure for generating solar power production scenarios with this data, and the procedure we use for testing the model. In the final subsection we present and discuss the results and performance of our implementation.

7.1 The Guinean Hybrid Power System

The Guinean hybrid hydro-solar system consists of two reservoirs in cascade, as described in Section 4. The upstream reservoir, Frankonédou, is significantly larger than the downstream reservoir Kogbédou. Discharge from Frankonédou flow into Kogbédou. The system is estimated to have a yearly power generation of 468 GWh (Lombardi 2022). A visualization of the planned reservoirs are given in Figure 7.

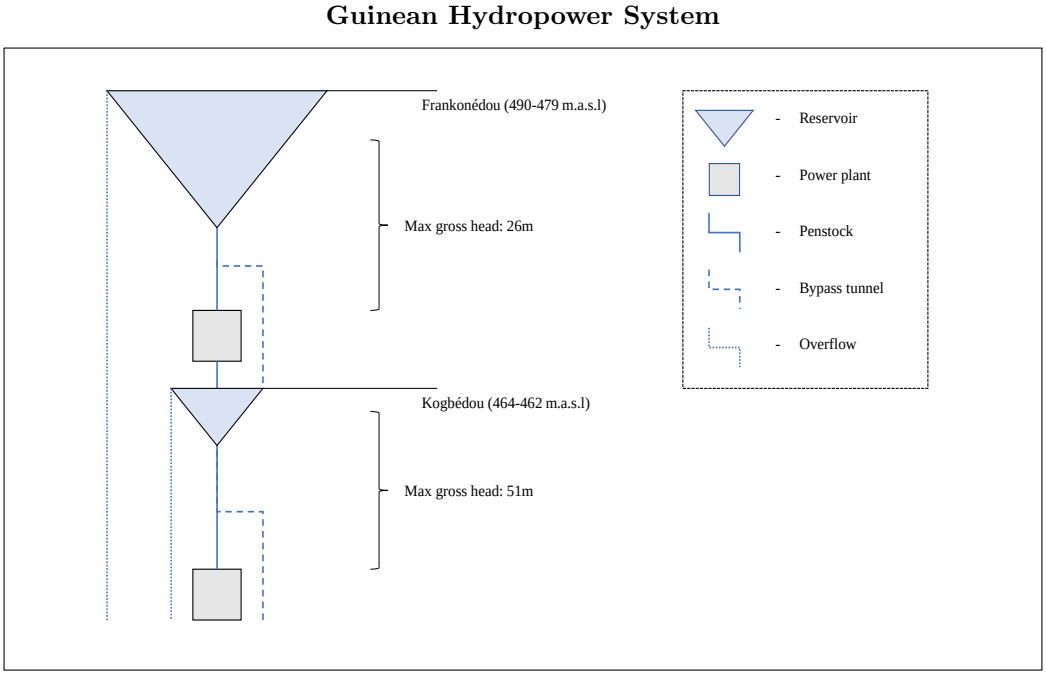

Figure 7: Visualization of the cascading reservoirs with connected power plants

Both reservoirs contain one power plant, each with two turbines. The turbines in each power plant are identical Kaplan turbines. This means that the turbine efficiency given some head and discharge combination is equal for both turbines in each power plant. As mentioned in Section 4, the turbines are connected to the reservoir through the same penstock, and it is possible to discharge different amounts of water to each turbine. Data for the power system is provided in Table 2.

	Frankonédou	Kogbédou
Reservoir Capacity (Mm^3)	1375	17.8
Power plants	1	1
Turbines in power plant	2	2
Max gross head (m)	26	51
Min discharge per turbine (m^3/s)	24	30
Max discharge per turbine (m^3/s)	80	100
Max discharge (m^3/s)	160	200
		Total
Grid capacity (MW)		135
Solar power production capacity DC (MWp)		147
Estimated power generation (GWh/year)		468

Table 2: Data for the Planned Power System

7.2 Data Handling

Most of the data used in this study was provided by Scatec and SINTEF. Some of this data had to be processed in order to use it in our optimization program, and some values had to be computed from this data. Some data was also possible to use directly. These processes will be explained in this section, as well as a description of the data used.

Breakpoints for the HPF

The breakpoints from the HPF are derived from the Hill chart of the turbines in the hydropower plant. As mentioned in Section 3.2, Hill charts are commonly used to create breakpoints. These Hill-charts were provided to us from SINTEF. The Hill chart for reservoir Frankonédou is shown in Figure 8.

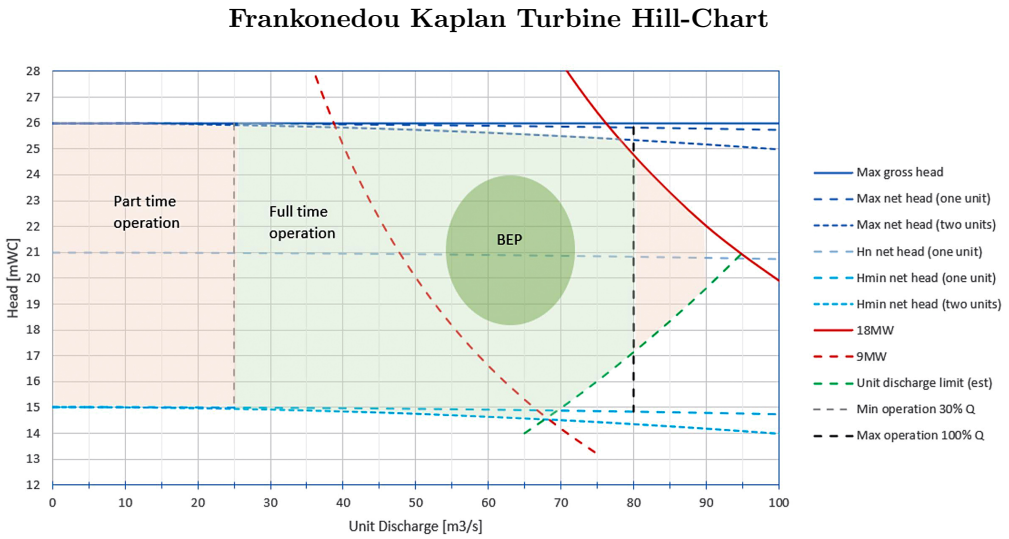

Figure 8: Hill chart for the Kaplan turbines at Frankonédou. Image provided by SINTEF.

Discharge (m^3)	*Net Head (m)*				
	14.53	**17.18**	**21.00**	**24.70**	**26**
24	82.9178%	86.1545%	87.8740%	86.1545%	84.6643%
35	89.9981%	92.6027%	93.8923%	92.6027%	91.4850%
42	93.3613%	94.8914%	95.8072%	94.8914%	94.3710%
46	94.2115%	95.8072%	96.3543%	95.8072%	95.1689%
54	95.2025%	96.3557%	96.9014%	96.4626%	96.2176%
63	95.8570%	96.6501%	97.2092%	96.7274%	96.4538%
68	95.8072%	96.5823%	97.0382%	96.6507%	96.4227%
72		96.3557%	96.9014%	96.4626%	96.2176%
80		95.8072%	96.3543%	95.8072%	95.1689%

Table 3: Turbine efficiencies for the Kaplan turbines at Frankonédou. Best efficiency points are in red.

Discharge (m^3)	*Head (m)*				
	47.66	**48.59**	**49.59**	**50.59**	**51**
30	93.5201%	94.0863%	94.3147%	94.0863%	93.8796%
49	94.9504%	95.1371%	95.2285%	95.1371%	95.0545%
58	95.2574%	95.3800%	95.4449%	95.3800%	95.3269%
68	95.4017%	95.5356%	95.6133%	95.5356%	95.4735%
79	95.4756%	95.6256%	95.7614%	95.6256%	95.5521%
90	95.4017%	95.5356%	95.6133%	95.5356%	95.4735%
100		95.3800%	95.4449%	95.3800%	95.3269%

Table 4: Turbine efficiencies for the Kaplan turbines at Kogbédou. Best efficiency points are in red.

Based on the Hill charts provided, it is possible to calculate the turbine efficiencies for given combinations of net head and discharge, as mentioned in Section 3.2. Table 3 and Table 4 show the turbine efficiencies derived from the Hill chart. The efficiencies were derived by SINTEF.

From the table we can create turbine efficiency curves for given head values. These are shown graphically in Figure 11 and Figure 10 for the Kogbédou reservoir in both two and three dimensions. The visualization of the turbine efficiencies showcase the importance of having discharge dependent net head when the production accuracy should be high.

Based on the efficiency tables we have calculated the power output for each discrete combination of net head and discharge. These values were computed using the formula for hydropower generation from Section 3:

$$P = G\eta_g\eta_t\bar{h}\bar{q} \tag{7.1}$$

where $\bar{h}$ and $\bar{q}$ are the discrete values from the table, and η_g is included in the term for turbine efficiency, η_t. This leads to identically dimensioned tables as Table 3 and Table 4, but the turbine efficiencies are instead replaced with the amount of power generated for the combinations of discharge and head.

Turbine Efficiency Curve for Kogbédou

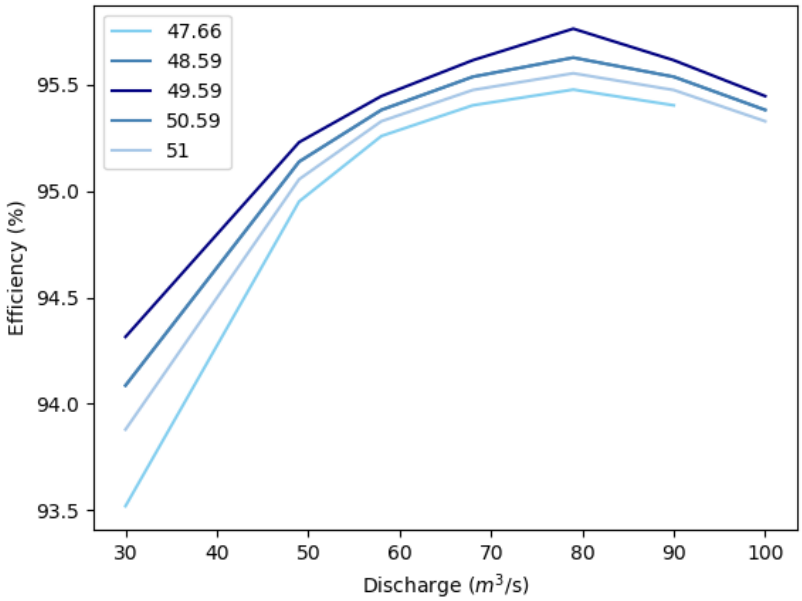

Figure 9: Turbine efficiency curves for different net head levels at Kogbédou. Notice that there are only 4 curves, as the curves for 48.59m and 50.59m net head lie on top of each other.

Turbine Efficiency as a Curved Plane for Kogbédou

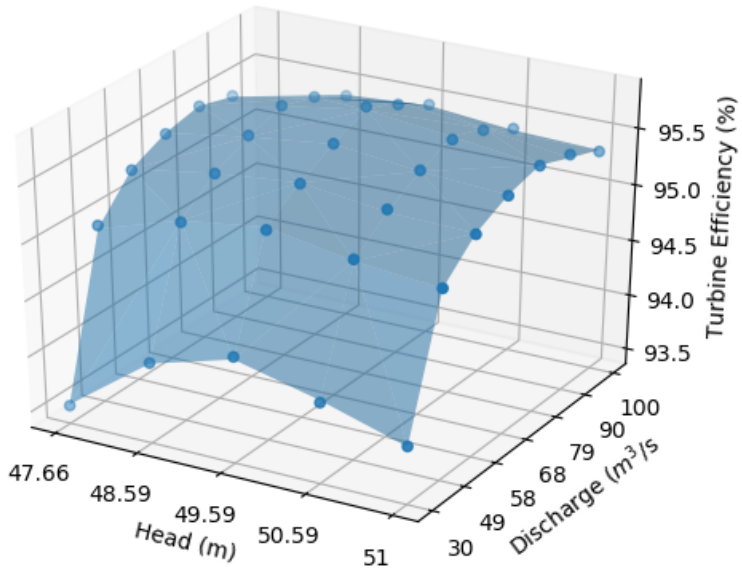

Figure 10: Turbine efficiency as a curved plane of a turbine in Kogbédou reservoir.

Approximation of Gross and Net Head

In addition to the power output, the relationship between gross head and water volume has been linearly approximized for each reservoir. We received data on the relationship between the water level in meters above sea level and the water volume for both reservoirs. This allowed us to easily create breakpoints and a piecewise linearization of the gross head/volume relation for each reservoir. For Frankonédou reservoir, some breakpoints on the linearization were omitted. In Kogbédou however, some artificial breakpoints were created. This was done to create lists of the same size without loosing too much accuracy.

Gross Head (m)	15	17	19	23	26
Volume (Mm^3)	206.375	329.875	484.875	916.875	1375

Table 5: Breakpoints in the calculation between gross head and volume for the Frankonédou reservoir.

Gross Head (m)	49.0	49.5	50.0	50.5	51
Volume (Mm^3)	5.5	7.5	10	13.5	17.8

Table 6: Breakpoints in the calculation between gross head and volume for the Kogbédou reservoir

Recall that the relationship between gross head and net head is dependent on discharge squared as well as a friction coefficient:

$$h_{r,t} = h^G_{r,t} - \mu_r(\sum_{k \in \mathcal{K}_r} q_{k,t})^2, \quad r \in \mathcal{R}, t \in \mathcal{T} \tag{7.2}$$

The friction coefficient was provided to us by SINTEF. We will refer to this curve as the net head curve. We approximate this function as a linear function, as mentioned in Section 6.1. This linear function was found creating a line that intersects the net head curve in minimum discharge and best efficiency discharge. These two points were selected as it was expected that the mathematical model would keep discharge near these two points most of the time. That is because the maximum efficiency point is the most resource effective point, and the minimum discharge point is the lowest possible discharge where the environmental restriction are kept but the power plant still profits off the water. Therefore we saw it as most important to keep these two approximated values as close to their true values as possible. With these two intersections, the largest approximation error is 0.1174 for Frankonédou and 0.2945m for Kogbédou. These errors are small enough to be negligable.

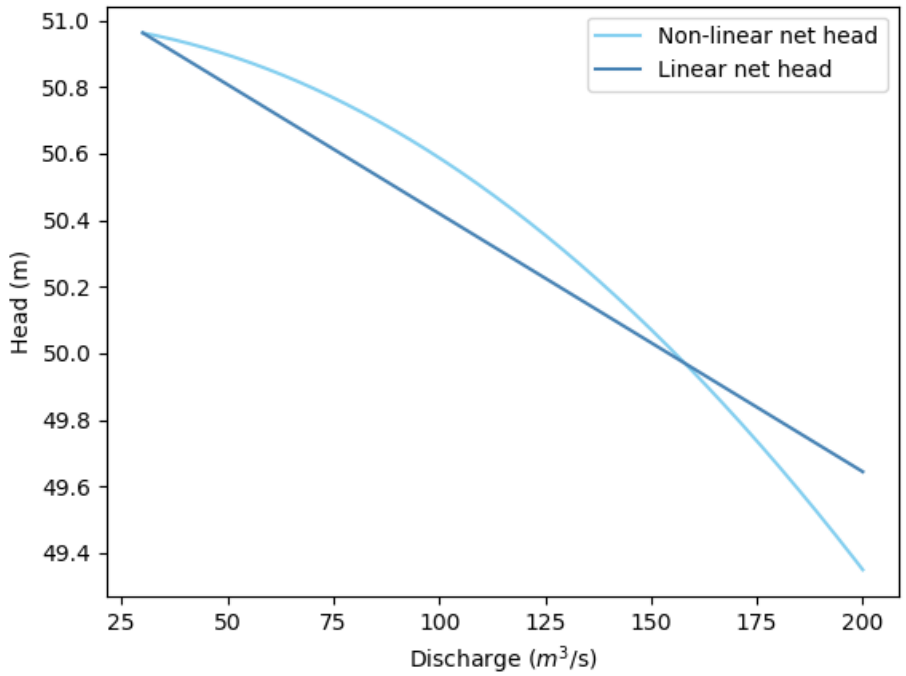

Figure 11: Net head linear approximation for Kogbédou reservoir. The reference head used is maximum gross head. Only feasible discharge values are plotted, i.e., $30 \leq$ discharge ≤ 200.

Weather Data

The scenario generation procedures, the planning models, and the simulation models all utilize external datasets. These has been gathered from several sources, and this section outlines where the different datasets originates from. In addition, we will describe the preprocessing that has been performed on some of them.

An overview of the monthly inflow to the reservoirs was provided by SINTEF, and spanned from 1970 to 2017. The inflow data is actual measured flow in the rivers that are suppose to make up the planned reservoirs of the hydropower plant. These values were originally provided as average m^3/s for each month. As we wanted more variation of inflows each day, we calculated the accumulated inflows of each month and interpolated the days in between each month end. We used monotonic cubic spline interpolation to ensure that there were no days of negative inflows. A comparison of the inflow before and after interpolation is shown in Figure 12. In reality, days of negative inflows could be possible in these regions, as the evaporation is non-negligible at times, but for the scope of this thesis, evaporation has been ignored. The interpolation gave us a smoother curve of inflows from day to day. For the intraday hourly inflows we simply divided the interpolated daily inflow by 24. An overview of the yearly variations is shown in Table 7 and an illustration of the seasonal variations can be seen in Figure 13.

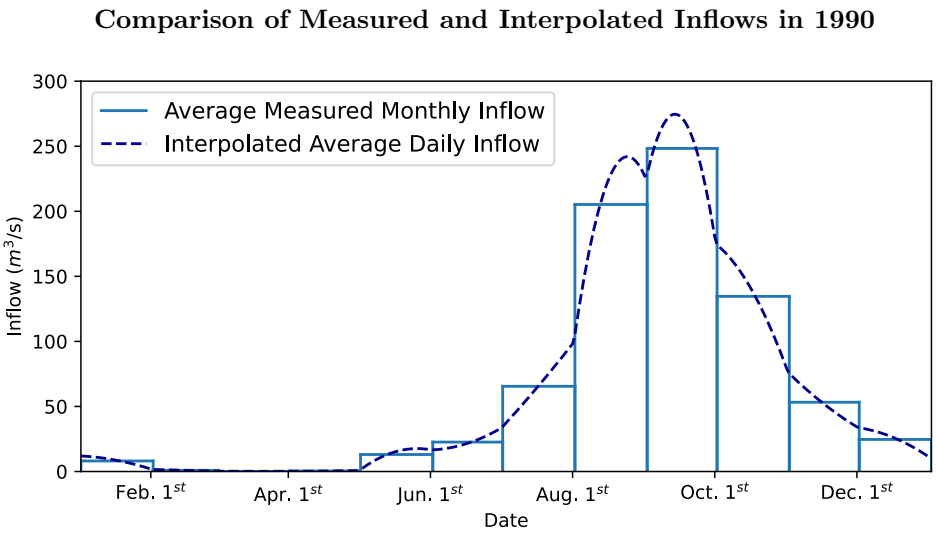

Figure 12: Comparison of measured and interpolated inflows in the Frankonedu reservoir in 1990.

Year	1987	1988	1989	1990	1991	1992	1993
Inflow	248	201	216	196	218	213	239

Table 7: The combined average daily inflow of both reservoirs in Mm^3.

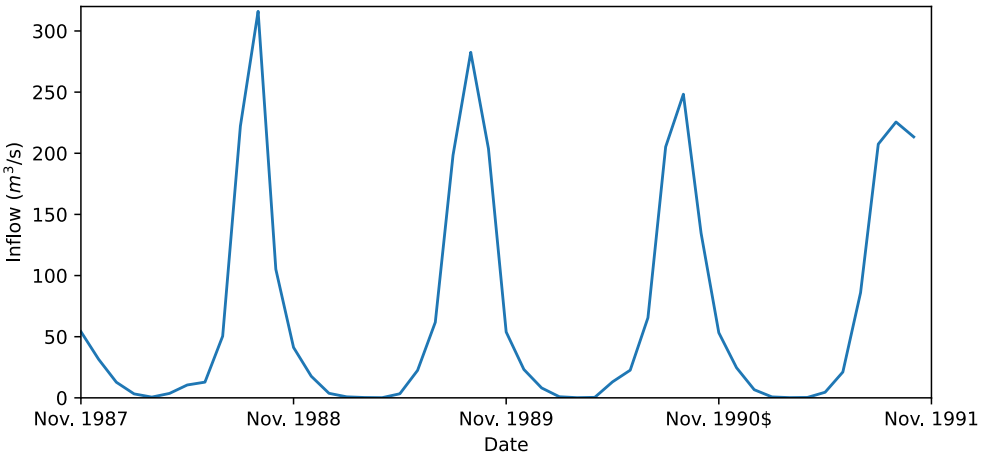

Figure 13: Average monthly inflow to the reservoirs.

The other weather related dataset provided by SINTEF was an estimation of PV generation at a hypothetical 147 MWp PV power plant, given in hourly MWh. The estimations are based on weather data from 1990, a year that is, according to SINTEF, considered a climatically representative for the region. In our simulations, this is the dataset we have used to simulate the actual PV power production in the hybrid power system.

The NWPs on wind, temperature, and irradiation used as input in our models are not actual historic weather predictions. They are taken from the ERA5 reanalysis dataset (Muñoz Sabater 2019). These are estimates made many years after but represent approximated NWPs based on analysis of complex weather systems. In a sense, this is similar to how an NWP for the future is made. For the purpose of this thesis, it is considered precise enough, and is treated in our models as actual forecasts.

The ERA5 irradiance data is given as hourly energy per m^2. Inside an accumulated hour, many fluctuations in instantanious irradiance can be hidden. To capture these fluctuations, we increased the granularity to minutes. This is done the same way as with the inflow, by interpolating every minute between the accumulated energy. This leaves us with the average instantaneous irradiance of every minute. Wind and temperature data is also taken from the ERA5 dataset but interpolated to minutely resolution by simple linear interpolation between hours. Wind and temperature are kept constant in all scenarios. Including them as a function of the scenario irradiance would introduce weather complexity beyond the scope of this thesis.

Additional Data

Other data regarding this specific hybrid power plant was given to us by SINTEF and Scatec. This includes the monetary values in the PPA with exception of the penalty cost, start-up costs for the turbines and the friction coefficient for discharge. Based on discussions with Scatec, we assumed the penalty cost to be slightly higher than the peak price, and chose this to be 150 \$/MWh compared to the peak price of 120 \$/MWh. The other prices from the PPA provided by Scatec were used driectly. Both start-up costs and friction coefficients can be challenging to calculate. Approixmations of these were provided by SINTEF. The start-up costs were the same for the turbines connected to both reservoirs. We chose to increase the start-up costs of the turbines for the lower reservoirs by 14% to reflect the significantly higher head of this reservoir.

All data concerning the direct physical attributes of the power plant, such as water volume, installed PV capacity, minimum and maximum discharge, grid capacity etc. was also provided. Most of this data was used directly without processing. However, grid capacity was increased by 7%. This modelling choice was made to not allow neither the hydropower plant nor the solar power plant to produce at maximum grid capacity. This adjustment makes sure that both power sources are always relevant. The intent is to introduce more variation to the simulations, and more varied results.

7.3 Scenario Generation Hyperparameter Tuning

Hyperparameters are fixed constants that influence the output of a model and can be adjusted prior to running it. In our solar scenario generation, described in Section 6.3, there are eleven tunable hyperparameters. In the original paper by Iversen, Morales et al. (2014), tuning is performed mathematically. They do however have access to the actual observed minutely weather data and predictions, something we do not. To determine the optimal values, we employ the brute force approach and run the model with thousands of different combinations of hyperparameters, evaluating each result. To assess the tuning, we examine the number of actual energy output observations falling within different prediction quantiles generated. Although it is generally discouraged to evaluate predictions on data used for tuning, we consider 1990 as a representative year in this region, assuming that the seasonal patterns will repeat the following year. Thus, we perform hyperparameter tuning on the entire available dataset. A comparison of the hyperparameter values used in this project report and the original paper by Iversen, Morales et al. (2014) is presented in Table 8. For detailed explanations of their functions, we refer to Section 6.3.

	μ_x	σ_x	σ_ϵ	β_x	γ	θ_α	μ_α	σ_α	ω_1	ω_2
Original paper	0.879	0.655	2.89	0.00298	0.887	1.16	-1.08	1.60	0.172	0.116
This project report	0.67	1.00	2.89	0.00898	2.40	0.15	-2.6	14	0.10	0.0

Table 8: Hyperparameters used in the scenario generation.

7.4 Simulation

This subsection explains what data we use when running the simulation procedures outlined in Section 6.4. As the solar data provided is from 1990, this is the year in which we will run all our simulations. The inflow data dates all the way back to 1970, allowing us to run the mid-term model over the necessary flooding seasons.

The first step of the general procedure is the mid-term model calculation of initial water volumes and water values. In this step, we use the inflow data from Section 7.2, and run the model from 1989 to 1991. In terms of calculating initial water volumes, allowing our model to run on future inflow data is legitimized by the fact that water volumes is something one would be able to measure in a real life setting. With the water values, we need some other argument to allow the usage of future data. Looking at the daily inflows in Table 7, we see an oscillation in the data. From this, it is expected that the values of 1990 are to be lower than in 1989, and that 1991 is more similar to 1989. With the rough granularity and long horizon of the mid-term model, it seems reasonable to use the future values as expected values without introducing unrealistic precision in the calculations of water values. We define the rainy season to end on October 31st every year, meaning we either run the mid-term up to this date in 1990 or in 1991, whichever is more than 32 weeks away. This is done to give the mid-term a sufficient time horizon to calculate the water value, as mentioned in Section 3.2

One prominent tendency we observe in our simulations is high starting water volumes. This is the result of two aspects of the model: our linearisation of the mid-term HPFs (6.2) and the fact that the model runs deterministically. Firstly, with the Taylor expansion around the mean head in the HPF, we observe that the mid-term model is actually able to generate power without discharging water. While this does not effect the calculation of water values significantly, it does mean that the water volume is kept unrealistically high. Secondly, the model runs deterministically. It knows exactly how much volume needs to be cleared to face each rainy season, hence it never empties the reservoirs to reduce the risk of overflow. In combination, these two aspects leads to the lowest starting volume of the upper, large reservoir being 1005 Mm^3. This represents a mere 32% of the total available discharge having left the upper reservoir. Simulating our configurations with these artificial head values means that the consequence of releasing too much water is reduced in the 14 day period. This is caused by the non linear relationship between volume and head, where the head, and consequently the turbine efficiency, would be reduced faster at lower volumes in the reservoirs. It is important to keep these effects in mind while interpreting the results.

Moving on to the different configurations of the simulations, they all run with the same, deterministic inflow data as the mid-term model. For the solar data, we first look at how we have run the three setups that utilize scenarios. The scenario generation algorithm is run with the NWP of the following day. These weather predictions are the interpolated datasets described in Section 7.2. In addition, it takes in the predicted PV power generation, what we reference as the deterministic dataset, and the actual PV power generation from the last 14 days. The two latter datasets are used to calculate the correlation of variation in the scenario generation. This leaves us with our desired number of solar power generation scenarios and their corresponding probabilities. Because of the use of deterministic equivalents, we limit the number of scenarios to three; one high generation, one low generation, and one highly likely scenario. An example of scenario sets from different seasons compared to the forecasted and actual power generation can be seen in Figure 14. This combination of scenarios allows the model to see and evaluate the extremes and the most likely scenarios.

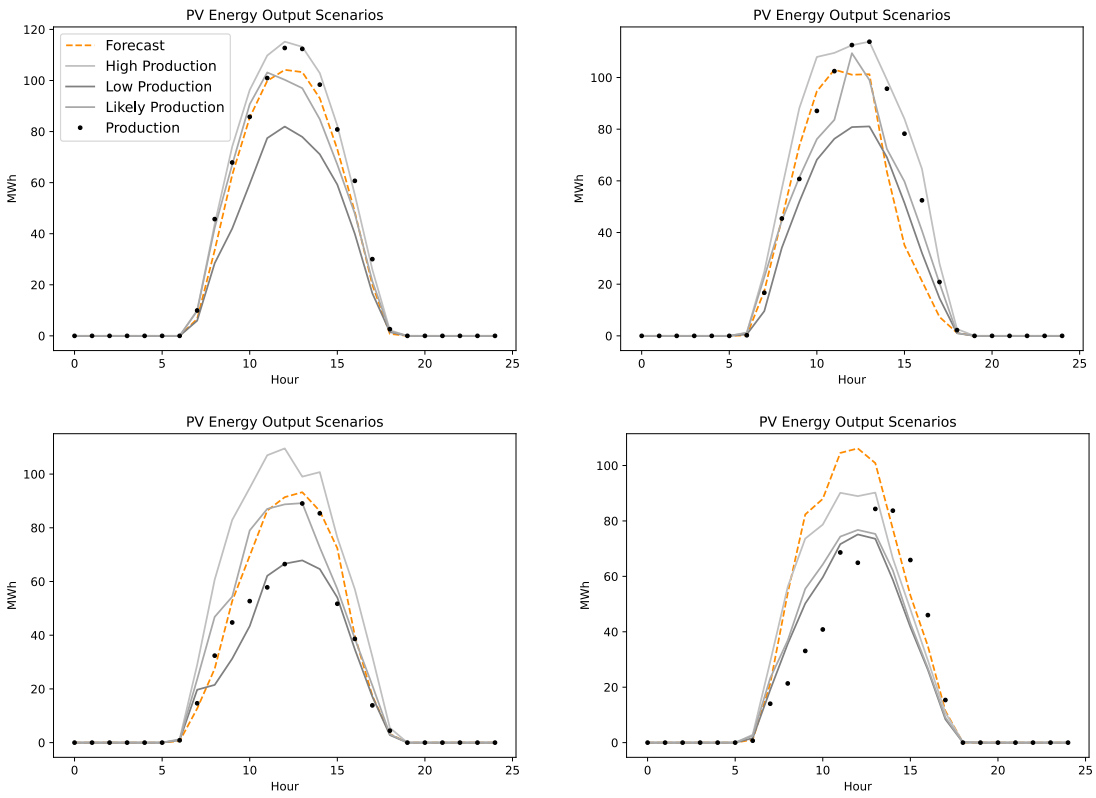

Figure 14: PV power generation scenarios, forecasts, and production for days in different seasons. The dates are January 18^{th}, April 5^{th}, July 2^{nd}, and October 10^{th}.

The scenarios are used in the planning phase. The deterministic configuration is run in planning mode with only the deterministic dataset, i.e., the predicted irradiance converted to power production. After the planning phase, all configurations are run with their load commitments fixed. The PV power generation data used in this step is the actual PV power production, simulating the production from the allready planned day. All configurations utilize the same PV production data. At this point, we save the outputs for use in analysis, before we run the entire sequence again. For the next iteration we use the volumes outputted by the short-term simulation, not the calculated volumes from the mid-term. Figure 15 and Figure 16 show an overview of the simualtion procedure and the use of external datasets for the hybrid and the separate configuration.

Even without scenarios, the complexity of our short-term model implementation is quite high. There are 48 interlinked timesteps with several linearized functions, using hundreds of binary variables at each timestep. To avoid simulations running for an unreasonable amount of time, we set the maximum solution time for each step of each configuration to three hours. If this limit is hit, the model returns the current best feasible solution. In our tests, the largest optimality gap when a time limit was hit was 0.47%. This assessed to not introduce severe problems to our results.

We begin the simulations with data from January 15^{th} 1990 in order to have two previous weeks to calculate the coefficient of variance for the scenario generation. Recall from Section 6.3 that we use the two previous weeks of NWPs and actual PV production in the scenario generation process. The simulation is run over 14 days. Covering all 14-day periods in 1990, except the first 14 days and the last 15, gives a total of 24 simulation periods. All tests are run on a system with Intel E5-2643v3, CPU 2x3.4 GHz processor, 12 cores and 512 Gb RAM. The python version is 3.10.8-GCCcore-12.2.0 and Gurobi version 10.0.

Data Flow of Hybrid Configuration Simulation

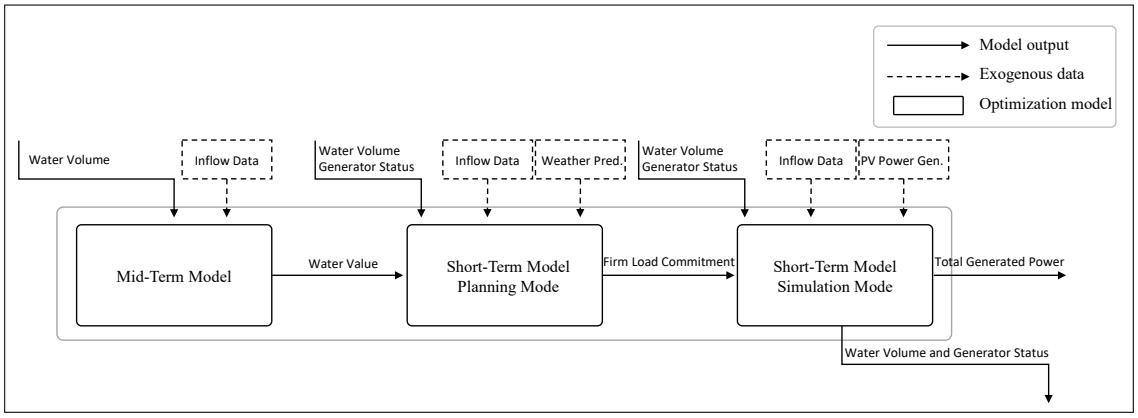

Figure 15: An overview of data flow in one day of simulation for a hybrid power system configuration.

Data Flow of Separate Configuration Simulation

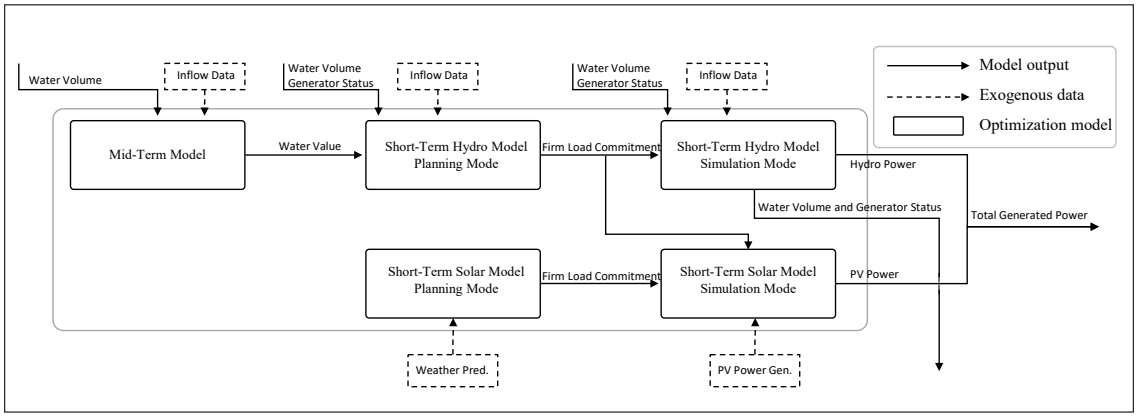

Figure 16: An overview of data flow in one day of simulation for the separate power system configuration.

The Impact of Data and Accuracy in Estimations

The attributes of the hybrid power system, such as size, location and layout, impacts both the solution time and the precision of the short-term production planning. Firstly, because of these attributes the input data consists of data in very large ranges. The variable $v_{r,t}$, which describes water volume of reservoir r in timestep t, has an order of magnitude of 10^9 in the largest reservoir. In comparison, the water value ϕ_r or the slope of the net head linearization a_r has an order of magnitude of 10^{-3}, where the water value has up to 8 significant decimals. These large size differences in coefficients and variables may lead to numerical instabilities and longer solution times. Scaling and rounding these variables so that they are closer in size first and foremost leads to a loss in precision, but it also lead to less numerical precision in our solver. This may be because several variables gets an increased amount of significant decimals, something which is hard for the solver to handle.

The power system is also constructed with two power plants, one for each reservoir, that each has two identical turbines. The turbines in the same power plant has the same head values, the same minimum and maximum discharge and the same start-up costs. This means that there are several identical solutions where it does not matter which turbine is in use. This leads to symmetrical solutions, which increases the solution time for the model. Had there been small differences between the turbines, the model might have been solved in a shorter amount of time.

The data handling leads to some imprecisions in our implementation. Firstly, some accuracy in the

representation of the HPF, gross head and net head is lost when approximating these as piecewise linear functions. These functions, especially the HPF, are necessary to approximate in order to solve the optimization problem. We have selected a linearization method for the HPF that is proven to be accurate as mentioned in Section 3.2, and essentially the same method is selected for the gross head linearization. In the case of the net head linearization the approximation error is low enough to be acceptable in our case. We therefore see these approximation errors as small enough to be insignificant to our solution.

Secondly, the granularity of both the inflow data and the irradiance data reduces the accuracy of our models. Though we solve this to some extent to some extent by the interpolation procedures, rapid changes in either dataset are not represented. Especially in the solar scenario generation procedure, large and rapid changes could effect the outcome. There might for instance be a short period of PV power generation that would have lead to the grid capacity being exceeded. As the solar power is averaged over one hour, this is not represented in the model.

As discussed previously in this section, the absence of historical volumes for the reservoirs and our inaccurate approximations also presents an imprecision in the simulations and the results. We chose to not introduce stochastic inflow in the mid-term model. This is a simplification based on the cyclic and relative predictability of inflows. Introducing some stochasticity in this data could however have affected the water values and as mentioned, the approximated starting reservoir volumes.

7.5 Results

This subsection presents the results. The simulation procedure has been run for 24 14-day periods on all configurations. Recall from Section 6.4 that we refrence the four configurations as the hybrid, the separate, the deterministic, and the heuristic configuration. We will first interpret the difference between the hybrid and the separate configuration. Then we will examine the effects, benefits, and costs of introducing stochasticity by comparing the hybrid and the deterministic configurations. Finally, we look at how planning with an exact solution compares to planning with its LP relaxation by comparing the hybrid and the heuristic configuration. For all configurations we will first present the results before we analyze the causes and implications of these.

The key results from all configurations are presented in Table 9. To highlight the effects of seasonal variations on the results, they are presented as semi-annual and annual results. The first half of the year is characterized by low inflows, as seen in Figure 13, and quite stable, high PV production. The forecasted PV power production in this period is on average 0.5% higher than the actual production. The second half sees high inflows, while the PV power production on average is 3.6 % lower. This period is also characterized by less accurate NWPs, as the forecasted PV power production is 9.63% lower than the actual production on average.

We present the revenue, costs, and profits, both including and excluding the cost of water. Because the short-term model is a minimization problem, revenue is calculated by summing all negative terms of the objective function for the first 24 timesteps. The cost of water is the value of the net difference in reservoir water volumes, i.e., inflow minus outflow. The costs presented in Table 9 does not include the cost of water to highlight operational costs between the different configurations. The costs are thus all the positive terms in the objective function except the cost of water. We present the profits as revenue subtracted costs. We do however present the profits with the cost of water subtracted as well. This value reflects the actual objective function value that our models try to minimize.

We have chosen to present both with and without the cost of water to highlight the differences between the four configurations. In some of the analyses we present calculations based on results that are not presented in Table 9. This data can be found in the complete results file in the appended file folder.

Period	Configuration	Revenue	Costs	Profits	Profits Incl. WC
First Half	Hybrid	39,588,399	459,478	39,289,922	15,706,178
	Separate	40,914,048	6,266,896	34,647,152	8,666,481
	Deterministic	39,260,125	417,155	38,842,970	15,711,738
	Heuristic	38,636,352	475,774	38,160,578	15,401,080
Second Half	Hybrid	46,189,204	587,898	45,601,307	45,006,636
	Separate	45,521,229	1,784,659	43,736,569	40,656,224
	Deterministic	46,178,708	582,807	45,595,901	44,979,248
	Heuristic	45,970,979	639,345	45,331,633	44,848,958
Full Year	Hybrid	85,777,604	1,047,375	84,730,229	60,712,814
	Separate	86,435,276	7,383,721	78,383,721	49,322,705
	Deterministic	85,438,833	999,962	84,438,871	60,690,986
	Heuristic	84,607,331	1,115,119	83,492,212	60,250,038

Table 9: Accumulated results over all simulations for all four configurations. Water costs abbreviated WC. All values in $.

Hybrid vs Separate

We first compare our hybrid to our separate configuration. The separate configuration results in Table 9 is the combined results of the hydropower and solar power producer. On average, we see that the annual revenue is 0.77% higher in the separate case. The costs are, however, as expected, much higher. The combined costs of penalty and generator start-ups are 769% higher in the separate configuration. In turn, this leads to the profits, excluding the costs of water, being 7.49% lower in the separate configuration compared to the hybrid configuration. Including the cost of water increases the profit gap to 18.76%. To explore this profit gap, we look at the utilization of resources. While the hybrid configuration curtails 298 MWh of potential solar power across all days in all simulation periods, the separate curtails 9952 MWh. Additionally, the separate configuration discharges 12.50% more water from the lower reservoir. On the other hand, it has 32.21% fewer generator stops and starts. Turning to the semi-annual results, we see that in the first half of the year, the costs excluding water are over 13 times higher in the separate configuration. The profits excluding water are 11.45% lower and the profits including costs of water are 54.82% lower. In the second half of the year, this gap is significantly smaller. In this period, the profits are 4.09% lower excluding water and 9.67% lower when including it.

Looking at some key takeaways from these results, we see that the setting we simulate in does not favour the separate producer. The way the PPA is constructed forces the separate PV power producer to take a large penalty in the timesteps when irradiance is low in order to balance its commitment. For the separate PV power producer, this represents a constant balancing penalty, while in the hybrid case it can be seen as a lower bound. The hybrid configuration has the option to balance out commitments by producing more hydropower rather than incurring the penalty cost, should water be less expensive than the penalty cost. The hybrid configuration's strength lies in the ability to coordinate the utilization of resources.

One metric where the separate configuration however outperforms the hybrid is on generator starts. Most likely this is because the separate configuration needs constant hydropower output to meet its obligations, while the hybrid system shuts generators down in periods of high PV power production. Since the costs of starting up a generator is hard to calculate exactly, this benefit may not be accurately represented in our calculations. Were it to be higher than what we have used in our models, the advantage of using hydro to balance out the intermittency of the PV production would be smaller. In the semi-annual results, the differences even out somewhat in the last half of

the year. This can be explained by water becoming less valuable, giving less of an advantage to the configuration with a better utilization of non-hydro resources.

Our simulations show a huge advantage in hybrid planning and operation. One could argue that the setting and market conditions we simulate are too favourable to the hybrid configuration. The hydro producer takes precedence the separate case, a mechanism that might weaken the results. Because of the favourable setting, testing in other settings and different market conditions would be valuable contributions to the research in the future.

Stochastic vs Deterministic

Turning to the effect of introducing stochasticity in the PV power production, we now compare the hybrid and the deterministic configuration. The differences between the configurations are significantly smaller than in the previous section. Without power production scenarios, i.e., in the deterministic configuration, the yearly revenues are 0.39% lower, while the costs are 4.53% lower. Combined, this gives the non-stochastic configuration a total of 0.34% lower profits, when excluding water, and only 0.04% lower profits when we include the costs of water. It should be noted that the profits including costs of water are actually slightly higher in the deterministic configuration in 18 out of 24 periods. In the first half of the year, the deterministic configuration has 0.83% lower revenues and 9.21% lower costs. Excluding cost of water, the profits are 0.73% lower. Including the cost of water, however, yields profits 0.04% higher than the stochastic configuration. In the second half of the year, the differences between the two configurations are similar. The deterministic one has revenues 0.02% lower and 0.87% lower costs. It has 0.01% lower profits when excluding, and 0.06% lower profits when including the costs of water.

Looking at the utilization of resources, they are almost identical. The deterministic configuration curtails 0.55% more solar power throughout the year, with 299.44 MWh curtailed, as opposed to 297.78 MWh. The use of water is also marginally lower. On average, the discharge in each 14-day simulation period is 0.67% lower than in the hybrid configuration. Another difference between the two configurations is the number of generator start-ups. The deterministic configuration has 1348 generator starts, while the hybrid has only 1310.

The differences in results between these two configurations are small. Figure 17 shows how the profits of the deterministic configuration, including the cost of water, compares to the hybrid configuration in all 24 14-day periods. To analyze the difference in operation, we present a detailed look at April 11^{th} and April 12^{12}. These two days represent one day where the NWP is too optimistic in terms of PV power production, and one day where it is too pessimistic. On the 11^{th}, the deterministic generates a profit, including the costs of water, that is 0.60% lower than in the hybrid. On the 12^{th} it generates 0.23% more.

Figure 18 gives an indication of the mechanics behind the difference. We see that on the 11^{th}, the predicted solar power production is too high. The hybrid configuration is able to see the possibility of lower production because of its stochastic scenarios, and it bids a lower load commitment (LC) than the deterministic configuration. When the actual production realizes and they have to produce to meet their commitments, the deterministic configuration must produce more hydropower and accumulates 5.99% higher water costs (WC). Though its revenue is 4.17% higher, its profit including water is 0.60% lower. On the 12^{th}, we see that the predicted solar power production is too low. The hybrid commits slightly higher than the deterministic configuration. This leads to it generating 2.17% more revenue while incurring 3.35% higher costs of water.

To explain the differences in the aggregated numbers, we start by looking at some numbers from the PPA. If you over-commit in a peak hour, the cost per MWh is maximum 30, i.e., the 120 you get from selling subtracted the 150 penalty cost you incur. On the other hand, the cost of under-committing is dramatically higher. If you produce more than you have committed to, you sell each excess MWh at 10, incurring an opportunity cost of 110. These differences give an advantage to the hybrid configuration. It is able to see the optimistic production scenario, no matter how low the probability of that scenario is. In fact, across all the daily production scenarios used in our simulations, the average probability of a high production scenario is almost 5% lower than that of

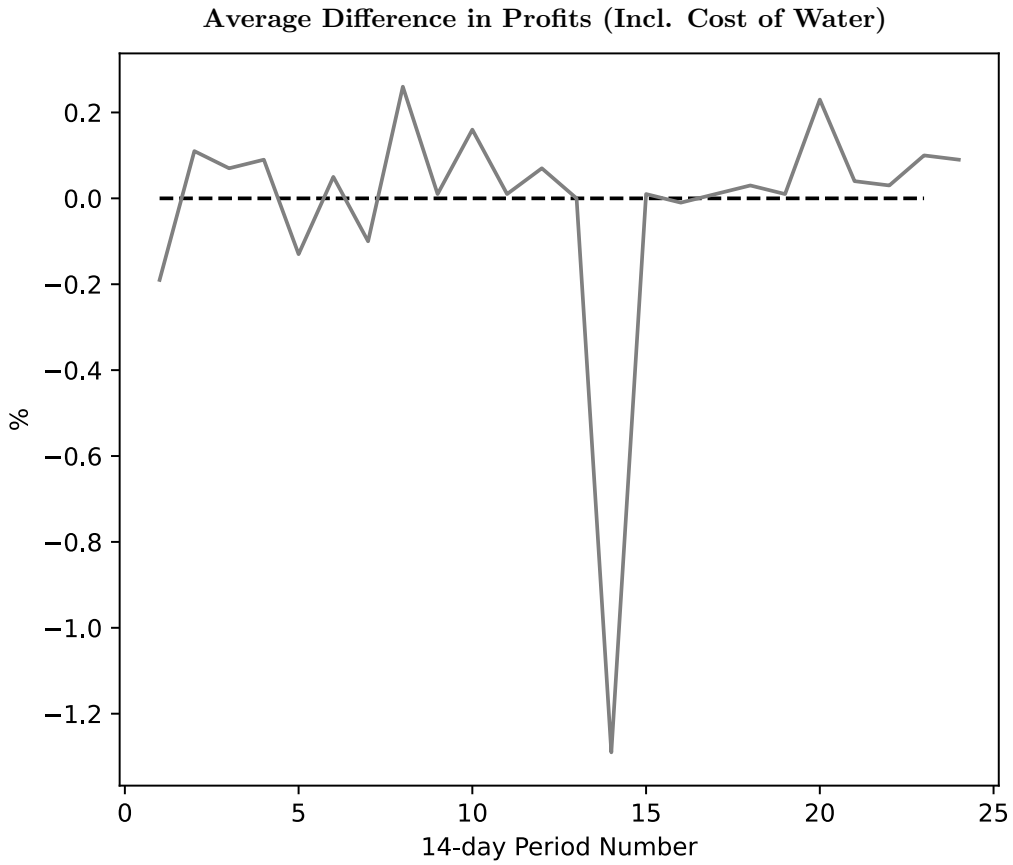

Figure 17: Plot of how the deterministic configurations accumulated profits compares to the hybrid.

low production. This means the probability of low production was higher than of high production. Yet, on average, the stochastic configuration commits slightly higher in the peak hours than the deterministic configuration.

Looking at the difference in turbine start-ups, the explanation most likely lies in the stochastic configuration committing slightly higher. When you under-commit, the peak PV production, typically around noon, would constitute a larger percentage of the committed load. This means it might not be profitable to keep the generators running, even at minimum, because the produced power can only be sold at an intermittent price. This might mean that introducing stochasticity that pushes the peak load commitment slightly higher brings a smaller toll on the generators in terms of stops and starts.

Looking at the semi-annual results, we see that the cost of introducing stochasticity is felt when the water value is high, i.e., in the first half of the year. The consequence of seeing those high production scenarios is more over-commitment that leads to more water used. The results make sense, as over-commitment in the second half of the year can easily be adjusted by hydro production using cheap water. Keeping in mind the discussion about the artificially large water volumes at the beginning of each 14-day period, more accurate water volumes could have emphasized the consequence of spending more water in the hybrid configuration. At lower water volumes, the head values and turbine efficiencies decrease more rapidly.

We might get the impression that the hybrid configuration always commits higher and therefore earns more. The effects of introducing stochasticity is however more nuanced. We see this in the detailed comparison in Figure 18. In this example, the advantage of the hybrid configuration is when it commits lower than its deterministic counterpart, i.e., on the 11^{th} of April. At the same time it sees less profits when committing higher, contradicting the analysis of the aggregated results. One logical explanation could be that the hybrid configuration performs better when the difference between the forecast and the actual PV power production is large, either on the upside

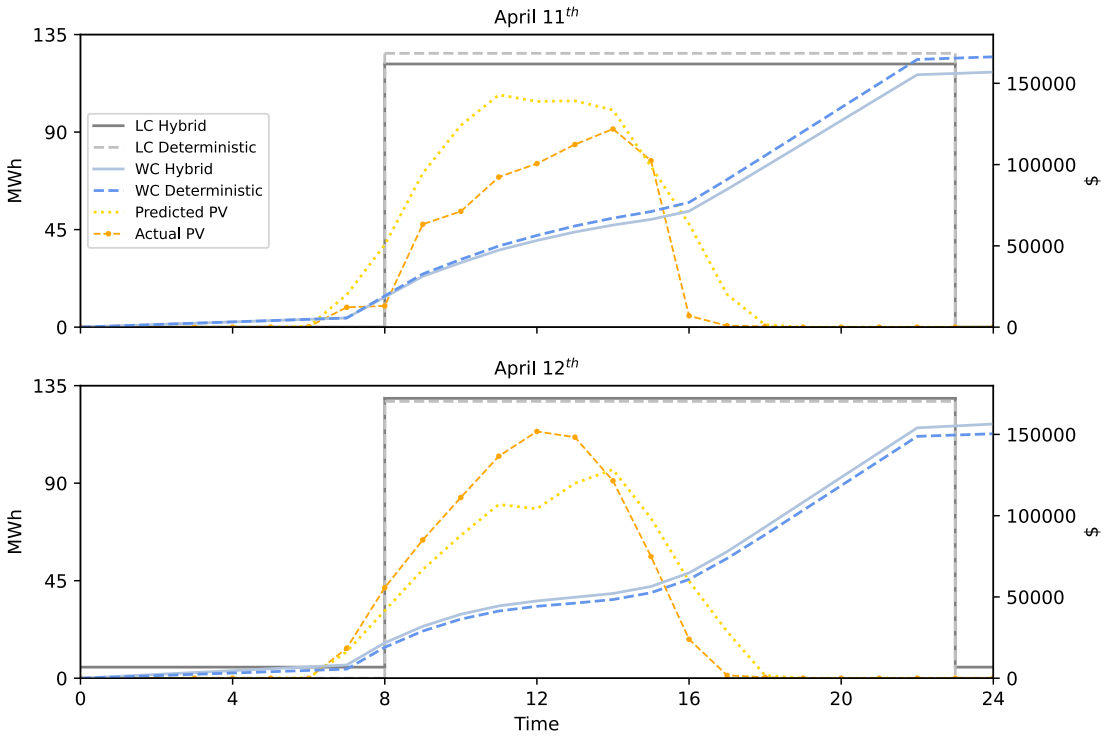

Figure 18: Load commitment (LC), accumulated costs of water (WC), and PV power prediction/generation for the hybrid and the separate configuration.

or the downside. This result is to be expected, as a non-stochastic model always performs better than a stochastic model if the non-stochastic dataset is close to the actual realisation (King and Wallace 2012). Recalling from Section 7.2 that neither the production nor the prediction data is actual data measured or predicted in 1990, we should be reluctant to conclude on the benefits of either configuration.

Exact Planning vs Approximation

The final comparison we look at is between the hybrid and the heuristic configuration, i.e., exact scenario planning using the deterministic equivalent and heuristic planning using its LP relaxation. The LP planner has 1.36% lower revenue, 6.47% higher costs, 1.56% lower profits, and 0.76% lower profits when including the cost of water. Looking at the detailed results, the heuristic planner always commits a minimum of about 7.5 MWh in the off-peak periods. This is significantly higher than in all other configurations. We know from all the other configurations we have looked at that this is by no means optimal. Additionally, the peak load commitment is lower on average in every 14-day simulation period where the commitment is not at maximum. From the comparison between the deterministic and stochastic configurations, we know that lower peak loads is no advantage either. The differences between seasons is not significant and is thus not explored further.

The explanation of the inefficient off-peak commitment lies in the relaxation of the generator status variable. With this relaxed, all generators are able to produce with the water running at the river flow minimum, which is lower than the actual generator minimum. The differences in profits and imprecision in load commitment emphasize the need for planning with an exact approximation, or a better heuristic. However, the LP-planner runs in less than a minute, while the other configurations seldom use less than ten. The exact planners average on approximately 30 minutes, often using more in the periods with high water values. If time is critical, a heuristic

plan based on the LP-relaxation could prove a valuable tool to hybrid planners.

7.6 Implementation and Testing of the D2-CBAC Algorithm

The D2-CBAC algorithm described in Section 6.5 was implemented in Python and solved with Gurobi. Our short-term mathematical model from Section 5 was translated to a master and subproblem on canonical form, with all matrices and vectors represented in sparse matrices. On this form, the constraint matrix of the subproblem was a (12960x9072) matrix, where 2592 of the 9072 variables were binary. In this section we will first describe how we tested the D2-CBAC algorithm, the issues we faced and some of the measures we took to overcome them. Then we will analyze the reasons for these issues, and discuss possible ways to overcome them in the future

After implementing the D2-CBAC algorithm, we ran it on the test-problem from Sen, Higle and Ntaimo (2003). This paper merely considers the D2 algorithm and not the Branch-and-Cut process. Therefore, the purpose of implementing this test problem was to see if the D2 part of our algorithm worked. In other words the creation of disjunctive cuts, the convexification of these cuts and adding them to the subproblem. Since we used the modified version of the objective function in the C3-SLP (6.22), as explained in Section 6.5, we ran the test-problem with both the non-modified C3-SLP and the modified C3-SLP. In the non-modified version the values of the cuts were exactly the same as in the paper, whereas in the modified version the values where somewhat different. This was not surprising, as the modified version has a slightly changed objective function in order to guarantee that a cut is found, as explained in Section 6.5. The correctness of the cuts from them modified objective value were manually checked by comparing them to the values that would have been created by Sen, Higle and Ntaimo (2003) had they also implemented this modification. The test-problem converged in 0.07 seconds and produced the same optimal solution as the paper in the same amount of iterations. We observed how our cuts correctly cut away the fractional solutions in each step.

After successfully testing the D2 part, we tested the full algorithm on the test-problem from Ntaimo and Sen (2007). This test-problem has the same structure as ours, with continuous first-stage variables and binary second-stage, although in this problem all second-stage variables are all binary, whereas in ours there are continuous second-stage variables as well. Once again, we tested the problem with both the modified and the non-modified C3-SLP. Both tests produced the same optimal solution as in Ntaimo and Sen (2007). The cuts cut away the fractional solutions and the first-stage solutions branched on the correct x-values.

After ensuring the implementation worked on the test problems, we began testing on our stochastic short-term scheduling model. The algorithm quickly branched to the first-stage variables we knew were the solution of the LP-relaxation of the problems deterministic equivalent. However, the algorithm never converged, and the iterations saw an increasing solution time, especially in the C3-SLP problem (6.22). Eventually, the algorithm would exit because the C3-SLP (6.22) became infeasible, or the disjunctive cut convexification problem (6.29) became unbounded. We know that our problem has large coefficient ranges, something that could suggest our model is ill conditioned. To gain more insight in the numerics we extracted information about the Gurobi solvers "Kappa" value. This value is the Condition Number and is a measure on how much the output value can be changed by a small input change. A large Kappa means that a problem is sensitive to numerical errors. The Gurobi documentation (GUROBI OPTIMIZATION LLC. 2023) states that this value should be as low as possible. In our case the Kappa value for some problems in the algorithm quickly increased to values of 12 an above, values explicitly stated in the documentation are too high.

To combat the numerical issues, we worked on scaling the input data and the data flowing between the subproblems. We changed the units of our inputs, e.g., all water volume units to Mm^3/s, and divided specific constraints by the greatest common divisor. After extensive user scaling, we were able to achieve a coefficient range of $10^4 - 10^{-2}$, well within the bounds recommended by Gurobi (GUROBI OPTIMIZATION LLC. 2023). With the scaled values, the Kappa reduced from 12 to 7 on the initial iterations but quickly rose as cuts where added. Implementing automatic scaling of the added cuts saw little effect, though no advanced automatic scaling was implemented. We

also implemented automatic rounding to combat the Kappa increase seen by adding cuts. This rendered the cuts useless, emphasizing the precision needed in the disjunctive cuts.

Another issue was identified in the branching scheme of the algorithm. The upper bound in this algorithm is set when a feasible solution is identified. As we were not able to find a feasible solution, no upper bound was set. In turn, this lead to no nodes being closed by bound, giving a large number of expanded nodes to explore.

To get a better overview in the troubleshooting of our problem, we generated a small version of the hydropower production problem. This had constant head and a linear HPF that was only dependent on the discharge. The only binary variables in this problem were the status variables of the turbines. This gave a problem with only 96 binary variables, enabling us to print and view all binary variables. Indeed, when iterating through the algorithm with the simple hydropower problem, the implemented algorithm successfully cut away the fractional solutions of the binary variables and the algorithm ran to completion. However, the model still did not get an optimal solution. This was because the problem did not branch, i.e., the algorithm got stuck in the first node. This node had x-values that were in a vertex of X, i.e., the feasible region of x but were not optimal. If the x-variables are not pushed out of the vertex solutions by the optimality cuts, branching does not occur. The convergence of the algorithm thus happened in the root node. This implies that the Benders' optimality cuts produced by the subproblem did not work correctly.

Summarizing the issues we faced:

- Ill conditioning of the initial problem.
- Numeric instability after iteratively adding cuts.
- Long solution times of C3-SLP (6.22).
- Weak disjunctive cuts.
- No upper bound on the problem.
- Imprecise branching scheme.
- Weak optimality cuts.

The rest of this subsection seeks to analyze the results seen in our implementation of the D2-CBAC algorithm. We will try to point out weaknesses in our implementation, weaknesses in the algorithm itself, and challenges in employing this specific algorithm on our specific two-stage stochastic problem. We suggest solutions or approaches that might fix the problems we have faced. In this work, we have reached out to Professor Lewis Ntaimo, one of the authors behind the D2-CBAC algorithm. This has allowed us to discuss our theories and come up with possible solutions that could bring value to future implimentations of the algorithm, or variations of it. All references to communications with Professor Ntaimo is from email correspondence between May 21^{st} and June 9^{th}, 2023.

Addressing first the conditioning of the problem and the numerical instability, we saw slight improvements in the Kappa value when applying extensive user scaling. Utilizing more advanced techniques might condition the problem even more. Another challenge in this is that the scaling needs to be automatic, as the coefficients, and especially the right hand side values, vary with seasons, and even day by day. Rounding could also be an approach to strengthen the matrix conditioning. Care must however be taken, as employing extensive rounding could potentially introduce more numeric instability (GUROBI OPTIMIZATION LLC. 2023). Additionally, the scaling should be performed on the cuts added throughout the algorithmic iterations. We saw the cuts increasing the Kappa value, a strong indication that the numeric instability in the solver rose. We suggest exploring the literature to find effective methods of performing automatic model scaling. This should be implemented into the iterations of the algorithm to ensure stability throughout repeated solves.

We have additionally looked at the solver itself. In Ntaimo (2010), a variation of the the D2 algorithm is successfully implemented using the solver CPLEX. We have not found documentation

other than discussions on different web forums on the numerical precision of CPLEX compared to the solver we have used, i.e., Gurobi. We do however know that Gurobi's built-in MILP solver operates with a integer precision of 10^{-5}. In some sense, the algorithm is a MILP solver using the LP-solvers of Gurobi. There is, however, no parameter that can enforce integer sensitivity in the LP solver. We have to round the outputs manually, which leads to imprecision in the variables that are not rounded. Additionally, as discussed, rounding often rendered the disjunctive cuts useless and could potentially introduce more numeric instability. We suggest conducting a comparison of the LP-mode of different commercial solvers on how they handle the different inputs it would get by running the D2-CBAC on a short-term scheduling problem. Parameters to internally control rounding of fractional values near their bounds would be an advantage. Changing language entirely, from Python to, e.g., C++ could also boost precision, as it supports extended precision floating point arithmetic.

Addressing the weak disjunctive cuts, Prof. Ntaimo in our correspondence points out that D2 cuts in high dimensional space might not produce as strong cuts as we need for the second-stage problem. For future implementations, one could try implementing some sort of Branch-and-Bound scheme together with the D2 cuts. Additionally, as we discussed in Section 7.4, symmetry breaking constraints or measures should be added to speed up solution time.

The weak D2 cuts is essentially also what caused the missing upper bound, as no feasible solution was ever found. An upper bound could be set from the start. An example could be solving the LP relaxation of the deterministic equivalent of the problem, using those first-stage variables and solving each subproblem individually using a standard MILP solver. From these solutions, a feasible upper bound could be calculated by taking the expectation over all second-stage solutions added to the first-stage solution of the LP relaxation. Another approach could be to change the search tactic in the algorithm branching tree. In the original paper (Ntaimo and Sen 2007), a best-first approach is used. This leads to many iterations on what is often the LP-relaxed solution. Focusing on first finding a feasible solution could see decreased run-times in the algorithm.

The long solution times of the C3-SLP problem could comprise several issues. As it uses the coefficient matrix of the subproblems, it is affected by the numerical instability discussed earlier. Prof. Ntaimo points out that it is in itself a simple recourse problem and could be solved by a decomposition algorithm if necessary. As the C3-SLP is what often becomes infeasible in our implementation, it could be worth looking into this part of the algorithm.

Lastly we look at the optimality cuts. Benders' optimality cuts are known to be less effective in some cases, and often many iterations are needed to get to the optimal solution (Rahmaniani et al. 2017). In our model, the subproblem is much larger than the master problem, and the first-stage decisions are only present in a very small part of the constraints in the second-stage problem. This structure may lead to weak Benders' cuts. With the optimality cuts numeric precision and conditioning could play a role as well. Dual values are affected by the precision of the solution, and they are in turn used to create the optimality cuts.

Other reasons why the Benders' optimality cuts do not work correctly are related to the LP relaxation of our subproblem. If the gap between the LP relaxation of the subproblem is too large, the optimal solutions gained from the LP relaxation may be far from the optimal solution of the non-relaxed problem. Since the dual values that constitute the cut are gathered from the LP relaxation, the cuts may be weak if the dual values do not adequately represent the problems optimal solution. Additionally, since the binary values in our subproblem are an important factor in capturing the combinatorial complexity of the HPF, the relaxation of these may result in a too-large loss of information in the subproblem. This may also lead to some accuracy loss in the Benders' cut.

Of course there is a chance that we have implemented the algorithm, or at least parts of it, incorrectly. However, the observed behavior in our different tests suggests that they are working as intended, for instance the output of all test problems, the cuts actually cutting away fractional solutions, the branching to the LP relaxation first-stage solution, and the convergence of the reduced problem.

The proposed solutions to the challenges we faced are all suggestions that should be explored in

future research. They could provide valuable input to future implementations of the D2-CBAC algorithm, both in hybrid hydro-solar production planning and general two-stage stochastic programming.

8 Concluding Remarks

The setting of our thesis is a hybrid power system consisting of a hydropower plant and a large set of PV panels. The area has limited grid capacity. The challenge is to schedule day ahead commitments under a power purchase agreement. The focus is on developing an optimization approach to this scheduling, as well as developing a framework for testing the performance of the scheduling of the hybrid system. The optimization model includes linearization three non-linear functions, i.e., the hydropower production function, the gross head function and the net head function. Additionally, we have formulated a mid-term model that runs in tandem with the short-term model, calculating the value of water on a daily basis. In the mid-term model we linearize the production function by using Taylor expansions around the mean head and mean discharge.

The solar power production in the hybrid power system has been introduced as scenarios generated by simulations governed by stochastic differential equations. Together, the scenario generation and the short-term planning model in the setting of the power system comprise a complex two-stage stochastic optimization problem. To solve this problem, we have implemented and tested an advanced decomposition method. Additionally, we have simulated an entire year of power production, estimating the value of hybrid planning and operation as opposed to separate. We have set up tests that helps us estimate the value of stochasticity introduced by our scenario generation, and we have tested the importance of exact planning, as opposed to using an LP relaxation.

The tests show a significant increase in both profits and resource utilization when planning and operating the hydro and solar power plant in hybrid as opposed to separately. Annual profits are 19% lower when planning and operating the power plants separately. This is partly explained by a significantly lower utilization of resources, i.e., water and solar irradiance. The separate configuration discharges 12% more water and curtails 33 times the amount of solar power as the hybrid configuration.

To evaluate the effects of introducing stochasticity, we have compared running the model on scenarios to running only on the weather forecast. The tests show a slight increase in yearly revenues when introducing stochasticity in the solar production. When the solar power production is stable and high and the water value is high, the stochastic configuration performs slightly worse than its deterministic counterpart. When the weather is less predictable and the value of water is lower, the stochasticity helps increase profits so that the deterministic configuration earns 0.06% less. For the full year, the hybrid configuration with stochasticity earned 0.04% more.

The final tests show that there are significant gains by solving these types of planning problems exactly as opposed to with an LP relaxation. Trading precision for time in the planning phase, by planning using an LP relaxation of the problem, reduces profits by 0.76% over the course of a year. The tests where performed using a deterministic equivalent when solving the two-stage stochastic optimization problem. As tests show that using the LP relaxation is not sufficient and that stochasticity can increase profits, the need for a more efficient solution algorithm is emphasized.

Our work with implementing the D2-CBAC algorithm as a solution method shows that the theory behind it fits the characteristics of our optimization problem. In practice, however, several challenges are uncovered. A combination of the wide ranges in the scale of input values, imprecisions in the solver used, weak optimality cuts, and missing upper bounds led to an unsuccessful implementation of the solution algorithm. Our suggestions on how to address these challenges are outlined in the next section.

8.1 Future Research

In the future, the D2-CBAC algorithm should be explored further. As its solution time theoretically does not increase drastically as a function of the number of scenarios, it could be used in a variety of hybrid power system settings. We suggest implementing it in a solver and programming language with high numerical precision. Additionally, the power production scheduling problem should be altered to work better with the algorithm. This includes automatic scaling to ensure

well conditioned matrices. A good approach to rounding of inputs and cuts without introducing numerical instability should be implemented as well.

The disjunctive cuts could be paired with some bounding scheme on the second stage variables. Additionally, problem specific cuts could be included, for instance symmetry breaking measures, reducing the issue of identical solutions because of identical turbines. Additionally, an effective heuristic to find a feasible upper bound would allow for fewer expanded nodes, which may lead to several benefits for the algorithm. Not needing to explore that many nodes will enable less memory to be used, which is important in problems of large magnitude. The search strategy in the node tree should also be looked at. One final direction to explore with the algorithm would be changing the method used to add optimality cuts. The Benders approach could be altered or exchanged for a more tailored method. This could allow faster branching and convergence.

The tests show that significant gains in solving the planning problem to optimality, rather than some approximation. This emphasizes the need for more research on a solution algorithm. The tests also show promising results from implementing scenarios generated around weather data. With more data available, more advanced methods could be used in the scenario generation, possibly yielding even higher profits.

Lastly, the tests performed in this thesis show the significant gains of planning and operating in hybrid. Expanding the research into different environmental and market settings could prove to be an important contribution to the current transition into renewables. The ability to rapidly introduce low marginal cost power production without having to invest significantly in infrastructure is an appealing idea.

Bibliography

Annear, R.L. and Wells, S.A. (2007). 'A comparison of five models for estimating clear-sky solar radiation'. *Water resources research* 43.10.

Antonanzas-Torres, F., Urraca, R., Polo, J., Perpiñán-Lamigueiro, O. and Escobar, R. (2019). 'Clear sky solar irradiance models: A review of seventy models'. *Renewable and Sustainable Energy Reviews* 107, pp. 374–387.

Asensio, M. and Contreras, J. (2016). 'Stochastic Unit Commitment in Isolated Systems With Renewable Penetration Under CVaR Assessment'. *IEEE Transactions on Smart Grid* 7.3, pp. 1356–1367.

Bakken, B.H. and Bjorkvoll, T. (2002). 'Hydropower unit start-up costs'. *IEEE Power Engineering Society Summer Meeting,* 3, pp. 1522–1527.

Balas, E., Ceria, S. and Cornuéjols, G. (1993). 'A lift-and-project cutting plane algorithm for mixed 0–1 programs'. *Mathematical Programming* 58.1, pp. 295–324.

Beale, E.M.L. and Forrest, J.J.H. (1976). 'Global optimization using special ordered sets'. *Mathematical Programming* 10.1, pp. 52–69.

Beltrán, F., Finardi, E.C. and de Oliveira, W. (2021). 'Two-stage and multi-stage decompositions for the medium-term hydrothermal scheduling problem: A computational comparison of solution techniques'. *International Journal of Electrical Power Energy Systems* 127, p. 106659.

Beluco, A., Kroeff de Souza, P. and Krenzinger, A. (2012). 'A method to evaluate the effect of complementarity in time between hydro and solar energy on the performance of hybrid hydro PV generating plants'. *Renewable Energy* 45, pp. 24–30.

Benders, J.F. (1962). 'Partitioning procedures for solving mixed-variables programming problems'. *Numerische Mathematik* 4.1, pp. 238–252.

Bhandari, B., Lee, K.T., Lee, C.S., Song, C.K., Maskey, R.K. and Ahn, S.H. (2014). 'A novel off-grid hybrid power system comprised of solar photovoltaic, wind, and hydro energy sources'. *Applied Energy* 133, pp. 236–242.

Breton, M., Hachem, S. and Hammadia, A. (2004). 'Accounting for losses in the optimization of production of hydroplants'. *IEEE Transactions on Energy Conversion* 19.2, pp. 346–351.

Carøe, C.C. and Schultz, R. (1999). 'Dual decomposition in stochastic integer programming'. *Operations Research Letters* 24.1, pp. 37–45.

Carøe, C.C. and Tind, J. (1998). 'L-shaped decomposition of two-stage stochastic programs with integer recourse'. *Mathematical Programming* 83.1, pp. 451–464.

Carpentier, P.L., Gendreau, M. and Bastin, F. (2013). 'Midterm Hydro Generation Scheduling Under Uncertainty Using the Progressive Hedging Algorithm'. *Water Ressources Research* 49.5, pp. 2812–2827.

Cassano, S., Sossan, F., Landry, C. and Nicolet, C. (2021). 'Performance Assessment of Linear Models of Hydropower Plants'. *2021 IEEE PES Innovative Smart Grid Technologies Europe (ISGT Europe)*, pp. 01–06.

Catalão, J.P.S, Mariano, S., Mendes, V.M.F. and Ferreira, L.A.F.M. (2009). 'Scheduling of Head-Sensitive Cascaded Hydro Systems: A Nonlinear Approach'. *IEEE Transactions on Power Systems* 24, pp. 337–346.

Cordova, M.M., Finardi, E.C., Ribas, F.A.C., de Matos, V.L. and Scuzziato, M.R. (2014). 'Performance evaluation and energy production optimization in the real-time operation of hydropower plants'. *Electric Power Systems Research* 116, pp. 201–207.

De Ladurantaye, D., Gendreau, M. and Potvin, J.Y. (2009). 'Optimizing profits from hydroelectricity production'. *Computers Operations Research* 36.2. Scheduling for Modern Manufacturing, Logistics, and Supply Chains, pp. 499–529.

Deshmukh, M.K. and Deshmukh, S.S. (2008). 'Modeling of hybrid renewable energy systems'. *Renewable and Sustainable Energy Reviews* 12.1, pp. 235–249.

Diniz, A.L. and Maceira, M.E.P. (2008). 'A Four-Dimensional Model of Hydro Generation for the Short-Term Hydrothermal Dispatch Problem Considering Head and Spillage Effects'. *IEEE Transactions on Power Systems* 23.3, pp. 1298–1308.

Durbin, J. and Watson, G.S. (1950). 'Testing for Serial Correlation in Least Squares Regression: I'. *Biometrika* 37.3/4, pp. 409–428.

Eichhorn, A., Heitsch, H. and Roemisch, W. (2010). 'Stochastic Optimization of Electricity Portfolios: Scenario Tree Modeling and Risk Management', pp. 405–432.

Ek Fälth, H., Mattsson, N., Reichenberg, L. and Hedenus, F. (2022). 'Exploring trade-offs between aggregated and turbine-level representations of hydropower in optimization models'. Available at SSRN: https://ssrn.com/abstract=4252603 or http://dx.doi.org/10.2139/ssrn.4252603.

European Commission (2022). *PVGIS data sources calculation methods*. URL: https://joint-research-centre.ec.europa.eu/pvgis-online-tool/getting-started-pvgis/pvgis-data-sources-calculation-methods_en (visited on 10th Mar. 2023).

Faiman, D. (2008). 'Assessing the outdoor operating temperature of photovoltaic modules'. *Progress in Photovoltaics: Research and Applications* 16.4, pp. 307–315.

Finardi, E.C. and da Silva, E.L. (2005). 'Unit commitment of single hydroelectric plant'. *Electric Power Systems Research* 75.2, pp. 116–123.

Finardi, E.C. and Scuzziato, M.R. (2013). 'Hydro unit commitment and loading problem for day-ahead operation planning problem'. *International Journal of Electrical Power Energy Systems* 44.1, pp. 7–16.

Finardi, E.C. and Silva, E.L. da (2006). 'Solving the Hydro Unit Commitment Problem via Dual Decomposition and Sequential Quadratic Programming'. *IEEE Transactions on Power Systems* 21, pp. 835–844.

Flatabø, N., Haugstad, A., Mo, B. and Fosso, O.B. (1998). 'Short-term and medium-term generation scheduling in the Norwegian hydro system under a competitive power market structure'. *EPSOM'98 (International Conference on Electrical Power System Operation and Management), Switzerland*.

Fleten, S.E. and Kristoffersen, T.K. (2007). 'Stochastic programming for optimizing bidding strategies of a Nordic hydropower producer'. *European Journal of Operational Research* 181.2, pp. 916–928.

Fleten, S.E. and Kristoffersen, T.K. (2008). 'Short-term hydropower production planning by stochastic programming'. *Computers Operations Research* 35.8. Queues in Practice, pp. 2656–2671.

Fosso, O.B., Gjelsvik, A., Haugstad, A., Mo, B. and Wangensteen, I. (1999). 'Generation scheduling in a deregulated system. The Norwegian case - Discussion'. *IEEE Transactions on Power Systems* 14, pp. 75–81.

Garcia-Gonzalez, J. and Castro, G.A. (2001). 'Short-term hydro scheduling with cascaded and head-dependent reservoirs based on mixed-integer linear programming'. *2001 IEEE Porto Power Tech Proceedings (Cat. No.01EX502)*. Vol. 3.

Gjelsvik, A., Mo, B. and Haugstad, A. (2010). *Handbook of Power Systems*. Springer-Verlag Berlin Heidelberg.

Guedes, L., De Mendonça Maia, P., Lisboa, A., Vieira, D. and Saldanha, R. (2016). 'A Unit Commitment Algorithm and a Compact MILP Model for Short-Term Hydro-Power Generation Scheduling'. *IEEE Transactions on Power Systems*, pp. 3381–3390.

Guedes, L.S.M., Mendonça Maia, P. de, Lisboa, A.C., Vieira, D.A.G. and Saldanha, R.R. (2017). 'A Unit Commitment Algorithm and a Compact MILP Model for Short-Term Hydro-Power Generation Scheduling'. *IEEE Transactions on Power Systems* 32.5, pp. 3381–3390.

GUROBI OPTIMIZATION LLC. (2023). *Guidelines for Numerical Issues*. URL: https://www.gurobi.com/documentation/9.5/refman/guidelines_for_numerical_i.html (visited on 9th June 2023).

Huld, T., Šúri, M. and Dunlop, E.D. (2008). 'Geographical variation of the conversion efficiency of crystalline silicon photovoltaic modules in Europe'. *Progress in Photovoltaics: Research and Applications* 16.7, pp. 595–607.

IEA, Paris (2022). *Solar PV*. URL: https://www.iea.org/reports/solar-pv (visited on 12th Dec. 2022).

Iversen, E.B., Morales, J.M., Møller, J.K. and Madsen, H. (2014). 'Probabilistic forecasts of solar irradiance using stochastic differential equations'. *Environmetrics* 25.3, pp. 152–164.

Iversen, E.B. and Pinson, P. (2016). 'RESGen: Renewable Energy Scenario Generation Platform'. English. *Proceedings of IEEE PES General Meeting*. United States: IEEE.

Kall, P. and Wallace, S.W. (1994). *Stochastic Programming*. Springer-Verlag Berlin Heidelberg.

Kang, C., Guo, M. and Wang, J. (2017). 'Short-Term Hydrothermal Scheduling Using a Two-Stage Linear Programming with Special Ordered Sets Method'. *Water Resources Management* 31.11, pp. 3329–3341.

King, A.J. and Wallace, S.W. (2012). *Modeling with Stochastic Programming*. Springer New York.

Koehl, M., Heck, M., Wiesmeier, S. and Wirth, J. (2011). 'Modeling of the nominal operating cell temperature based on outdoor weathering'. *Solar Energy Materials and Solar Cells* 95.7, pp. 1638–1646.

Kong, J., Skjelbred, H.I. and Fosso, O.B. (2020). 'An overview on formulations and optimization methods for the unit-based short-term hydro scheduling problem'. *Electric Power Systems Research* 178, p. 106027.

Küçükyavuz, S. and Sen, S. (2017). 'An introduction to two-stage stochastic mixed-integer programming'. INFORMS TutORials in Operations Research null.null, pp. 1–27.

Laporte, G. and Louveaux, F.V. (1993). 'The integer L-shaped method for stochastic integer programs with complete recourse'. *Operations Research Letters* 13.3, pp. 133–142.

Li, F.F. and Qiu, J. (2016). 'Multi-objective optimization for integrated hydro–photovoltaic power system'. *Applied Energy* 167, pp. 377–384.

Li, P., Zhou, K. and Yang, S. (2018). 'Photovoltaic Power Forecasting: Models and Methods'. *2018 2nd IEEE Conference on Energy Internet and Energy System Integration (EI2)*, pp. 1–6.

Lombardi (2022). *Frankonedou and Kogbedou HPP (Guinea)*. URL: https://www.lombardi.ch/en-gb/pages/References/Hydroelectric%20plants/References_5113.aspx (visited on 12th Dec. 2022).

Lorenz, E., Hurka, J., Heinemann, D. and Beyer, H.G. (2009). 'Irradiance Forecasting for the Power Prediction of Grid-Connected Photovoltaic Systems'. *IEEE Journal of Selected Topics in Applied Earth Observations and Remote Sensing* 2.1, pp. 2–10.

Mariano, S., Catalão, J.P.S., Mendes, V.M.F. and Ferreira, L.A.F.M. (2008). 'Optimising power generation efficiency for head-sensitive cascaded reservoirs in a competitive electricity market'. *International Journal of Electrical Power Energy Systems* 30.2, pp. 125–133.

Matevosyan, J. and Soder, L. (2007). 'Short-term hydropower planning coordinated with wind power in areas with congestion problems'. *Wind Energy* 10, pp. 195–208.

Ming, B., Liu, P., Cheng, L., Zhou, Y. and Wang, X. (2018). 'Optimal daily generation scheduling of large hydro–photovoltaic hybrid power plants'. *Energy Conversion and Management* 171, pp. 528–540.

Morales, J.M., Conejo, A.J., H.M., Pinson, P. and Zugno, M. (2014). *Integrating Renewables in Electricity Markets*. Springer New York.

Munir, M.A., Khattak, A., Imran, K., Ulasyar, A. and Khan, A. (2019). 'Solar PV Generation Forecast Model Based on the Most Effective Weather Parameters'. *2019 International Conference on Electrical, Communication, and Computer Engineering (ICECCE)*, pp. 1–5.

Muñoz Sabater, J. (2019). *ERA5-Land hourly data from 1981 to present*. Copernicus Climate Change Service (C3S) Climate Data Store (CDS).

Nore, I.B. and Winther, K. (2022). 'Optimizing Hybrid Hydro-Solar Power Systems Using Two-Stage Stochastic Programming'. [Project thesis, Norwegian University of Science and Technology. Available upon request].

Ntaimo, L. (2010). 'Disjunctive Decomposition for Two-Stage Stochastic Mixed-Binary Programs with Random Recourse'. *Operations Research* 58.1, pp. 229–243.

Ntaimo, L. and Sen, S. (2007). 'A branch-and-cut algorithm for two-stage stochastic mixed-binary programs with continuous first-stage variables'. *International Journal of Computational Science and Engineering* 3, pp. 232–241.

Paska, J., Biczel, P. and Kłos, M. (2009). 'Hybrid power systems – An effective way of utilising primary energy sources'. *Renewable Energy* 34.11, pp. 2414–2421.

Pedro, H.T.C. and Coimbra, C.F.M. (2012). 'Assessment of forecasting techniques for solar power production with no exogenous inputs'. *Solar Energy* 86.7, pp. 2017–2028.

Pinson, P., Madsen, H., Nielsen, H.A., Papaefthymiou, G. and Klöckl, B. (2009). 'From probabilistic forecasts to statistical scenarios of short-term wind power production'. *Wind Energy* 12.1, pp. 51–62.

Qazi, S. (2017). 'Chapter 7 - Solar Thermal Electricity and Solar Insolation'. *Standalone Photovoltaic (PV) Systems for Disaster Relief and Remote Areas*. Elsevier, pp. 203–237.

Rahmaniani, R., Crainic, T.G., Gendreau, M. and Rei, W. (2017). 'The Benders decomposition algorithm: A literature review'. *European Journal of Operational Research* 259.3, pp. 801–817.

Raygani, S.V. (2019). 'Robust unit commitment with characterised solar PV systems'. *IET Renewable Power Generation* 13.6, pp. 867–876.

Rios, I., Wets, R. and Woodruff, D. (2015). 'Multi-period forecasting and scenario generation with limited data'. *Computational Management Science* 12.

Saad, M., Turgeon, A., Bigras, P. and Duquette, R. (1994). 'Learning disaggregation technique for the operation of long-term hydroelectric power systems'. *Water Resources Research* 30.11, pp. 3195–3202.

Séguin, S., Fleten, S.E., Côté, P., Pichler, A. and Audet, C. (2017). 'Stochastic short-term hydropower planning with inflow scenario trees'. *European Journal of Operational Research* 259.3, pp. 1156–1168.

Sen, S. and Higle, J.L. (2005). 'The C3 Theorem and a D2 Algorithm for Large Scale Stochastic Mixed-Integer Programming: Set Convexification'. *Mathematical Programming* 104.1, pp. 1–20.

Sen, S., Higle, J.L. and Ntaimo, L. (2003). 'A Summary and Illustration of Disjunctive Decomposition with Set Convexification'. *Network Interdiction and Stochastic Integer Programming*. Boston, MA: Springer US, pp. 105–125.

Sen, S. and Sherali, H.D. (1987). 'Nondifferentiable reverse convex programs and facetial convexity cuts via a disjunctive characterization'. *Mathematical Programming* 37.2, pp. 169–183.

Sherali, H.D. and Shetty, C.M. (1980). *Optimization with Disjunctive Constraints*. Springer-Verlag Berlin Heidelberg.

Sherali, H.D. and Zhu, X. (2009). 'Two-stage stochastic mixed-integer programs: algorithms and insights'. *Advances in Applied Mathematics and Global Optimization* 17.1, pp. 1–31.

Singh, G.K. (2013). 'Solar power generation by PV (photovoltaic) technology: A review'. *Energy* 53, pp. 1–13.

Skjelbred, H.I., Kong, J. and Fosso, O.B. (2020). 'Dynamic incorporation of nonlinearity into MILP formulation for short-term hydro scheduling'. *International Journal of Electrical Power Energy Systems* 116, p. 105530.

Staid, A., Watson, J.P., Wets, R. and Woodruff, D. (2017). 'Generating short-term probabilistic wind power scenarios via nonparametric forecast error density estimators'. *Wind Energy* 20.

Thyregod, H. and Madsen, P. (2011). *Introduction to General and Generalized Linear Models*. CRC Press.

Tong, B., Zhai, Q. and Guan, X. (2013). 'An MILP Based Formulation for Short-Term Hydro Generation Scheduling With Analysis of the Linearization Effects on Solution Feasibility'. *IEEE Transactions on Power Systems* 28.4, pp. 3588–3599.

Vagropoulos, S.I., Kardakos, E.G., Simoglou, C.K., Bakirtzis, A.G. and Catalão, J.P.S. (2016). 'ANN-based scenario generation methodology for stochastic variables of electric power systems'. *Electric Power Systems Research* 134, pp. 9–18.

Van Slyke, R.M. and Wets, R. (1969). 'L-Shaped Linear Programs with Applications to Optimal Control and Stochastic Programming'. *SIAM Journal on Applied Mathematics* 17.4, pp. 638–663.

Wallace, S.W. and Fleten, S.E. (2003). 'Stochastic Programming Models in Energy'. *Stochastic Programming*. Vol. 10. Handbooks in Operations Research and Management Science. Elsevier, pp. 637–677.

Wets, R. (1974). 'Stochastic Programs with Fixed Recourse: The Equivalent Deterministic Program'. *SIAM Review* 16.3, pp. 309–339.

Wiener, N. (1923). 'Differential-Space'. *Journal of Mathematics and Physics* 2.1-4, pp. 131–174.

Zhang, Y., Ma, C., Yang, Y., Pang, X., Liu, L. and Lian, J. (2021). 'Study on short-term optimal operation of cascade hydro-photovoltaic hybrid systems'. *Applied Energy* 291, p. 116828.

Appendix

A Short-Term Model

Nomenclature

Sets and Indices

$\mathcal{R}$	-	set of reservoirs, index $r \in \mathcal{R}$
$\mathcal{K}$	-	set of power generating units, index $k \in \mathcal{K}$
$\mathcal{K}_r$	-	set of power generating units connected to reservoir r, index $k \in \mathcal{K}_r$
$\mathcal{T}$	-	set of timesteps in the planning period, index $t \in \mathcal{T}$
$\mathcal{T}_d$	-	set of timesteps in the days of the planning horizon, index $t \in \mathcal{T}_d$. $d \in \{1, 2\}$
$\hat{\mathcal{T}}$	-	set of peak period timesteps in the planning horizon, index $t \in \hat{\mathcal{T}}$, $\hat{\mathcal{T}} \subset \mathcal{T}_1$
$\tilde{\mathcal{T}}$	-	set of off-peak period timesteps in the planning horizon, index $t \in \tilde{\mathcal{T}}$, $\tilde{\mathcal{T}} \subset \mathcal{T}_1$

Parameters

P_t	-	power selling price at timestep t (\$/MWh)
P^I	-	intermittent power selling price (\$/MWh)
C^U	-	penalty cost of not meeting load commitment (\$/MWh)
C^S_k	-	start-up cost of generating unit k (\$)
V^{MIN}_r, V^{MAX}_r	-	minimum and maximum water volume in reservoir r (m^3)
Q^{MIN}_r	-	environmental restriction on minimum water discharge from reservoir r (m^3/h)
Q^{MIN}_k, Q^{MAX}_k	-	minimum and maximum amount of water dischargeable to unit k (m^3/h)
D^{MAX}	-	grid capacity (MW)
ξ_t	-	solar power production in timestep t (MWh)
$\delta_{k,0}$	-	input status for generating unit k (bin)
ϕ_r	-	water value in reservoir r at end of planning horizon (\$/m^3)
V^{INIT}_r	-	water volume in reservoir r at start of planning horizon (m^3)
$Q^{NI}_{r,t}$	-	natural inflow to reservoir r in timestep t (m^3/h)

Variables

$v_{r,t}$	-	water volume in reservoir r in timestep t (m^3)
$q_{k,t}$	-	water discharge to unit k in timestep t (m^3)
$h_{r,t}$	-	net head level in reservoir r in timestep t (m)
$h^G_{r,t}$	-	gross head level in reservoir r in timestep t (m)
$q^{BP}_{r,t}$	-	controlled water spillage through bypass gate in reservoir r in timestep t (m^3)
$q^{OF}_{r,t}$	-	water overflow in reservoir r in time t (m^3)
$q^{TOT}_{r,t}$	-	total regulated water discharge from reservoir r at time t (m^3)
$\delta_{k,t}$	-	status of unit k in timestep t (bin)
$\lambda_{k,t}$	-	status change of production at plant k in timestep t (bin)
ξ^{CURT}_t	-	excess solar power in time t (MWh)
$p_{k,t}$	-	hydropower production at unit k in timestep t (MWh)
p^U_t	-	total unfulfilled commitment based on the load commitment in timestep t (MWh)
p^I_t	-	total amount of power delivered in excess of the load commitment in timestep t (MWh)
x_t	-	firm power commitment in timestep t (MWh)
x^P	-	firm power commitment in the peak period (MWh)
x^O	-	firm power commitment in the off-peak period (MWh)

Functions

$h_r^G(v_{r,t})$	-	gross head of reservoir r at timestep t (m)
$h_r(h_{r,t}^G, q_{k,t})$	-	net head for the power plant in reservoir r in timestep t (MWh)
$p_k(h_{r,t}, q_{k,t})$	-	hydropower production function for unit k in timestep t (MWh)

$$min \quad \sum_{r \in \mathcal{R}} \phi_r(V_r^{INIT} - v_{r,T}) + \sum_{t \in \mathcal{T}} \sum_{k \in \mathcal{K}} C_k^S \lambda_{k,t} + \sum_{t \in \mathcal{T}} C^U p_t^U - \sum_{t \in \mathcal{T}} (P_t x_t + P_t^I p_t^I) \tag{.1}$$

s.t.

$$v_{r,1} = V_r^{INIT}, \quad r \in \mathcal{R} \tag{.2}$$

$$v_{r,t} = v_{r,t-1} + Q_{r,t-1}^{NI} + q_{r+1,t-1}^{TOT} - q_{r,t-1}^{TOT} - q_{r,t-1}^{OF}, \quad r \in \mathcal{R}, t \in \mathcal{T} \backslash \{1\} \tag{.3}$$

$$q_{R+1,t}^{TOT} = 0, \quad t \in \mathcal{T} \tag{.4}$$

$$q_{r,t}^{OF} \geq v_{r,t} + Q_{r,t}^{NI} + q_{r+1,t}^{TOT} - q_{r,t}^{TOT} - V_r^{MAX}, \quad r \in \mathcal{R}, t \in \mathcal{T} \tag{.5}$$

$$V_r^{MIN} \leq v_{r,t} \leq V_r^{MAX}, \quad r \in \mathcal{R}, t \in \mathcal{T} \tag{.6}$$

$$q_{r,t}^{TOTAL} = \sum_{k \in \mathcal{K}_r} q_{k,t} + q_{r,t}^{BP}, \quad r \in \mathcal{R}, t \in \mathcal{T} \tag{.7}$$

$$Q_r^{MIN} \leq q_{r,t}^{TOT}, \quad r \in \mathcal{R}, t \in \mathcal{T} \tag{.8}$$

$$Q_k^{MIN} \delta_{k,t} \leq q_{k,t} \leq Q_k^{MAX} \delta_{k,t}, \quad k \in \mathcal{K}, t \in \mathcal{T} \tag{.9}$$

$$q_{r,t}^{BP} \leq Q_r^{BP}, \quad r \in \mathcal{R}, t \in \mathcal{T} \tag{.10}$$

$$h_{r,t}^G = h_r^G(v_{r,t}), \quad r \in \mathcal{R}, t \in \mathcal{T} \tag{.11}$$

$$h_{r,t} = h_r(h_{r,t}^G, q_{k,t}) \quad r \in \mathcal{R}, k \in \mathcal{K}_r, t \in \mathcal{T} \tag{.12}$$

$$p_{k,t} = p(h_{r,t}, q_{k,t}), \quad r \in \mathcal{R}, k \in \mathcal{K}_r, t \in \mathcal{T} \tag{.13}$$

$$\lambda_{k,t} \geq \delta_{k,t} - \delta_{k,t-1}, \quad k \in \mathcal{K}, t \in \mathcal{T} \tag{.14}$$

$$\xi_t + \sum_{k \in \mathcal{K}} p_{k,t} + p_t^U = x_t + p_t^I + \xi_t^{CURT}, \quad t \in \mathcal{T} \tag{.15}$$

$$x_t = x^P, \quad t \in \hat{\mathcal{T}} \tag{.16}$$

$$x_t = x^O, \quad t \in \tilde{\mathcal{T}} \tag{.17}$$

$$x_t + p_t^I \leq D^{MAX}, \quad t \in \mathcal{T} \tag{.18}$$

$$\lambda_{k,t}, \delta_{k,t} \in \{0, 1\}, \quad k \in \mathcal{K}, t \in \mathcal{T} \tag{.19}$$

$$p_{k,t}, q_{k,t} \geq 0, \quad k \in \mathcal{K}, t \in \mathcal{T} \tag{.20}$$

$$q_{r,t}^{BP}, q_{r,t}^{TOT}, q_{r,t}^{OF}, v_{r,t}, h_{r,t}^G, h_{r,t} \geq 0, \quad r \in \mathcal{R}, t \in \mathcal{T} \tag{.21}$$

$$\xi_t^{CURT}, p_t^I, p_t^U, x_t \geq 0, \quad t \in \mathcal{T} \tag{.22}$$

$$x^O, x^P \geq 0 \tag{.23}$$

B Mid-Term Model

Nomenclature

Sets and Indices

$\mathcal{R}$	-	set of reservoirs, index $r \in \mathcal{R}$
$\mathcal{K}$	-	set of power generating units, index $k \in \mathcal{K}$
$\mathcal{K}_r$	-	set of power generating units connected to reservoir r, index $k \in \mathcal{K}_r$
$\mathcal{T}$	-	set of timesteps in planning horizon, index $t \in \mathcal{T}$

Parameters

P_t	-	power selling price at timestep t (\$/MWh)
P^I	-	intermittent power selling price (\$/MWh)
C^U	-	penalty cost of not meeting load commitment (\$/MWh)
V_r^{MIN}, V_r^{MAX}	-	minimum and maximum water volume in reservoir r (Mm^3)
Q_r^{MIN}	-	environmental restriction on minimum water discharge from reservoir r (Mm^3/day)
Q_k^{MAX}	-	maximum amount of water dischargeable to unit k (Mm^3/day)
D^{MAX}	-	grid capacity (MW)
ξ_t	-	solar power production in timestep t (MWh)
V_r^{INIT}	-	water volume in reservoir r at start of planning horizon (Mm^3)
$Q_{r,t}^{NI}$	-	natural inflow to reservoir r in timestep t (Mm^3)

Variables

$v_{r,t}$	-	water volume in reservoir r in timestep t (Mm^3)
$h_{r,t}$	-	net head level in reservoir r in timestep t (m)
$q_{k,t}$	-	water discharge to unit k in timestep t (Mm^3)
$q_{r,t}^{BP}$	-	controlled water spillage through bypass gate in reservoir r in timestep t (Mm^3)
$q_{r,t}^{OF}$	-	water overflow of reservoir r in time t (Mm^3)
$q_{r,t}^{TOTAL}$	-	total regulated water discharged from reservoir r at time t (Mm^3)
ξ_t^{CURT}	-	excess solar power in time t
$p_{k,t}$	-	hydropower production at unit k in timestep t (MWh)
p_t^U	-	total unfulfilled commitment based on the load commitment in timestep t (MWh)
p_t^I	-	total amount of power delivered in excess of the load commitment in timestep t (MWh)
x_t	-	firm power commitment in timestep t (MWh)

Functions

$h_r(v_{r,t})$	-	net head for the power plant in reservoir r in timestep t. (MWh)
$p_k(h_{r,t}, q_{k,t})$	-	hydropower production function for unit k in timestep t. (MWh)

$$min \sum_{t \in \mathcal{T}} (C^U p_t^U) - \sum_{t \in \mathcal{T}} (P_t x_t + P_t^I p_t^I) \tag{.24}$$

s.t.

5.6 - 5.12 , 5.14 and 5.22

$$v_{r,1} = V_r^{INIT}, \quad r \in \mathcal{R} \tag{.25}$$

$$v_{r,t} = v_{r,t-1} + Q_{r,t-1}^{NI} + q_{r+1,t-1}^{TOT} - q_{r,t-1}^{TOT} - q_{r,t-1}^{OF}, \quad r \in \mathcal{R}, t \in \mathcal{T} \backslash \{1\} \tag{.26}$$

$$q_{R+1,t}^{TOT} = 0, \quad t \in \mathcal{T} \tag{.27}$$

$$q_{r,t}^{OF} \geq v_{r,t} + Q_{r,t}^{NI} + q_{r+1,t}^{TOT} - q_{r,t}^{TOT} - V_r^{MAX}, \quad r \in \mathcal{R}, t \in \mathcal{T} \tag{.28}$$

$$V_r^{MIN} \leq v_{r,t} \leq V_r^{MAX}, \quad r \in \mathcal{R}, t \in \mathcal{T} \tag{.29}$$

$$q_{r,t}^{TOTAL} = \sum_{k \in \mathcal{K}_r} q_{k,t} + q_{r,t}^{BP}, \quad r \in \mathcal{R}, t \in \mathcal{T} \tag{.30}$$

$$Q_r^{MIN} \leq q_{r,t}^{TOT}, \quad r \in \mathcal{R}, t \in \mathcal{T} \tag{.31}$$

$$q_{r,t}^{BP} \leq Q_r^{BP}, \quad r \in \mathcal{R}, t \in \mathcal{T} \tag{.32}$$

$$x_t + p_t^I \leq D^{MAX}, \quad t \in \mathcal{T} \tag{.33}$$

$$q_{k,t} \leq Q_k^{MAX}, \quad k \in \mathcal{K}, t \in \mathcal{T} \tag{.34}$$

$$h_{r,t} = h_r(v_{r,t}), \quad r \in \mathcal{R}, t \in \mathcal{T} \tag{.35}$$

$$p_{k,t} = p(h_{r,t}, q_{k,t}), \quad r \in \mathcal{R}, k \in \mathcal{K}_r, t \in \mathcal{T} \tag{.36}$$

$$p_{k,t}, q_{k,t} \geq 0, \quad k \in \mathcal{K}, t \in \mathcal{T} \tag{.37}$$

$$q_{r,t}^{BP}, q_{r,t}^{TOTAL}, q_{r,t}^{OF}, v_{r,t}, h_{r,t} \geq 0, \quad r \in \mathcal{R}, t \in \mathcal{T} \tag{.38}$$

$$\xi_t^{CURT}, p_t^I, p_t^U, x_t \geq 0, \quad t \in \mathcal{T} \tag{.39}$$

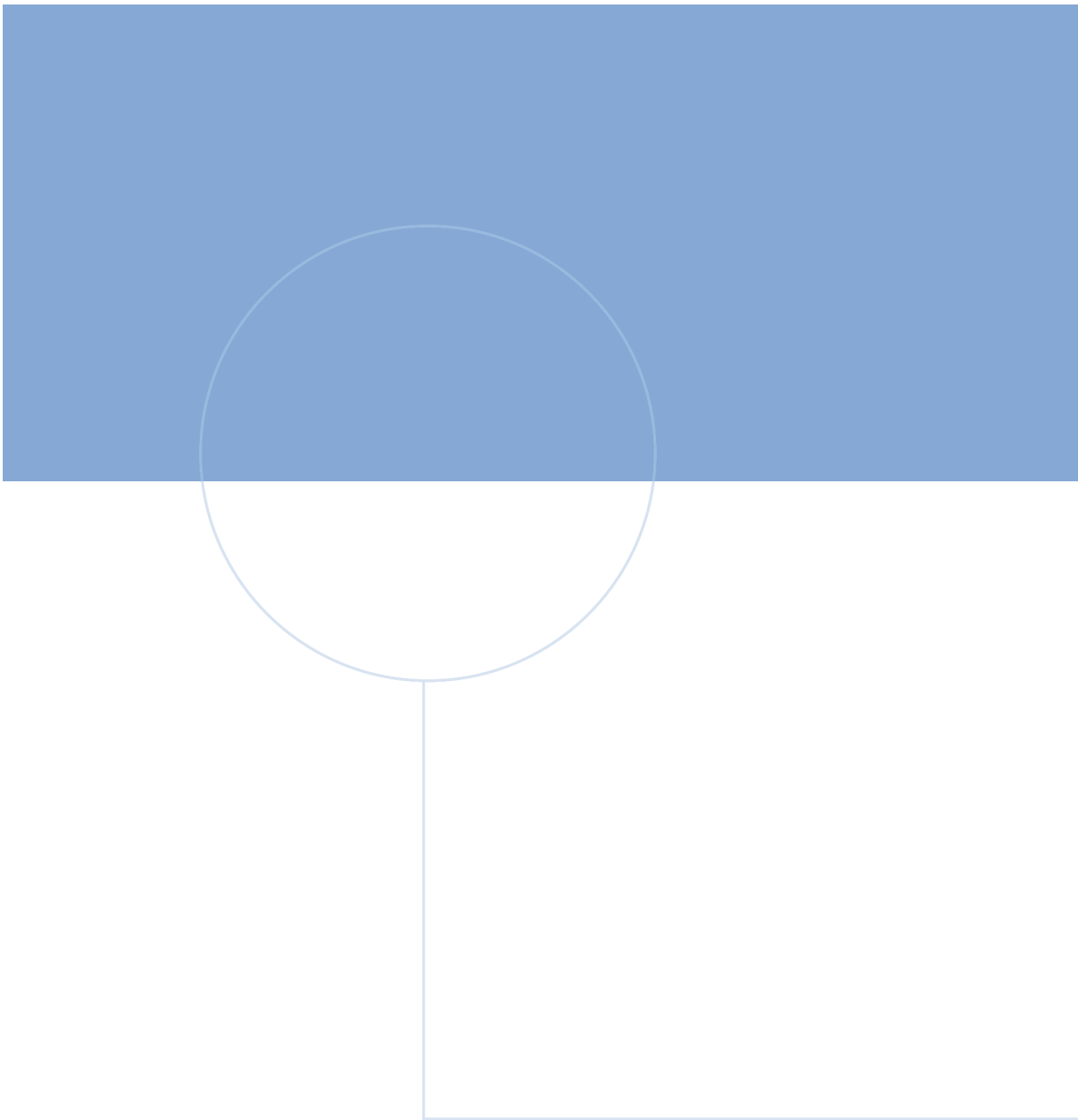

NTNU

Norwegian University of
Science and Technology